Theses and Dissertations   1. Thesis and Dissertation Collection, all items

2013-09

Novel Concept for High Dielectric Constant Composite Electrolyte Dielectrics

Fromille, Samuel S., IV

Monterey, California. Naval Postgraduate School

https://hdl.handle.net/10945/53408

NAVAL POSTGRADUATE SCHOOL

MONTEREY, CALIFORNIA

THESIS

NOVEL CONCEPT FOR HIGH DIELECTRIC CONSTANT COMPOSITE ELECTROLYTE DIELECTRICS

by

Samuel S. Fromille, IV

September 2013

Thesis Advisor:	Jonathan Phillips
Thesis Co-Advisor:	Young W. Kwon

THIS PAGE INTENTIONALLY LEFT BLANK

July 29, 2016

SUBJECT: Change in distribution statement for *Novel Concept for High Dielectric Constant Composite Electrolyte Dielectrics.* – September 2013.

1. Reference: Fromille, Samuel S. *Novel Concept for High Dielectric Constant Composite Electrolyte Dielectrics*. Monterey, CA: Naval Postgraduate School, Department of Mechanical and Aerospace Engineering, September 2013.

    UNCLASSIFIED [Distribution authorized to U.S. Government Agencies only, Premature Dissemination, September 2013. Other requests for this document must be referred to President, Code 261, Naval Postgraduate School, Monterey, CA 93943-5000 via the Defense Technical Information Center, 8725 John J. Kingman Rd., STE 0944, Ft. Belvoir, VA 22060-6218.].

2. Upon consultation with NPS faculty, the School has determined that this thesis may be released to the public with unlimited distribution effective July 29, 2016.

                                University Librarian
                                Naval Postgraduate School

THIS PAGE INTENTIONALLY LEFT BLANK

REPORT DOCUMENTATION PAGE		*Form Approved OMB No. 0704-0188*

Public reporting burden for this collection of information is estimated to average 1 hour per response, including the time for reviewing instruction, searching existing data sources, gathering and maintaining the data needed, and completing and reviewing the collection of information. Send comments regarding this burden estimate or any other aspect of this collection of information, including suggestions for reducing this burden, to Washington headquarters Services, Directorate for Information Operations and Reports, 1215 Jefferson Davis Highway, Suite 1204, Arlington, VA 22202-4302, and to the Office of Management and Budget, Paperwork Reduction Project (0704-0188) Washington DC 20503.

1. AGENCY USE ONLY *(Leave blank)*	2. REPORT DATE September 2013	3. REPORT TYPE AND DATES COVERED Master's Thesis
4. TITLE AND SUBTITLE NOVEL CONCEPT FOR HIGH DIELECTRIC CONSTANT COMPOSITE ELECTROLYTE DIELECTRICS		**5. FUNDING NUMBERS**
6. AUTHOR(S) Samuel S. Fromille, IV		
7. PERFORMING ORGANIZATION NAME(S) AND ADDRESS(ES) Naval Postgraduate School Monterey, CA 93943-5000		**8. PERFORMING ORGANIZATION REPORT NUMBER**
9. SPONSORING /MONITORING AGENCY NAME(S) AND ADDRESS(ES) N/A		**10. SPONSORING/MONITORING AGENCY REPORT NUMBER**

11. SUPPLEMENTARY NOTES The views expressed in this thesis are those of the author and do not reflect the official policy or position of the Department of Defense or the U.S. Government. IRB Protocol number ____N/A____.

12a. DISTRIBUTION / AVAILABILITY STATEMENT ~~Distribution authorized to U.S. Government Agencies only (Premature Dissemination) (September 2013). Other requests for this document must be referred to President, Code 261, Naval Postgraduate School, Monterey, CA 93943-5000 via the Defense Technical Information Center, 8725 John J. Kingman Rd., STE 0944, Ft. Belvoir, VA 22060-6218.~~ Approved for public release; distribution is unlimited	**12b. DISTRIBUTION CODE**

13. ABSTRACT (maximum 200 words)

This research was part of an ongoing program studying the concept of multi-material dielectrics (MMD) with dielectric constants much higher than homogenous materials. MMD described in this study have dielectric constants six orders of magnitude greater than the best single materials. This is achieved by mixing conductive particles with an insulating surface layer into a composite matrix phase composed of high surface area ceramic powder and aqueous electrolyte. Specifically examined in this study was micron-scale nickel powder treated in hydrogen peroxide (H_2O_2) loaded into high surface area alumina powder and aqueous boric acid solution. This new class of dielectric, composite electrolyte dielectrics (CED), is employed in an electrostatic capacitor configuration and demonstrated dielectric constant of order 10^{10} at approximately 1 Volt.

Additionally, it is demonstrated that treated nickel can be loaded in high volume fractions in the CED configuration. Prior studies of composite capacitors indicated a general limitation due to shorting. This results from the onset of percolation due to excess loading of conductive phases. Insulated particles described herein are successfully loaded up to 40% by volume, far above typical percolation thresholds. Simple models are presented to explain results.

14. SUBJECT TERMS Dielectric, Dielectric Constant, Relative Permittivity, Composite Dielectric, Capacitor, Energy Storage			**15. NUMBER OF PAGES** 143
			16. PRICE CODE
17. SECURITY CLASSIFICATION OF REPORT Unclassified	**18. SECURITY CLASSIFICATION OF THIS PAGE** Unclassified	**19. SECURITY CLASSIFICATION OF ABSTRACT** Unclassified	**20. LIMITATION OF ABSTRACT** UU

NSN 7540-01-280-5500

Standard Form 298 (Rev. 2-89)
Prescribed by ANSI Std. 239-18

THIS PAGE INTENTIONALLY LEFT BLANK

NOVEL CONCEPT FOR HIGH DIELECTRIC CONSTANT COMPOSITE ELECTROLYTE DIELECTRICS

Samuel S. Fromille, IV
Lieutenant, United States Navy
B.S.S.E., United States Naval Academy, 2006

Submitted in partial fulfillment of the
requirements for the degree of

MASTER OF SCIENCE IN MECHANICAL ENGINEERING

from the

NAVAL POSTGRADUATE SCHOOL
September 2013

Author: Samuel S. Fromille, IV

Approved by: Jonathan Phillips, PhD
                Thesis Advisor

                Young W. Kwon, PhD
                Thesis Co-Advisor

                Knox T. Millsaps, PhD
                Chair, Department of Mechanical and Aerospace Engineering

iii

THIS PAGE INTENTIONALLY LEFT BLANK

ABSTRACT

This research was part of an ongoing program studying the concept of multi-material dielectrics (MMD) with dielectric constants much higher than homogenous materials. MMD described in this study have dielectric constants six orders of magnitude greater than the best single materials. This is achieved by mixing conductive particles with an insulating surface layer into a composite matrix phase composed of high surface area ceramic powder and aqueous electrolyte. Specifically examined in this study was micron-scale nickel powder treated in hydrogen peroxide (H_2O_2) loaded into high surface area alumina powder and aqueous boric acid solution. This new class of dielectric, composite electrolyte dielectrics (CED), is employed in an electrostatic capacitor configuration and demonstrated dielectric constant of order 10^{10} at approximately 1 Volt.

Additionally, it is demonstrated that treated nickel can be loaded in high volume fractions in the CED configuration. Prior studies of composite capacitors indicated a general limitation due to shorting. This results from the onset of percolation due to excess loading of conductive phases. Insulated particles described herein are successfully loaded up to 40% by volume, far above typical percolation thresholds. Simple models are presented to explain results.

THIS PAGE INTENTIONALLY LEFT BLANK

TABLE OF CONTENTS

LIST OF FIGURES

xi

THIS PAGE INTENTIONALLY LEFT BLANK

LIST OF TABLES

THIS PAGE INTENTIONALLY LEFT BLANK

LIST OF ACRONYMS AND ABBREVIATIONS

3D	three-dimensional
AC	alternating current
$BaTiO_3$	barium titanate
BST	$Ba_{0.65}Sr_{0.35}TiO_3$
CED	composite electrolyte dielectric
cm	centimeter
ECP	electric conducting polymer
EDS	energy dispersive X-ray spectroscopy
EDLC	electric double-layer capacitor
ESR	equivalent series resistance
DC	direct current
F	farads
FIB	focused ion beam
g	gram
H_2O	water (distilled)
H_2O_2	hydrogen peroxide
HSA	high surface area acid
Hz	hertz (sec^{-1})
J	joule
kg	kilograms
KOH	potassium hydroxide
kV	kilovolts
kx	thousand times (magnification)
$k\Omega$	kiloohms
L	liters
M	molarity
m	meters
mA	milliamps

MCP	microchannel plates
mL	milliliter
mm	millimeter
MMD	multi-material dielectric
MΩ	megaohms
nA	nanaamp
nF	nanofarad
Ni	nickel
nm	nanometer
pA	picoamp
R	resistance
RC	resistor/capacitor
S	dielectric or breakdown strength
s	seconds
SEM	scanning electron microscopy
V	volts
W	watts
Wh	watt-hours
XRD	X-ray Diffraction
ε_R	dielectric constant
µF	microfarads
µm	micrometers

ACKNOWLEDGMENTS

I would like to thank Professor Jonathan Phillips for his guidance, insight, and support during this process. I greatly appreciate his confidence and trust, as well as the interesting conversations we shared throughout my time at NPS.

I would also like to thank Professor Sarath Menon for his limitless patience and willingness to help with characterization efforts. His dedication and support to the students in the materials science curriculum are invaluable. Professor Claudia Luhrs was also instrumental in providing advice and support to keep this project on track. Additionally, I would like to thank Professor Young Kwon for his assistance in the completion of this thesis, as well as his accessibility and cooperation as co-advisor.

I would like to acknowledge Professor Luke Brewer for his commitment and enthusiasm while teaching his classes. His influence was certainly instrumental in my selection to focus in materials science, and I appreciate all of his input and advice in and out of class.

I am also grateful to my fellow students who assisted and labored alongside me during this process. Particularly, LT Jason Downs, LT Jamie Cook, and LT Ashley Maxson were valuable resources and appreciated partners.

Finally, I would like to thank my wife, Molly, and my children, Quinn and Lanie, for their unconditional love and support.

THIS PAGE INTENTIONALLY LEFT BLANK

I.   INTRODUCTION

A.   SUMMARY OF FINDINGS

This research is part of a program to explore the dielectric properties of multi-material dielectrics (MMD). It is hypothesized that such materials can have dielectric constants orders of magnitude greater than homogeneous material. A particular variant of MMD studied herein, composite electrolyte dielectrics (CED), demonstrated extremely high dielectric constants, of the order 10^{10} operating at greater than 1 V. This result is notably many orders of magnitude higher than any other reported result for relative permittivity of a single material.

The devices produced using this particular MMD configuration were demonstrated to have consistent capacitor-like behavior, with multiple stable charge and discharge cycles in a parallel plate electrostatic configuration. This new general class of CED is composed of conductive particles with an insulating surface layer embedded in a matrix of high surface area powder wetted with aqueous acidic or basic solution. It is additionally demonstrated that this new class of dielectric material retains exceptional relative permittivity at loading fractions traditionally considered in excess of the percolation threshold. Specifically in this study, composites are loaded up to 40% conductive particle loading by volume.

This initial work focuses on a single sub-class of this novel dielectric material. Specifically, micron-scale nickel powders are treated with hydrogen peroxide (H_2O_2) and embedded in high surface area alumina powder wetted with aqueous solution of boric acid. Critical parameters of dielectric constant and operating voltage appear to be a function of several relevant variables including metal particle volume loading, dielectric thickness, and degree of metal particle surface treatment.

Operating voltage remains a significant performance limitation. Specifically, consistent dielectric properties were not observed in excess of approximately 1 V. Higher voltages bleed off of CED capacitors almost immediately. However, there is

reason to believe that other CED material compositions could achieve superior operating voltages without sacrificing superior capacitance.

Potential solutions for compact and inexpensive energy storage in a variety of applications motivate continued investigation. At present, a recognized benchmark is to design a capacitor with energy density of 1 J/cm^3 or greater. This result of this research achieved approximately 2% of this objective. However, over the course of one year, this study achieved approximately a factor of 75 increase in energy density. Alternate component materials and new compositions suggest rich potential for further improvement.

B.   BACKGROUND THEORY AND MOTIVATION

Capacitance is defined as the ability of an object to store electrical charge. The governing expression which relates the voltage potential (*V*) between objects of charge +*q* and –*q*, defines the capacitance (*C*), as

$$C = \frac{q}{V}.$$

Equation 1

Electrical capacitors are devices that exist in several different forms and are used in a variety of applications including filter circuits and energy storage. The foundational concept of this device is the storage of charge via an electric field in the space between two conducting electrodes according to Equation 1. After the charging power source is disconnected, the energy remains stored until an electric circuit is completed between the electrodes. The stored energy can then be delivered to the circuit load. The capacitance of a device can generally be calculated as a function of geometry and constituent materials. Electrodes are traditionally separated by a non-conducting material known as a dielectric. Dielectrics have a characteristic property that determines their capacity to store charge under the influence of an electric field. This parameter is referred to as the relative permittivity, or dielectric constant, of a material. The capacitance of a simply configured electrostatic device with two parallel conducting plates separated by dielectric material can be expressed as

$$C = \varepsilon_0 \varepsilon_R \frac{A}{d} \ , \qquad\qquad\qquad \text{Equation 2}$$

where ε_0 is the permittivity of free space and ε_R is the dielectric constant. The area of the plate surface is A and the distance between plates occupied by dielectric is d. It follows from **Error! Reference source not found.** that in order to maximize capacitance of a simply configured device, dielectric constant and surface area must be maximized while minimizing conductor separation. These performance concerns, along with considerations for cost, durability, operating voltage, and frequency, inform the design of capacitors for specific functions.

There are many uses for capacitors that require different attributes. Capacitors can be used for rapid energy delivery to provide running current or starting surges for electric motors, or provide pulse power for high energy laser systems. Other applications include signal rectification, which consists of converting source alternating current (AC) power to smooth direct current (DC) power for electronic devices [1]. The nature of capacitive energy storage and power delivery could be a pivotal aspect of future smart grid concepts [2]–[3]. The energy density of present capacitors must be improved for practical applications in energy storage.

Realizing the employment of capacitors for energy storage is the overall goal of this work in novel dielectric materials. This is not a typical application of capacitors, as they are inferior to chemical batteries in terms of energy density. Hence, capacitors are generally restricted to applications requiring rapid power delivery and fast charging [4]. Capacitors are superior to batteries in these applications as a result of the inherent limits of chemical batteries regarding high power delivery. The rate of energy released by a battery is dependent on ionic flux kinetics. Chemical reactions are the mechanism of energy release in batteries, and are restricted by rates of ionic diffusion. Conversely, capacitors store energy in an electric field and can consequently release that energy nearly instantaneously.

The energy stored in the electric field of a capacitor is expressed as

$$E_C = \frac{1}{2} C V^2 \ , \qquad\qquad\qquad \text{Equation 3}$$

where C is the capacitance and V is the voltage. As capacitance is directly proportional to dielectric constant, and energy varies as voltage squared, selecting an appropriate dielectric material is paramount in maximizing energy density. The objectives of maximizing voltage and dielectric constant while minimizing volume are constrained by an inherent limitation of capacitors known as dielectric breakdown. Breakdown occurs when the applied potential exceeds the limit of the non-conductive dielectric to sufficiently prevent shorting between the electrodes. Resistance to breakdown is referred to as breakdown strength or dielectric strength [5]. These factors point to the critical attributes of a suitable dielectric material for energy storage applications, namely a high relative permittivity and high dielectric strength. Examples of some common dielectric materials are listed in Table 1 with respective dielectric constants (ε_R), breakdown strengths (S), and theoretical energy densities (W_{max}/Vol). Improved energy density along with superior power delivery could allow capacitors to rival batteries in applications such as automotive and electronics power supplies, or energy storage systems for dynamic renewable energy sources.

Material	ε_r	S [kV/cm]	$\varepsilon_r S^2$ [(kV/cm)^2]	Wmax/Vol [J/cm^3]
Teflon	2.1	400 - 800	3.4E5 - 1.3E6	0.015 - 0.058
Epoxy/Araldit	3.7	160	9.5E4	0.0042
Polyethylene	2.3	470	5.1E5	0.023
Ba-Titanate	1300	29	(1.1E6)	0.049
Polyethylene - Teraphtalate	3.2	1600	8.2E6	0.36
Ruby Mica	5.4	1500 - 2200	12E6 - 26E6	0.53 - 1.2
CPN17	7000	400	(1.1E9)	5.8
SiO$_2$ Semi-crystalline	3.8	9800	3.6E8	16
SiO$_2$ amorphous: [2]	3.9	3000		
[3]	3.8...3.9	5000-10000		
[4]	3.9	6000-9000		

Table 1.   Common Dielectric Material Characteristic Parameters.From [6].

Clean, renewable energy sources are a worldwide topic of emphasis. One of the challenges hindering broader employment of these systems is the unstable nature of the power output. Unlike traditional power generation schemes, solar, wind, tidal, and other similar sources don't produce energy in a constant predictable fashion. This requires adaptation of energy storage and distribution infrastructure systems to effectively integrate these dynamic sources [7]–[9]. Supercapacitors have begun to bridge the gap into energy storage and delivery for specific applications such as mass transit and industrial machinery. With short duration loading and fast charge and discharge dynamics, these applications are well-suited for capacitive energy storage systems [10]. The potential for a durable, inexpensive, stable, and fast charging energy storage solution beyond chemical batteries motivates further study.

C.   CAPACITOR TECHNOLOGIES

Advances in capacitor performance are based on combinations of specialized configurations and material developments. Capacitor technology has evolved to meet

demands in different applications via a range of alternate configurations. Each alternate configuration may offer specific improved characteristics, but suffer from other inherent limitations. The wide variety of capacitor types leads to a high degree of specialization according to application. Specifications of capacitance, voltage, energy density, power density, cycle lifetime, and temperature stability contribute to determine the most appropriate class of device for each application. Figure 1 illustrates the configurations of standard electrostatic, electrolytic, and double-layer capacitors.
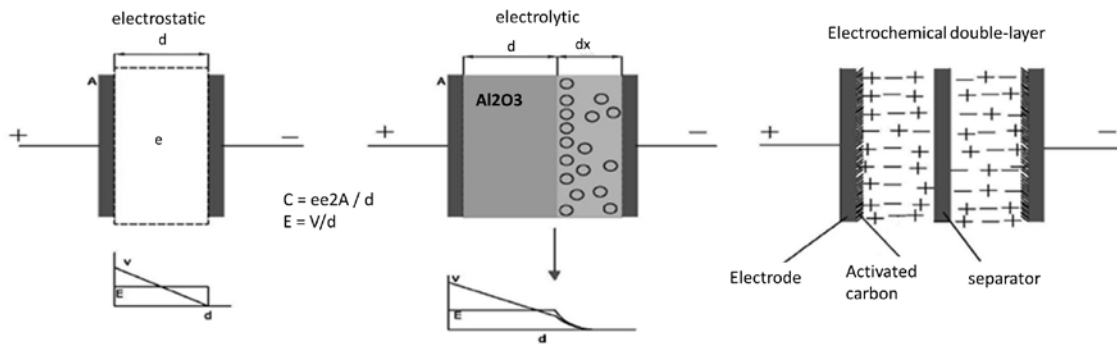
Figure 1.   Diagram of Different Capacitor Configurations (After [11])

1.   Electrolytic Capacitors

Electrolytic capacitors couple a non-conducting dielectric to a layer of electrolyte that acts as one electrode. This configuration improves practical specific capacitance and energy density, but results in other disadvantages. These naturally polarized devices suffer from higher equivalent series resistance, shortened operating life, temperature sensitivity, and can only operate in one polar orientation [12]–[13]. Typically constructed from aluminum or tantalum, electrolytic capacitors use a thin oxide layer on one parallel plate as the dielectric element with an electrolytic spacer acting as an ion conductor to the opposite electrode. The spacer may be soaked in liquid electrolyte, or consist of solid electrolyte material. Using solid organic semiconductive electrolyte, aluminum lead-type electrolytic capacitors can be rated for 2200 µF at 30 V [14]. Composite conducting polymers are also employed as solid electrolyte to improve leakage performance and temperature and frequency characteristics [15].

2. Supercapacitors

Supercapacitors, or electric double-layer capacitors (EDLC), capitalize on high surface area materials employed as electrodes wetted by an ion-conducting electrolyte solution. This configuration provides for two different modes of charge storage, namely double-layer capacitance and pseudocapacitance [16]. As a result, supercapacitors have become commercially viable devices with superior specific capacitance. Continuing research into high surface area carbon structure electrodes and advanced electrolyte chemistries has yielded specific capacitance values of 250 F/g [17] and specific energy of 80 Wh/kg [18]. Further experimental work into electrodes coated with active oxide materials has produced specific capacitance of 600 F/g [19]. Alternative arrangements of three-dimensional structures of $Ba_{0.65}Sr_{0.35}TiO_3$ (BST)/$NiSi_2$/silicon microchannel plates (MCP) have yielded specific capacitance of 792 F/g with low loss over hundreds of cycles [20]. However, the double-layer arrangement suffers from limited operating voltages across individual cells [4]. Studies varying electrolyte composition and electrode material have improved on this parameter, but devices remain limited to less than approximately 4 V [18], [21]. The implementation of electric conducting polymers (ECP) as electrodes also seeks to address the performance issues of supercapacitors at higher voltage [22]–[23]. One possible means to improve operating voltage is to connect multiple cells in series, with the net voltage equal to the sum of the individual cell voltages. However, this results in a net reduction in capacitance because the capacitances of devices connected in series add as inverses. Supercapacitors are also relatively expensive to produce and often require advanced materials processing techniques to fabricate electrodes of high surface area and current capacity.

3. Alternate Configurations

Non-conducting ferroelectric ceramics are the present state of the art in dielectric materials. Barium titanate ($BaTiO_3$) is the best of this class and may have a dielectric constant of the order 10^4 [24]–[26]. However, the dielectric constant has strong dependence on the form, purity, and synthesis of the material and observed values are often significantly lower than the best reported. A novel approach incorporates high-

dielectric constant materials into all-solid-state supercapacitor configurations. $BaTiO_3$ films can be employed as electrolytes with an effective dielectric constant on the order of 2,000, resulting in capacitance of 2 $\mu F/cm^2$ [27]. These materials suffer from high dielectric loss however, and further investigation addresses coating individual particles with low dielectric loss silica glass phases using advanced spark plasma sintering. Dielectric permittivity greater than 10^5 has been reported by this method [28]. In lower cost applications or those requiring greater stability, materials such as paper, glass, or polyethylene may be sufficient with dielectric constants less than 10 [11], [29].

The configuration of supercapacitors is not strictly analogous to electrostatic capacitors, and therefore the concept of an effective dielectric constant in a supercapacitor is not obvious as presented by Equation 2. This is discussed in the theory of volumetric capacitance behavior of supercapacitors [30]. Unlike electrostatic capacitors that demonstrate performance linear with electrode surface area and dielectric constant, supercapacitors tend to behave linearly with electrolyte ionic conductivity [27] and can achieve volumetric capacitance inconsistent with the relationship of Equation 2 [30].

A different configuration employing ceramics with high relative permittivity is the multi-layer ceramic capacitor (MLCC). This technology has been particularly successful in integrated circuit applications by achieving high capacitance and reliability in a small footprint [31]. Additionally, this concept has been adapted for larger energy storage applications but remains commercially unproven [32]–[33].

Another approach to achieving an effective balance of high capacitance and energy density is the development of supercapacitor-battery hybrids. These may include singular devices which employ an EDLC type positive electrode with a lithium ion battery type negative electrode, or a combined system with a supercapacitor bank in parallel with a typical lithium ion battery or similar fuel cell. The former configuration has achieved an energy density of 147 Wh/kg and power density of 150 W/kg, or energy density of 86 Wh/kg and power density of 2587 W/kg [34]. The latter configuration is shown to provide significant improvement in power supply lifetime and pulsed-power performance compared to individual battery or capacitor systems [35].

D.   ADVANCED DIELECTRIC MATERIALS

Material processing to improve dielectric constants presents a rich opportunity for study with the potential to advance the suitability of capacitors as efficient energy storage devices.   One focus area centers on the inclusion of conductive elements in a non-conducting ceramic matrix.   Specific examples include loading nickel particles into $BaTiO_3$ [36] or carbon nanotubes into barium zirconate titanate [37] to improve the bulk dielectric constant compared to the ceramic. Three-phase composites have also been studied, combining $BaTiO_3$ and carbon nanotubes with polymers to achieve dielectric constant on the order of 5,000 with improved stability and loss characteristics [38]. Metals and other conductors theoretically have high relative permittivity, but their utilization in dielectrics is hindered by the propensity to form an electrical shorting path between electrodes.

This behavior is a classic example of percolation theory, which describes the change in bulk parameters of a heterogeneous composite as an additive conducting phase is loaded into a non-conducting matrix phase. As the conducting phase is loaded above a certain volumetric threshold, the bulk composite takes on the conductive properties of the additive as opposed to the matrix.   Once the elements of the conductive phase form a continuous string or cluster with sufficient contact between elements, an electrical or thermal shorting path is created.   This behavior has been studied extensively with a variety of theoretical modeling strategies [39]–[42].

Theoretical models of metal-ceramic composite dielectrics predict increasing bulk relative permittivity up to the percolation threshold, and expect shorting behavior above the threshold. Some theoretical work suggests a singularity at the percolation threshold. It is predicted that dielectric constant will exhibit divergent behavior at the value of maximum loading before the onset of uninterrupted conductivity [43]–[44]. The existing body of work on metal-composite dielectrics does not describe loading fractions far in excess of the percolation threshold for electrical applications. One theoretical treatment proposes a relation for effective dielectric constant of composites of insulating particles with percolative characteristics, namely the dielectric constant of the inclusion is significantly greater than that of the matrix [45]. This theory addresses the full range of

9

volumetric loading and eliminates the singularity at the percolation threshold, but the experimentation addresses only optical properties.

E.   FOCUS OF PRESENT STUDY

The founding theory for this study asserts that the principal characteristic of dielectric materials is that they should be polarizable under the influence of an electric field [46]–[47]. More specifically, the material should permit a redistribution of charge when an external influence is applied, such as the electrical potential from the parallel plates of a capacitor. While dielectric material is fundamentally constrained by the requirement to insulate against shorting, it must be recognized that the most polarizable materials are generally electrical conductors. It follows that consideration of conductive materials as a class of dielectrics suggests potentially significant advantages. Hence, a hypothesis is advanced that a conductive particle with an electrically insulated surface should be a superior dielectric material. The objective of this study was to further validate that construct.

1.   Preceding Investigation

Prior to the study described herein, an investigation was initiated to validate the concept of using insulated metal particles as capacitor dielectrics [48]. Phillips and Scanlan measured the capacitance of various combinations of conductive particles and insulating layers using basic meters. Exceptional dielectric constants were initially observed and shown in Table 2, but the materials proved impractical when examined as dielectrics in basic capacitor configurations. Apparent charge leakage limited operation to only small fractions of a volt. This reveals a key limitation of measuring capacitance with basic meters. Specifically, the method generally uses low amplitude current square wave signals to charge and discharge the capacitor, and is therefore only appropriate at very low voltage and capacitance.

10

Sample	Material /treat	Measured C (thickness)	Dielectric Constant	Measured R /normalized R (1 cm)
1	Barium Titanate Powder	1.01 nF (1.9 mm)	50	600KΩ
2	Barium Titinate, sintered pellet [1]	10 nF	500	Not available
3	Teflon	16 pF (10 mm)	2.3	>10 MΩ
4	Ni/34cc*	15.0 µF	1,200,000^	N/A
5	Ni/34cc*	15.2 µF (3mm)	650,000	65K/215 KΩ
6	Cu/15cc*	0.33µF (1.6mm)	50,000	2K/13KΩ
7	Fe / 34 cc; Double bake**	2.61 µF (1.6 mm)	60,000	6.3K/41KΩ
8	Zn/TEOS	7.2 µF (1.8mm)	84,000	9.5 K/136KΩ
9	Cr/34ccDouble bake	0.10 µF (1.8 mm)	3,000	20 K/277 KΩ
10	Ni/TEOS	65 µF (1.8mm)	~3,200,000	2.7 KΩ/18 KΩ
11	Zn/TEOS	0.6 µF (1.8mm)	18,020	9.0 K/129KΩ
12	VX-72 TEOS	>500 µF (1.6mm)	$>10^6$	1.1K/18 KΩ
13	'Puck' Ni-TEOS/ Wax	>500 µF	$>10^6$	
14	'Puck' V7H TEOS/wax	0.8 µF	55,000	24K/150 KΩ

TABLE I: TABLE I: Reliable MMD Data, from measurement or literature.
Simple tests with standard Agilent capacitance meter yield values consistent with those anticipated for well known dielectrics (Samples 1-3). Remarkably, samples made from MMD materials produced unprecedented dielectric constants (Samples 4-9). Indeed, Barium titanate (Sample 3) is generally considered 'best'. Some values independently verified at Los Alamos National Lab. 'Pucks' made with MMD particles sealed in wax (see Text) were further tested for time constant directly by measuring discharge through a known resistance.

[1] Derived from dimensional values provided in recommended literature.
* 20 gms of metal (all metals Sigma Aldrich, reported better than >98% purity, and mean size 5-10 µ) powder, slowly mixed with noted number of cc of 20% hydrogen peroxide, then baked in air at 100 C for approximately 10 hours.
** Same procedure as *, but done in two steps, each step using half the hydrogen peroxide listed.
^ Independent measurement by Los Alamos National Lab team.

Table 2.   Multi-Material Dielectric Data Observed in Preceding Investigation. From [48].

To mitigate charge leakage, a two-layer system was developed. An electrolyte layer was added to one electrode with a second layer of insulated metal particles loaded into melted wax. The polarized orientation prevents net flow of charge through the capacitor. The geometry of the resulting electrolytic capacitor is depicted in Figure 2. The electrolyte layer consisted of a high surface area acid (HSA) powder, namely boric acid solution in high surface area alumina powder. This configuration was successful in

arresting leakage current, and demonstrated exceptional capacitance with dielectric constant greater than 10^6 at voltages less than 3 V.
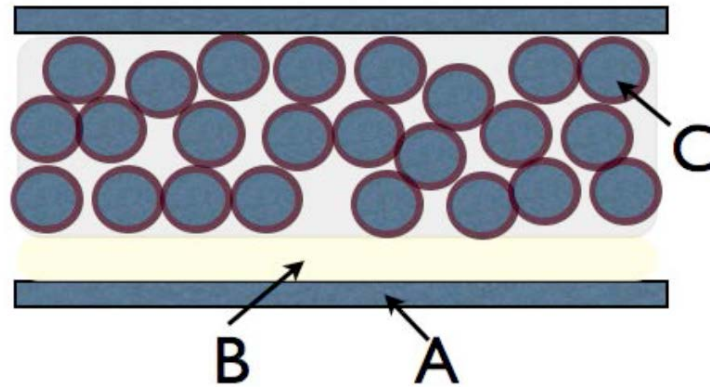
Figure 2.   Predecessor Composite Capacitor in Electrolytic Configuration with (A) aluminum electrodes, (B) HSA electrolyte, and (C) insulated conductor particles in wax. From [48].

Careful control studies were undertaken to gain insight into the mechanism of this remarkable capacitance. An unanticipated result of these tests was exceptional natural capacitance of the electrolyte, independent of the primary dielectric layer. The dielectric constant is observed to be on the order of 10^8 at approximately 0.7 V. There is no known theory to describe this result, specifically that a simple electrolyte consisting of high surface area powder wetted with acid solution should have unprecedented relative permittivity.

2.   Present Objective

In this work, further examination of MMD characteristics was conducted on a particular variant. One example of insulated metal particles derived from the previous work was employed. Micron-scale nickel powder is treated with H_2O_2 to create an insulating oxide layer, and is loaded into a matrix of electrolyte material to form an electrostatic capacitor dielectric. This geometry is termed a composite electrolyte dielectric (CED).

A similar concept is reported using nano-sized silver particles coated in alumina and doped in polyimide to form composite thin films, achieving a dielectric constant of greater than 25 in that configuration [49]. Rather than use nano-sized particles for thin film applications, this study seeks to employ the resulting composite with exceptional dielectric constant for capacitive energy storage.

The effect on dielectric constant is studied as metal particles are incrementally loaded, including in excess of percolation limits. Loading of metal particles into the dielectric matrix aims to improve capacitance and energy density of an electrostatic capacitor. The general CED capacitor geometry is depicted in Figure 3. Pieces of Grafoil, a carbon-based foil sheet material, is used as a convenient purely conductive platform to deposit the dielectric material for electrical testing between external aluminum electrodes.
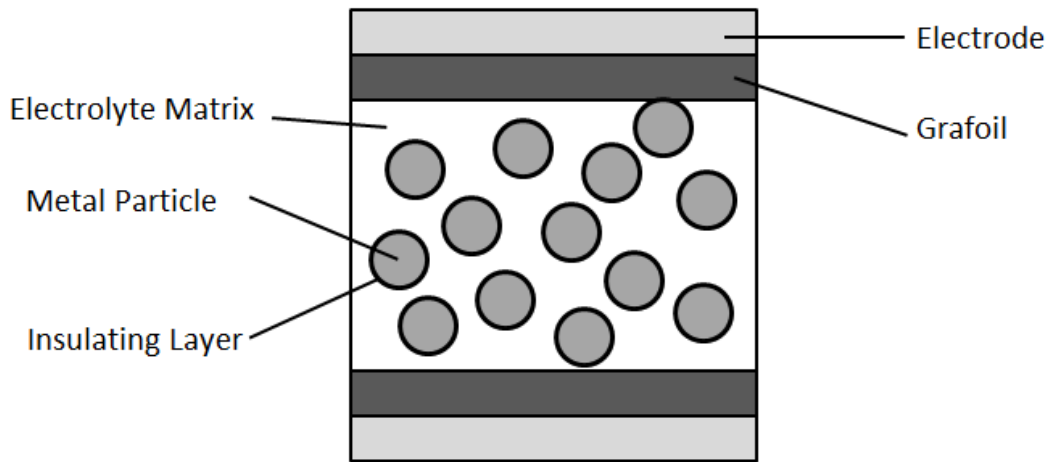
Figure 3.   Diagram of CED Capacitor Geometry

THIS PAGE INTENTIONALLY LEFT BLANK

II.   EXPERIMENTAL METHODS

A.   EXPERIMENTAL SETUP

Standard multimeters generally have a capacitance setting and are nominally able to measure the capacitance of standard circuit elements. Typically, this is accomplished using high frequency square wave signals at very low voltage in order to measure capacitance on the order of nano- or picofarads. This measurement does not provide a complete understanding of the capacitive behavior of a material. To more completely understand dielectric material properties, charge and discharge kinetics must be investigated. This is particularly true for novel materials with very high capacitance.

To measure capacitance generically, a device is connected in parallel with a DC voltage source and a resistor in a standard resistor/capacitor (RC) discharge circuit as shown in Figure 4.
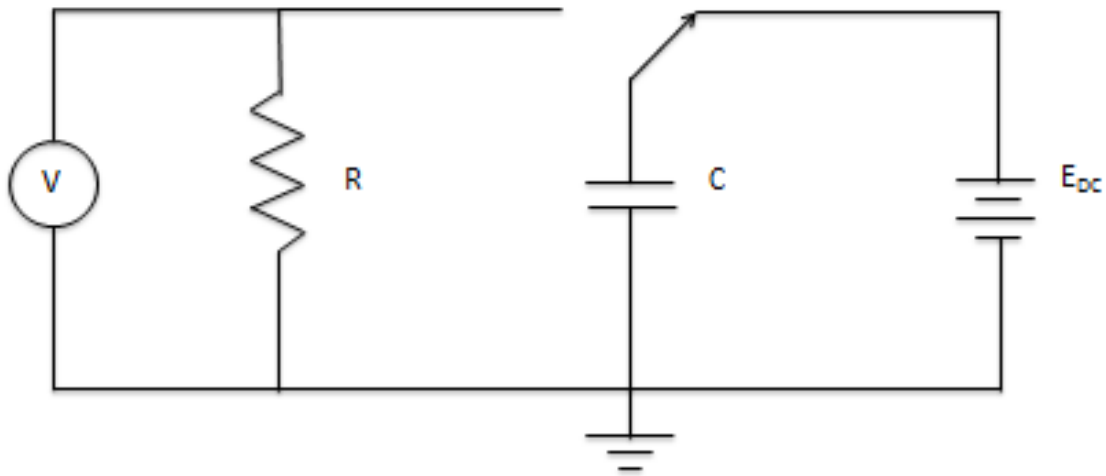
Figure 4.   Diagram of Experimental Discharge Circuit

A DC voltage bias is applied to charge the capacitor for a defined time interval, then the switch is repositioned and the capacitor discharges through the load resistor [50]. Voltage drop across the circuit is measured by a voltmeter connected in parallel. The voltage drop in a RC circuit during discharge is expressed as

$$V(t) = V_0 e^{\frac{-t}{RC}}.$$ Equation 4

It follows from Equation4 that a plot of $\ln(V/V_0)$ vs. t has slope (-1/RC). Given the value of the discharge resistor and the capacitor geometry, the dielectric constant can be calculated according to Equation 2. Figure 5 is an example of a characteristic discharge plot from an experiment conducted with the circuit depicted in Figure 4 using a commercial 100 µF capacitor. The capacitor is shown in Figure 6. Using a multimeter, the capacitance of the commercial capacitor was measured as 109 µF.
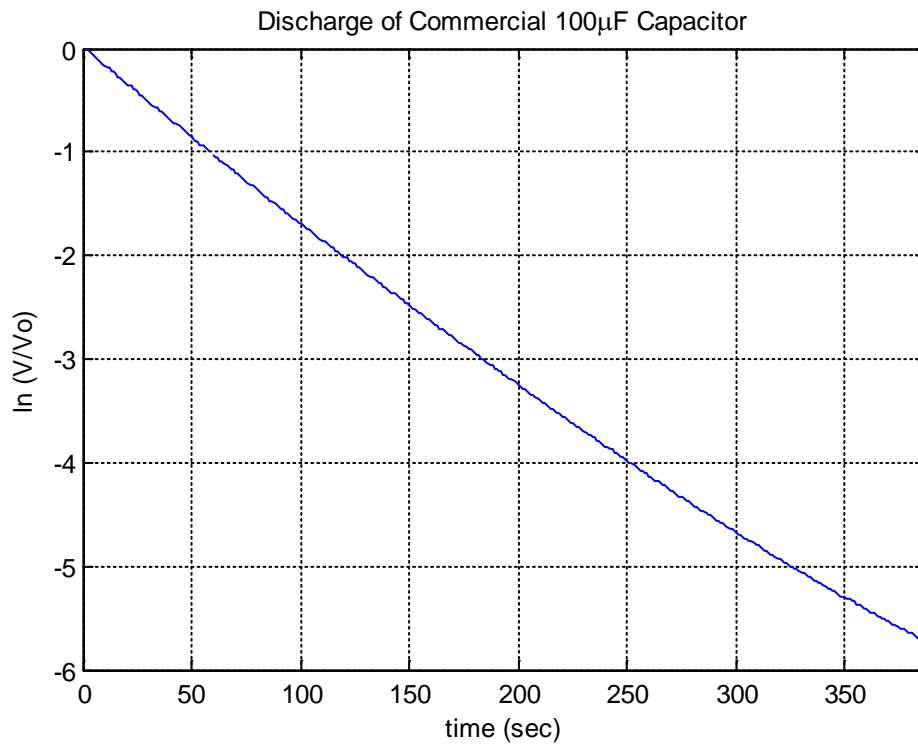
Figure 5.   Commercial Capacitor Example Discharge Characteristic Plot

16
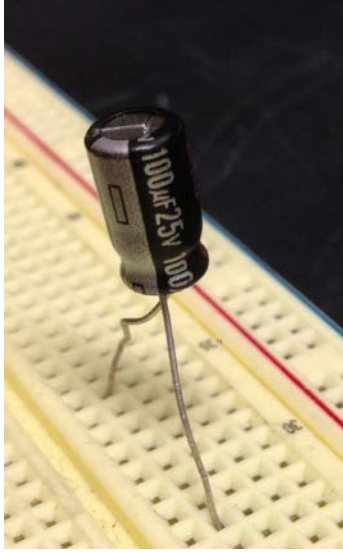
Figure 6.   Commercial Capacitor

The constant slope of the discharge characteristic is indicative of constant capacitance over the entire range of voltage during the discharge. The vertical axis represents a logarithmic display of the ratio of measured voltage to initial voltage. As a result, actual voltage is not strictly represented on the plot. A flatter slope indicates a slower discharge, and therefore higher capacitance. Figure 7 is an example discharge plot of an aforementioned electrolyte layer without addition of metal particles.
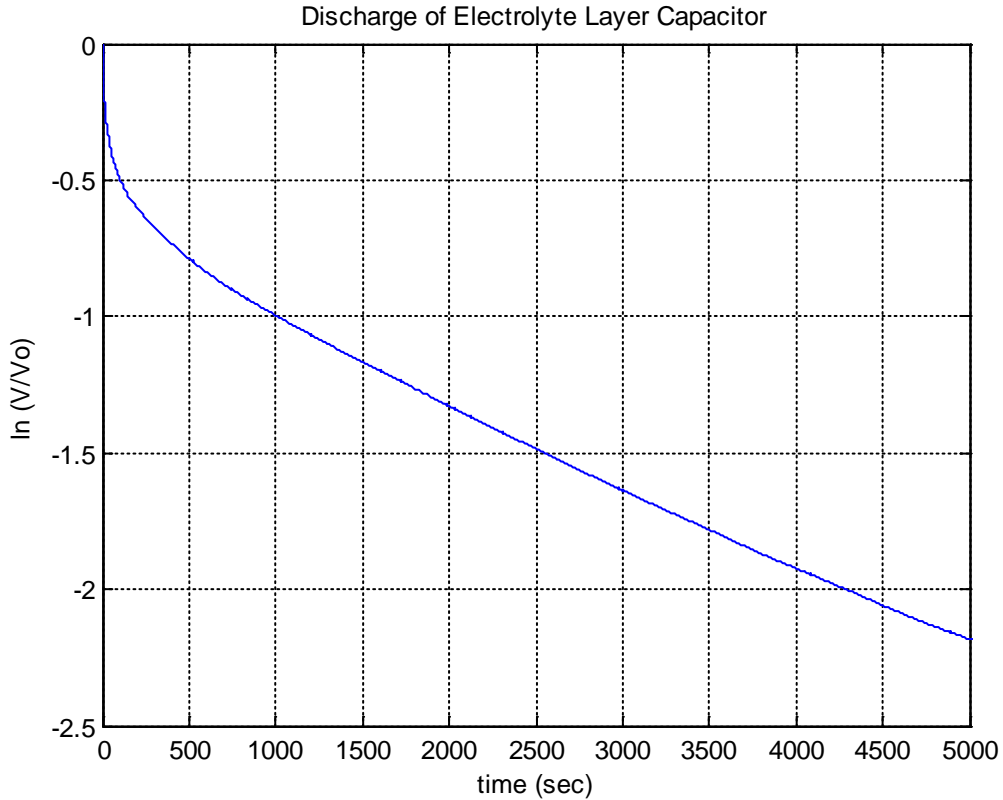
Figure 7.   Electrolyte Capacitor Example Discharge Characteristic Plot

The initial drop in discharge voltage is non-linear on the log plot, and unremarkable in terms of capacitance. The subsequent linear region better represents a constant capacitance at lower voltage, and its slope is the characteristic parameter measured in this study.

B.   EXPERIMENTAL PROCESS

To arrive at an optimal capacitor configuration incorporating the insulated composite dielectric material, a series of experiments was conducted for the first phase of this study. Subsequent experiments were designed to validate the capacitive behavior of the CED configuration. This validation was accomplished by performing repeated charge and discharge cycles using a modified test circuit shown in Figure 8. This modified circuit configuration allows monitoring of the capacitor voltage during charge and discharge through repeated cycles. The charge characteristics are determined using

18

Error! Reference source not found., which defines the voltage of the capacitor during charge. This calculation is analogous to the determination of discharge characteristics from Equation 4.

$$V(t) = V_0(1 - e^{\frac{-t}{RC}})$$ Equation 5
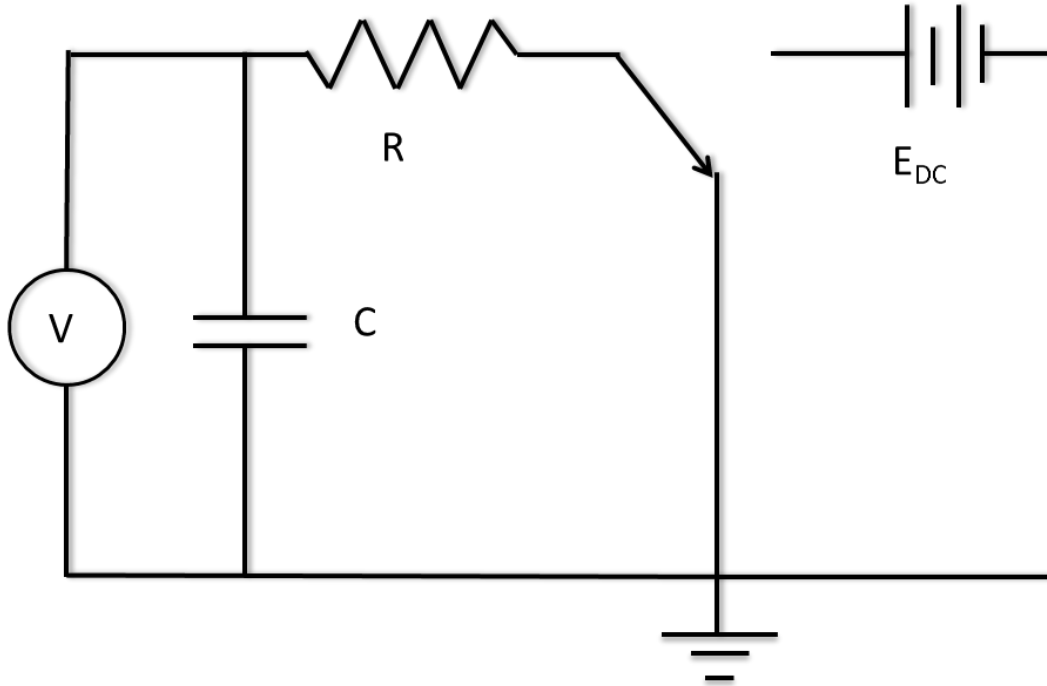
Figure 8.   Diagram of Experimental Charge/Discharge Circuit

1.   Variables and Controls

Variables examined in the first phase of study include dielectric layer thickness, metal particle volumetric loading, and degree of metal particle treatment. Initial control variables include electrolyte matrix composition, capacitor geometry, metal particle treatment process, charge time and voltage, and load resistance. Some variables, such as charge time and load resistance, have been previously investigated leading up to this study. Initial results generally failed to yield definitive impact on performance, and therefore these variables were established as controls for independent optimization

portions of this investigation. Specifically, convenient values were selected for charge voltage, charge time, and load resistance for each series of independent tests.

The impact of load resistance, and therefore current draw and supply, was re-examined in the verification phase of testing. Additional adjustments to the dielectric composition were also explored in the later testing phase to further examine how the impact of metal particle loading is related to the presence of the other composite constituents.

2. Materials and Equipment

The materials employed in this study consist of aluminum oxide powder (Alfa Aesar, γ-phase, 99.97%, 3 micron APS Powder, S.A. 80-120 m^2/g, CAS 1344-28-1), boric acid powder (BDH, 99.5% H_3BO_3, CAS 10043-35-3), nickel powder (Alfa Aesar, -100 mesh, 99+%, CAS 7440-02-0), and H_2O_2 (Sigma-Aldrich, 30 wt% in H_2O, CAS 7722-84-1). The primary test platform was a National Instruments ELVIS II electronics prototyping board implemented with LabView 2011 software. An additional multimeter, Agilent U1252A, was used for independent parameter verification. Capacitors were constructed for testing in a custom test jig consisting of two aluminum electrodes fitted into a plastic cylindrical containment, depicted in Figure 9. The test jig diameter is 5.042 cm, or approximately two inches. Based on this cross-sectional area, approximately 4 mL of material produces a dielectric thickness of approximately 2 mm when placed in the jig for testing.

Figure 9. Capacitor Test Jig

Disks of Grafoil, a conductive graphite-based foil similar to products provided by GrafTech International Ltd., were cut from sheet and used as a platform to deposit the dielectric material. This additionally helps to ensure effective electrical contact in the test jig, as illustrated in Figure 3. The Grafoil sheet is approximately 0.76 mm in thickness and is portrayed in Figure 10.

Figure 10.   Grafoil Sheet and Cut Disk

To control the pressure applied to the dielectric during capacitor testing, 250 g of weight was placed on top of the capacitor test jig. This was achieved with a fabricated stainless steel collar and flask filled with water placed on the top electrode. The arrangement is shown in Figure 11.

Figure 11.   Capacitor Test Jig Weight Arrangement

3.   Dielectric Composition

a.   *High Surface Area Acid (HSA) Electrolyte*

The HSA electrolyte is composed of a mixture of alumina and boric acid powders in a ten to one ratio by weight. Dry powders are combined by hand to produce a homogenous mixture. A sufficient amount of distilled water was added to achieve a pasty consistency. The desired consistency was derived from the need for the dielectric material to be workable or spreadable, but not too soft to support a structurally stable capacitor in the test jig. This balance was achieved with one milliliter of water for each gram of alumina in the HSA electrolyte mixture. The mixture was combined manually with a small laboratory spatula for deposition on Grafoil disks. The dielectric material was spread evenly to achieve complete coverage of the Grafoil disk with a layer of uniform thickness.   This HSA electrolyte matrix composition was maintained as a standard through the first phase of experimentation. The preparation process is shown in Figure 12.

Figure 12.   HSA Electrolyte Capacitor Preparation Process

b.   *Metal Particle Surface Treatment*

To generate the insulating surface layer on the nickel particles, the metal powder is thoroughly wetted with H_2O_2. The relative amounts are not required to be specific, as the powder is soaked with excess liquid just to the point of standing liquid over the powder in a beaker. Approximately 50 g of nickel is wetted with approximately 15 mL of H_2O_2 in a 150 mL beaker and swirled for uniform mixing. The wetted powder is illustrated in Figure 13.

Figure 13. Nickel Powder wetted with H_2O_2

The liquid was allowed to evaporate off at room temperature until the powder was completely dried. After approximately 24 hours, the powder was manually stirred to aid in drying. Complete dryout is generally achieved in 48 to 72 hours with intermittent stirring every 24 hours. The treated powder is shown in Figure 14, before and after stirring and completely dried. No change in mass is noted after completion of a treatment process. This process comprises one surface treatment, and was repeated to achieve the required number of treatments.

Figure 14.   Nickel Powder Surface Treatment Drying Process

To verify the effect of the surface treatment process, resistance checks were performed on beds of untreated and treated powders. A voltage divider circuit was established according to Figure 15, and the capacitor test jig filled with 4 mL of nickel powder to form a 2 mm thick bed. A DC voltage bias was applied, and the resistance of the powder bed measured. The resistance of the powder was checked in series with a 99.2 kΩ resistor with DC voltages from 0 V to 4 V in increments of 0.5 V.
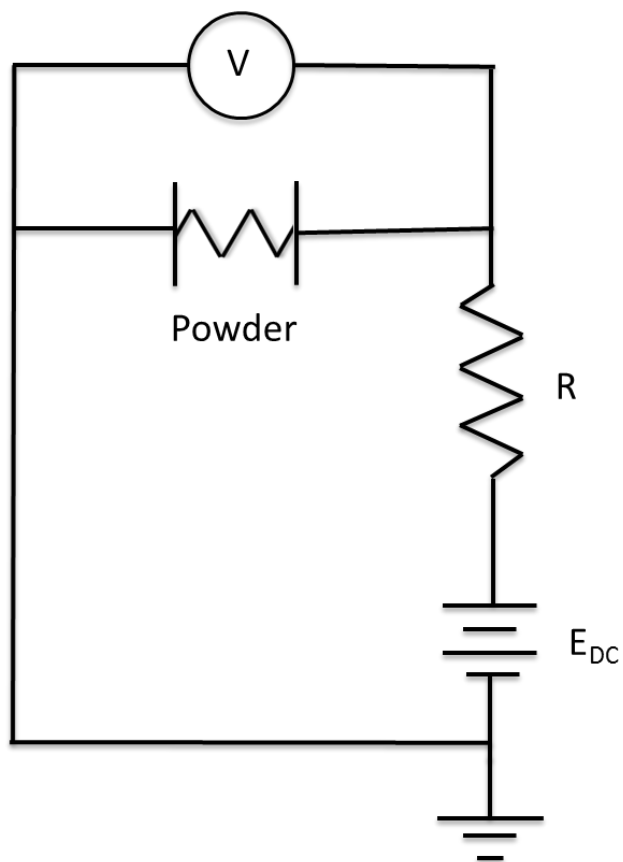
Figure 15.   Diagram of Voltage Divider Circuit

The powder was also examined using scanning electron microscopy (SEM) with energy dispersive X- ray spectroscopy (EDS) and X-ray diffraction (XRD). These characterization methods are used in addition to electrical testing to ascertain the effect of the H_2O_2 treatment process on the nickel powder. The results of these analyses are presented in Chapter IV.

c.   Composite Dielectric Construction

To create the CED dielectric, treated or untreated nickel powder was added to the dry powder HSA mixture. Again, dry powders are combined by hand to create a homogenous mixture before adding distilled water to achieve the desired consistency for spreading. The amount of water added varied according to nickel loading, and was primarily determined by trial and error. Higher nickel loadings require more water to achieve the desired consistency for sufficient workability. Volumetric

loading of nickel into HSA is varied to observe the influence of the percolation threshold on dielectric performance. The composite dielectric preparation process is shown in Figure 16.

Figure 16.   Composite Dielectric Capacitor Preparation Process

4.   Design of Experiments

A methodology was employed to sequentially optimize individual factors. The resulting best configuration from each test series was used as the control for the follow-on series, so that only one factor was varied in each series. This approach initially presumes that the factors of thickness, surface treatment, and metal particle loading are primarily independent. This is likely not the case and alternative compositions must be revisited based on the results of this analysis. All tests were conducted using the discharge circuit shown in Figure 4.

a.   *Thickness*

The first series of tests addressed the thickness of the dielectric, using the HSA electrolyte as the control composition. Four thicknesses were tested based on

convenient workable quantities. Capacitors were charged for 16 minutes at 6 V and discharged through a load resistor of 528 kΩ. For subsequent tests, the charging voltage and resistance are reduced based on observed operating voltage and to limit test run times.

b.   *Loading with Untreated Nickel*

The next series of tests was designed to find the best volumetric loading using untreated nickel powder. This loading level with the highest dielectric constant was used as the control during the next test series to determine the best level of metal particle surface treatment. This test also demonstrated the observed percolation threshold for this configuration of nickel powder loaded into HSA electrolyte matrix. Untreated nickel powder was loaded volumetrically in increments of 10% until the impact of percolation was verified, and 5% increments to find the maximum dielectric constant achievable before the onset of percolation. Capacitors were charged for 16 min at 4 V and discharged through a resistor of 99.2 kΩ.

c.   *Treatments at Best Loading*

The next series of tests uses the best volumetric loading determined in the previous test series to determine the best number of metal particle surface treatments. Nickel powder was treated with H_2O_2 as described previously, and powders of increasing treatments were used to create CED capacitors for testing. Treatments increased until a drop-off in performance was observed with increasing treatment. Capacitors were charged for 16 minutes at 4 V and discharged through a resistor of 99.2 kΩ.

d.   *Loading with Treated Nickel*

The final test series revisits volumetric loading using the treatment level resulting from the previous series. Treated nickel powder was loaded volumetrically in 10% increments until performance deteriorated. Capacitors were charged for 16 minutes at 4 V and discharged through a resistor of 99.2 kΩ.

5. Verification of Capacitor Behavior

After determination of the best composite capacitor configuration by using RC circuit discharge tests, the resulting product must be verified to behave like a capacitor. Specifically, the component should be subjected to charge and discharge cycles to verify consistency and characteristics. This was accomplished using the charge and discharge circuit shown in Figure 8. Capacitors were charged with 4 V and cycled with a 99.2 kΩ resistor.

Additionally, smaller load resistances should be used to verify the capability to deliver power quickly, a key attribute of capacitors compared to batteries. This is accomplished by performing charge and discharge cycles through resistors of 20.2 kΩ and 2.67 kΩ. Capacitors are charged with 4 V.

6. Revisited Parameters and Alternate Compositions

Upon selecting and verifying a CED configuration, additional parameters were revisited. The influence of dielectric thickness is reevaluated using the composite dielectric structure. The influence of charging voltage is also considered, as informed by the results of previous tests.

Because variables were treated independently, many possible combinations of number of treatments and volume loadings were not tested. Additionally, using dielectric constant as the parameter for optimization neglects other important factors. Operating voltage is a key performance aspect, and was considered alongside dielectric constant when selecting the best configuration. However, the stability of the individual responses should also be addressed. Characteristic charge and discharge curves showed a high degree of variability in capacitance over the operating voltage range. An alternate compositions was examined for the impact on response stability and voltage. Specifically, a CED capacitor is produced using potassium hydroxide (KOH) as the aqueous electrolyte instead of boric acid.

29

THIS PAGE INTENTIONALLY LEFT BLANK

III.   RESULTS

A.   COMPOSITE DIELECTRIC OPTIMIZATION

1.   Thickness

This test series was designed to determine empirically if the dielectric constant is a function of the thickness of the dielectric. In this first test series, capacitors without any nickel were charged for 16 minutes at 6 V and discharged through a load resistor of 528 kΩ. The specific parameters of the tested capacitors are shown in Table 3, and the discharge characteristic curves are shown in Figure 17. The operating voltage is taken as the maximum voltage at which the device begins to exhibit constant capacitance. This series was also valuable in establishing the impact of nickel particle loading on dielectric performance.

Composition	Dielectric Thickness (*d*)	Initial Discharge Voltage (V_0)	Dielectric Constant (ε_R)	Operating Voltage
3 g alumina 0.3 g boric acid 3 mL H_2O	1.47 mm	2.20 V	1.81E9	0.7 V
4 g alumina 0.4 g boric acid 4 mL H_2O	2.46 mm	2.16 V	5.78E8	0.8 V
5 g alumina 0.5 g boric acid 5 mL H_2O	2.87 mm	1.85 V	4.44E8	0.9 V
8 g alumina 0.8 g boric acid 8 mL H_2O	4.13 mm	2.18 V	4.43E8	0.8 V

Table 3.   Electrolyte Dielectric Thickness Test Data
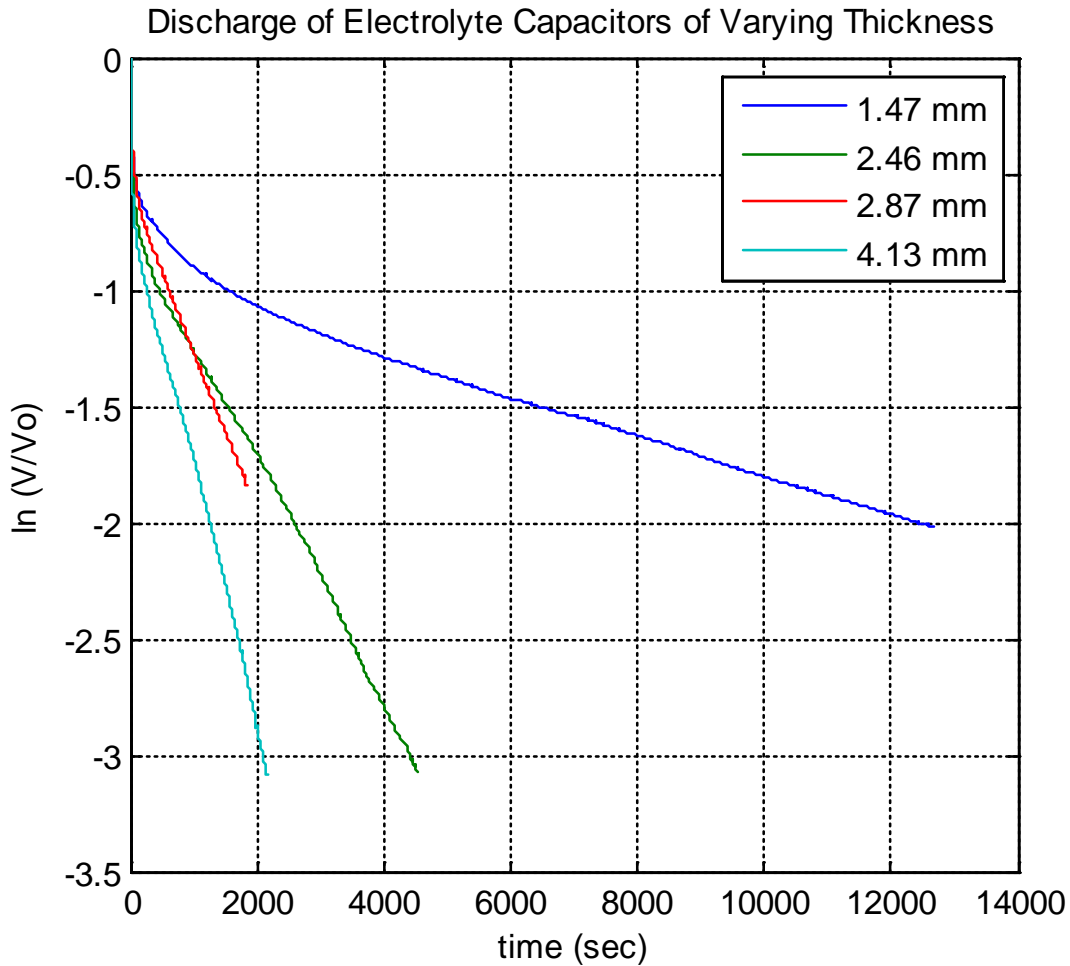
Figure 17.   Discharge of Electrolyte Capacitors of Varying Thickness

This test series suggests that thickness is a factor in determining the dielectric constant.   The thinnest dielectric resulted in a factor of two improvement in dielectric constant over the next thinnest.   However, the physical constraints of constructing the capacitors also influence the optimal layer thickness.   In order to ensure a dielectric layer of reasonably uniform thickness and complete coverage of the Grafoil disk, the minimum thickness produced in this test series is not consistently achievable.   This is particularly true after introducing metal particles for the composite construction.   The outcome of this test series informs follow on experiments in that it suggests the thinnest achievable layer is preferred.

2.   Loading with Untreated Nickel

This test series was designed to establish a percolation threshold for loading of untreated nickel powder into the electrolyte dielectric matrix. It was hypothesized, based on the previously discussed theory, that at some loading in excess of this threshold, the individual metal particles should form a continuous chain from one electrode to the other. This circumstance should be evidenced by a precipitous drop-off in capacitive performance. Additionally, this test series will establish the preferred volume loading to be held constant when analyzing different surface treatment levels.   The specific parameters of the tested capacitors are shown in Table 4, and the discharge characteristic curves are shown in Figure 18.

In the preceding tests of this study, as well as many investigative and familiarization tests, the maximum voltage observed across the capacitor did not exceed 3 V. Therefore, the charging voltage was reduced from 6 V to 4 V for the remainder of tests. Also, based on the very high capacitances, and consequently long test run times, the load resistance was reduced from 528 kΩ to 99.2 kΩ.

Nickel Volume Loading	Composition	Dielectric Thickness (d)	Initial Discharge Voltage (V_0)	Dielectric Constant (ε_R)	Operating Voltage
10%	13.5 mL alumina (2.8 g) 0.28 g boric acid 1.5 mL nickel 3.5 mL H_2O	2.01 mm	1.81 V	6.01E8	1.19 V
20%	12 mL alumina (2.4 g) 0.24 g boric acid 3 mL nickel 3.5 mL H_2O	1.93 mm	1.75 V	5.34E9	1.17 V
25%	11.25 mL alumina (2.2 g) 0.22 g boric acid 3.75 mL nickel 3.5 mL H_2O	1.88 mm	1.69 V	5.25E9	1.15 V
30%	10.5 mL alumina (2.2 g) 0.22 g boric acid 4.5 mL nickel 3.5 mL H_2O	2.06 mm	0.91 V	2.04E8	0.55 V
40%	9 mL alumina (1.8 g) 0.18 g boric acid 6 mL nickel 3.5 mL H_2O	1.91 mm	0.70 V	8.23E6	0.70 V

Table 4.   Untreated Nickel Composite Dielectric Volumetric Loading Test Data
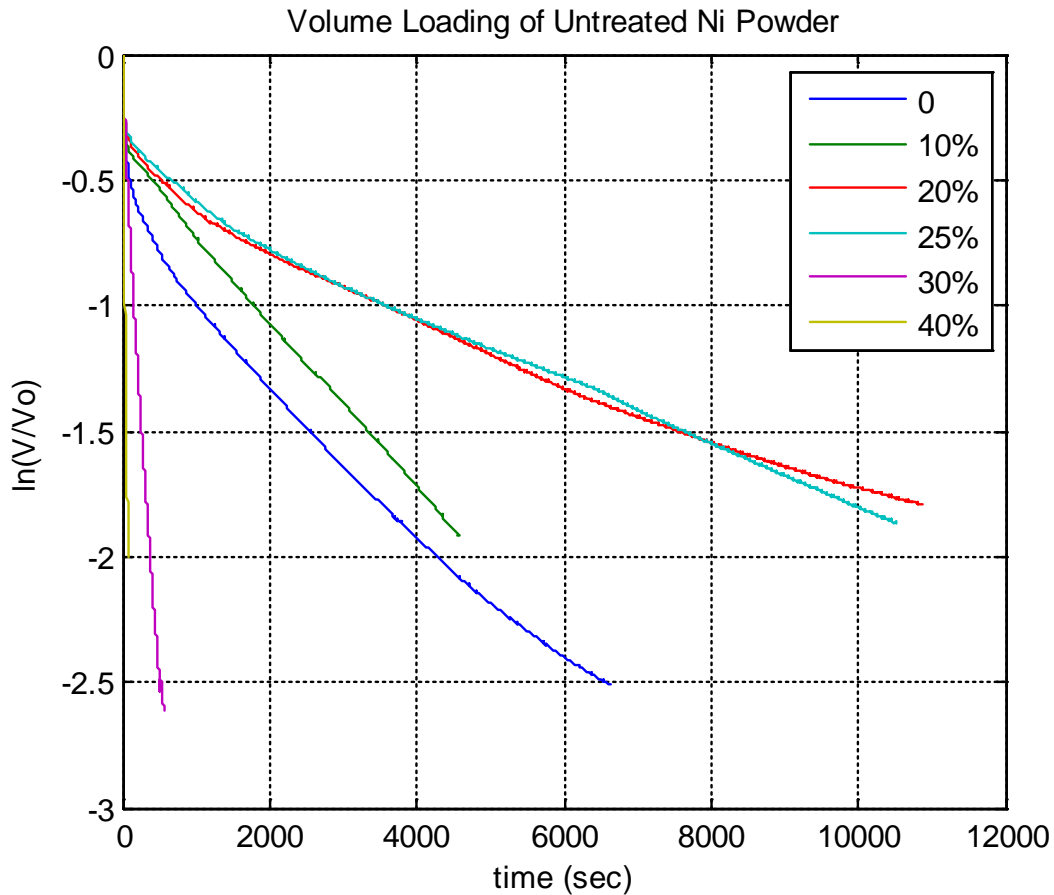
Figure 18. Discharge of CED Capacitors with Varying Untreated Nickel Loading

The discharge characteristics show the influence of the percolation threshold at loading of 30% or higher. While the observed dielectric constant seems to remain very high, the initial discharge voltage was less than 1 V. As a result, the operating voltage for constant capacitance is very low and this result is not considered significant. Seeking to further define the volume loading associated with percolative behavior, a 25% volume load test is conducted. This test also showed stable performance, comparable to the 20% volume load. However, the 20% volume load did exhibit slightly higher voltage, and the constituent volumes are more convenient to measure. Consequently, 20% volume load is established as the control loading for the surface treatment test series.

3. Metal Particle Surface Treatment

This test series is designed to determine the preferred number of surface treatments for nickel powder embedded in the HSA matrix. All capacitors were produced with 20% volume loading of treated or untreated nickel powder. The composition was constant, consisting of:

- 12 mL alumina (2.5 g)
- 0.25 g boric acid
- 3 mL untreated or treated nickel powder
- 3.5 mL H_2O.

The specific parameters of the tested capacitors are shown in Table 5, and the discharge characteristic curves are shown in Figure 19.

Surface Treatments	Dielectric Thickness (d)	Initial Discharge Voltage (V_0)	Dielectric Constant (ε_R)	Operating Voltage
0	1.93 mm	1.75 V	5.34E9	1.17 V
1	1.85 mm	1.90 V	5.26E9	1.17 V
2	2.29 mm	1.82 V	1.16E10	1.30 V
3	2.21 mm	1.87 V	5.20E9	1.25 V
4	2.77 mm	1.82 V	6.80E9	1.21 V

Table 5.   Varying Surface Treatments with 20% Volume Nickel Load Test Data
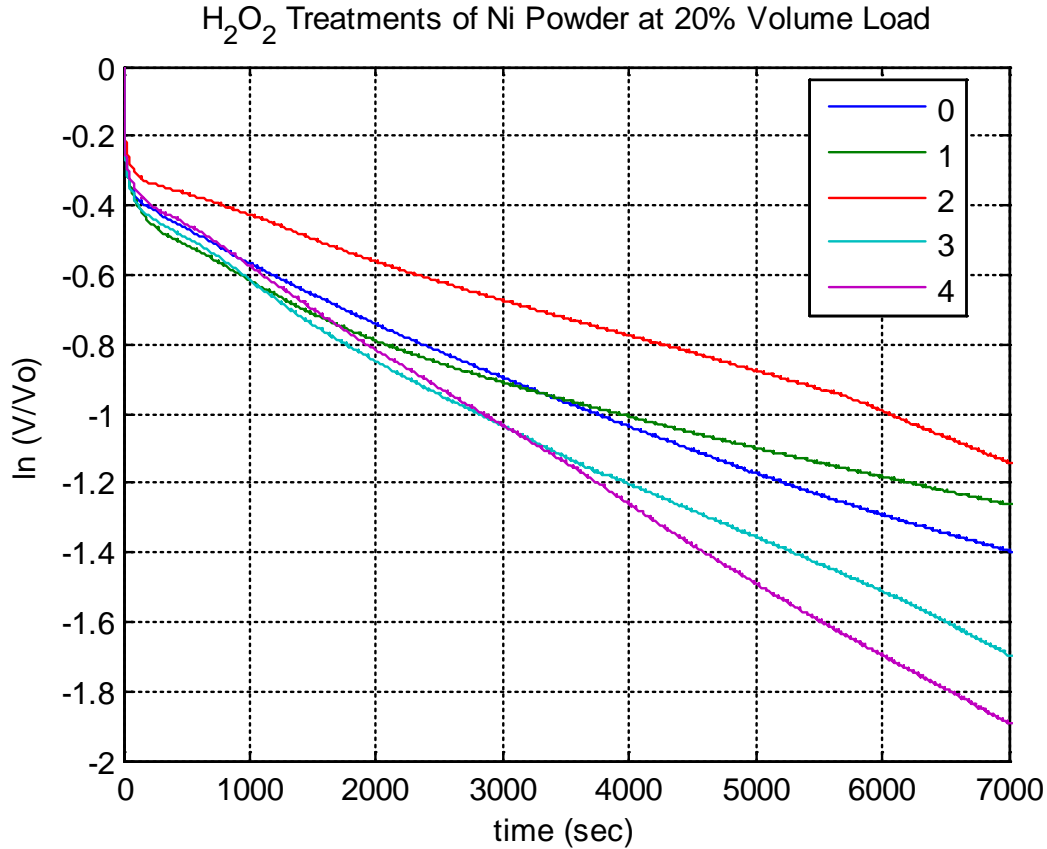
Figure 19. Discharge of CED Capacitors with Varying Treatments of Nickel Powder at 20% Volume Load

This test series showed that at 20% volume load, a range of treatments produced a reasonably consistent response. The capacitor using nickel powder subjected to two treatments was the only example of notably superior performance. Specifically, it showed the highest operating voltage, and the only observed instance of dielectric constant greater than 10^{10}. The discharge characteristic is also remarkably stable for greater than 5,000 seconds. The result is a capacitance of 89.5 mF at 1.30 V in a volume of 4.57 cm^3. Based on this dielectric constant, thickness, and operating voltage, the energy density is 0.017 J/cm^3.

4. Loading with Treated Nickel

This test series is designed to determine if treated nickel can be loaded in higher volume fractions than untreated nickel and produce a superior dielectric constant. All

capacitors were constructed with nickel powder subjected to two H_2O_2 surface treatments. The specific parameters of the tested capacitors are shown in Table 6, and the discharge characteristic curves are shown in Figure 20.

Nickel Volume Loading	Composition	Dielectric Thickness (d)	Initial Discharge Voltage (V_0)	Dielectric Constant (ε_R)	Operating Voltage
10%	13.5 mL alumina (2.8 g) 0.28 g boric acid 1.5 mL treated nickel 3.5 mL H_2O	1.88 mm	1.78 V	2.25E9	1.16 V
20%	12 mL alumina (2.5 g) 0.25 g boric acid 3 mL treated nickel 3.5 mL H_2O	2.29 mm	1.82 V	1.16E10	1.30 V
30%	10.5 mL alumina (2.2 g) 0.22 g boric acid 4.5 mL treated nickel 3.5 mL H_2O	2.26 mm	1.72 V	5.27E9	1.25 V
40%	9 mL alumina (1.8 g) 0.18 g boric acid 6 mL treated nickel 4 mL H_2O	2.21 mm	1.75 V	7.86E9	1.26 V
50%	7.5 mL alumina (1.7 g) 0.17 g boric acid 7.5 mL treated nickel 4.3 mL H_2O	2.11 mm	0.64 V	(No measurable result)	

Table 6.   Twice Treated Nickel Composite Dielectric Volumetric Loading Test Data
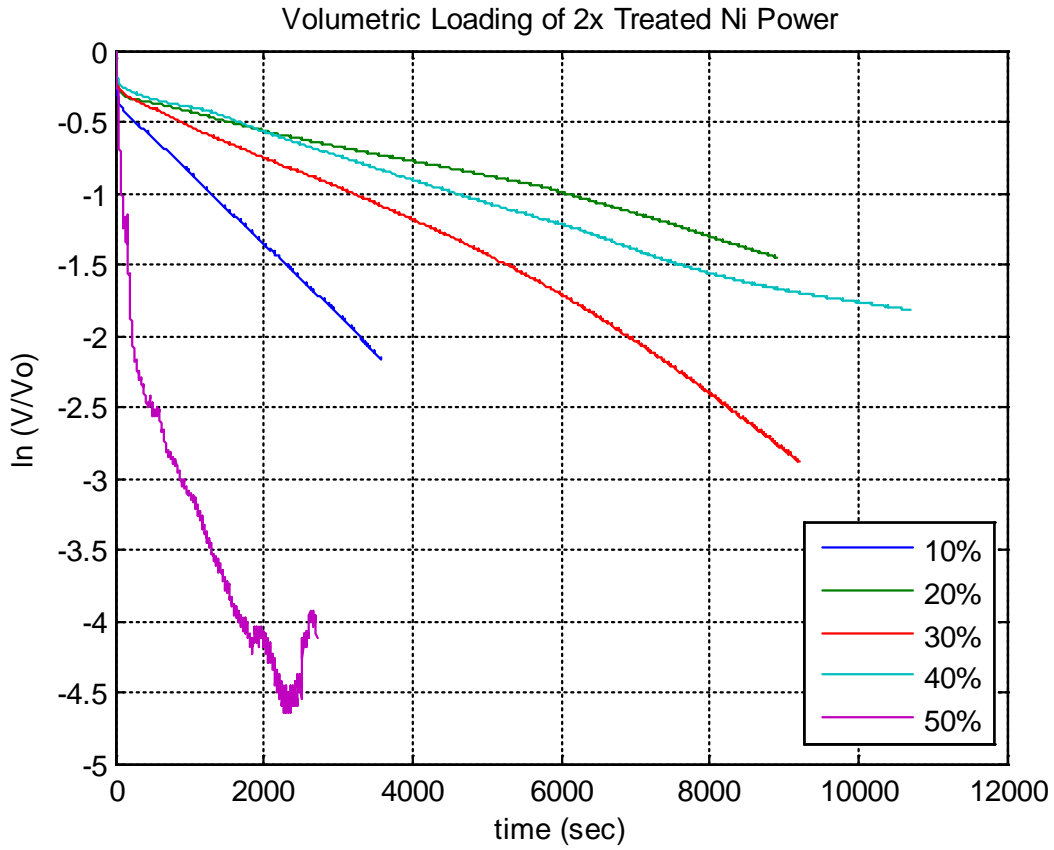
Figure 20.   Discharge of CED Capacitors with Varying 2x Treated Nickel Loading

The result of this test series showed that nickel subjected to surface treatment can in fact be loaded in excess of the previously demonstrated percolation threshold with no observed drop in performance. The capacitor with 40% nickel load demonstrated a particularly high capacitance, close to that observed with the best 20% nickel load capacitor. As shown in the rescaled plot of Figure 21, the 40% load capacitor actually performs comparably to the 20% load capacitor for approximately 1500 seconds. The dielectric constant over this limited initial linear portion of the discharge is 1.11E10 at 1.25 V. It is also clear that the initial operating voltage for capacitors constructed with treated nickel particles does not decrease at higher volume loadings. This is in contrast to observations from capacitors constructed with untreated nickel.
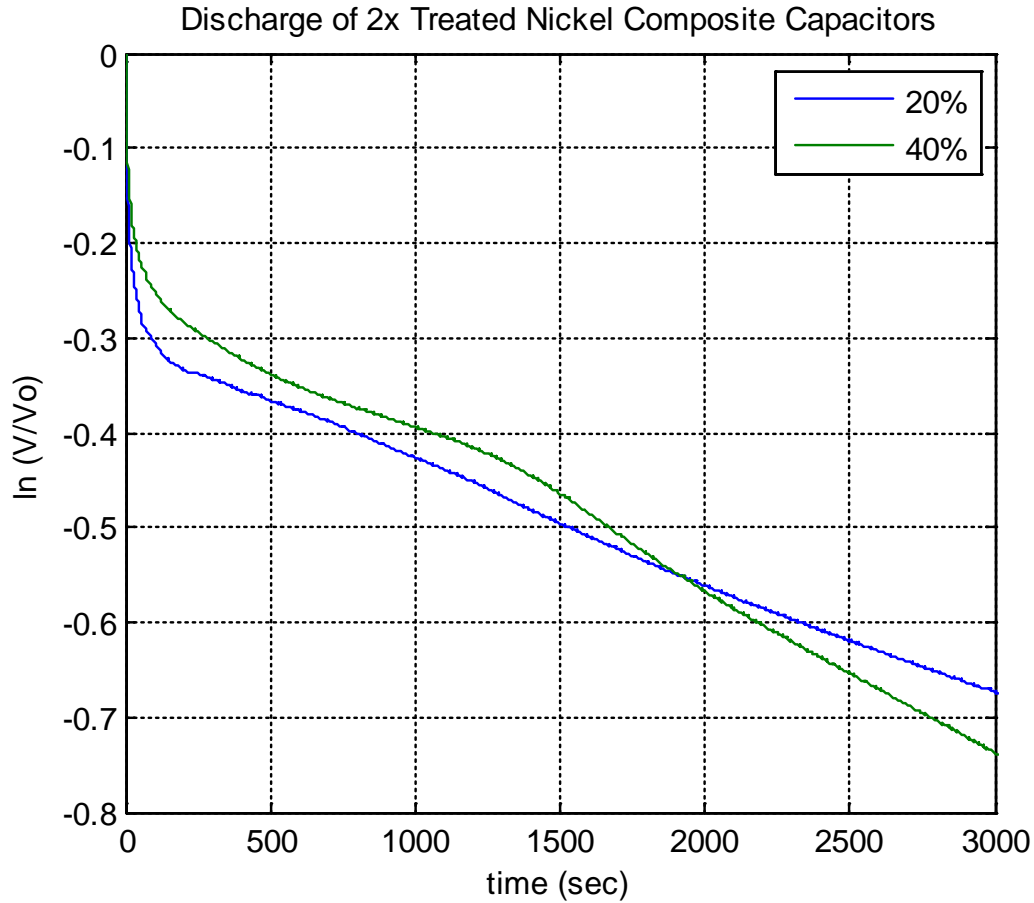
Figure 21.   Discharge Characteristic Curves for 20% and 40% Volume Load with 2x
Treated Nickel

While this shows remarkable performance of a CED capacitor loaded with treated nickel above the previous threshold limit, the 20% loaded capacitor is the configuration with the best and most stable performance. Hence, this configuration was selected as the subject for verification of capacitive behavior in follow on testing. In support of this selection, the dielectric constant, voltage, and thickness results are accounted for by calculating the energy density for each discharge test. Energy density, E_C/Vol, is determined by combining Equations 2 and 3 with the definition of cylindrical volume according to Equation 6.

$$\frac{E_C}{Vol} = \frac{\varepsilon_0 \varepsilon_R V^2}{2d^2}$$ Equation 6

The observed energy density associated with each discharge test is shown in Figure 22. Previously unmentioned duplicate test results are also shown in the Figure and can be reviewed in the Appendix. It can be seen that the 20% volume load with twice treated nickel was clearly the superior result in terms of energy density.

Energy Density Summary of CED Capacitors by Treatment and Volume Load
(Standard Thickness Discharge Test with 99 kΩ)
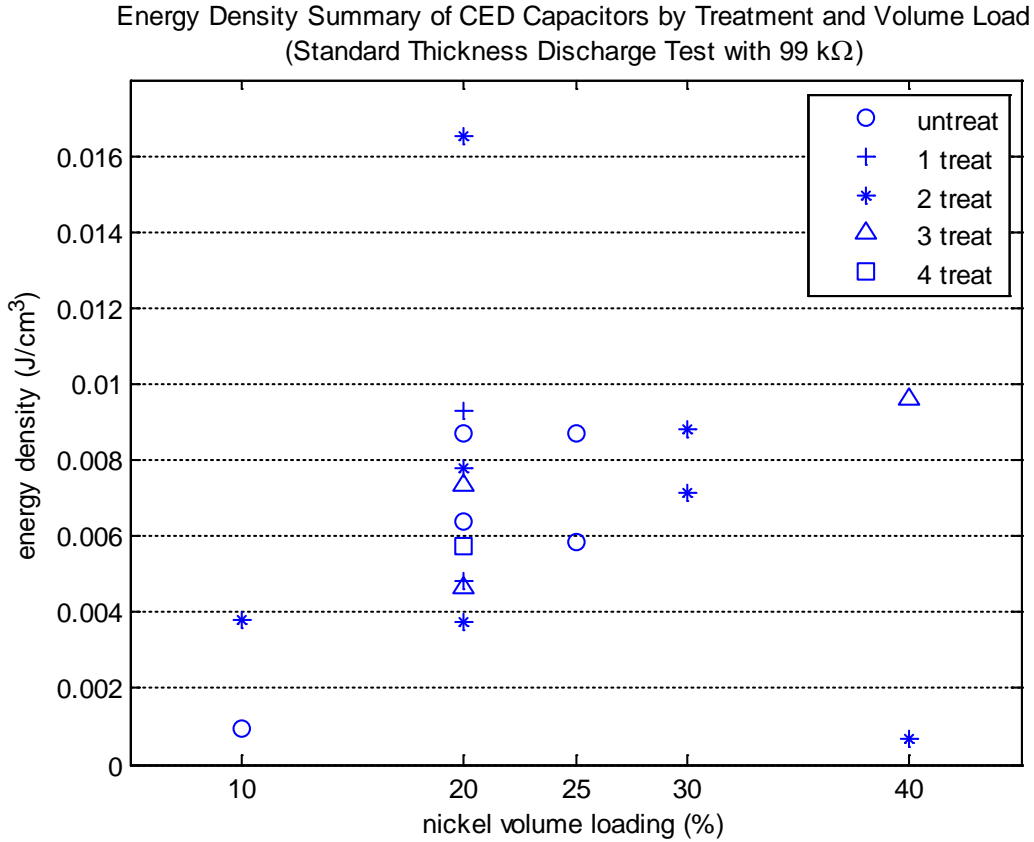
Figure 22.   Energy Density Summary of CED Capacitor Discharge Tests by Nickel Treatment and Volume Load

B.   VERIFICATION OF CAPACITOR BEHAVIOR

1.   Charge and Discharge Cycling

The circuit shown in Figure 8 was used to conduct capacitor charge and discharge cycles. To validate the test method, the previously described commercial 100 µF capacitor is tested with a charge voltage of 10 V and cycled with a 99.2 kΩ resistor. The

resulting voltage response is shown in Figure 23. This typical "shark-fin" curve shape is consistent with the expected response for a capacitor in a charge/discharge cycle.
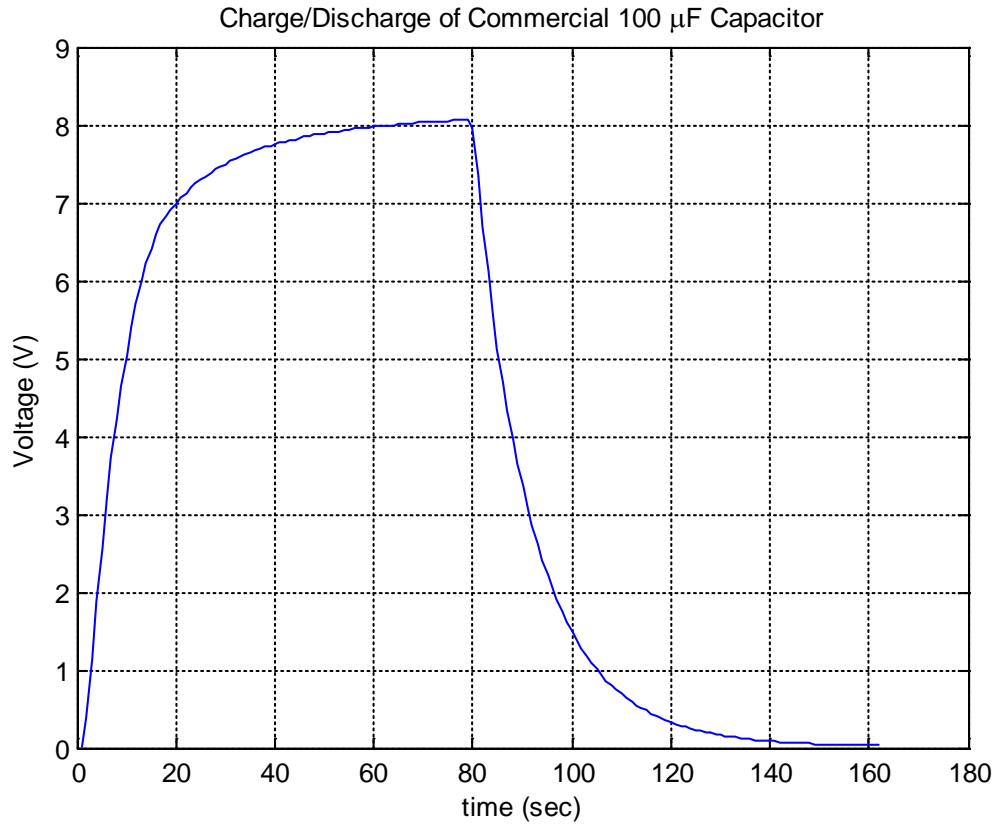
Figure 23. Charge/Discharge cycle of Commercial 100 µF Capacitor

A CED capacitor is then tested in the same manner. Using the selected dielectric configuration of 20% volume load with twice treated nickel powder, the capacitor is charged with 4 V and cycled through a 99.2 kΩ resistor. The dielectric thickness, d, is measured as 1.80 mm. The resulting voltage response is shown in Figure 24.
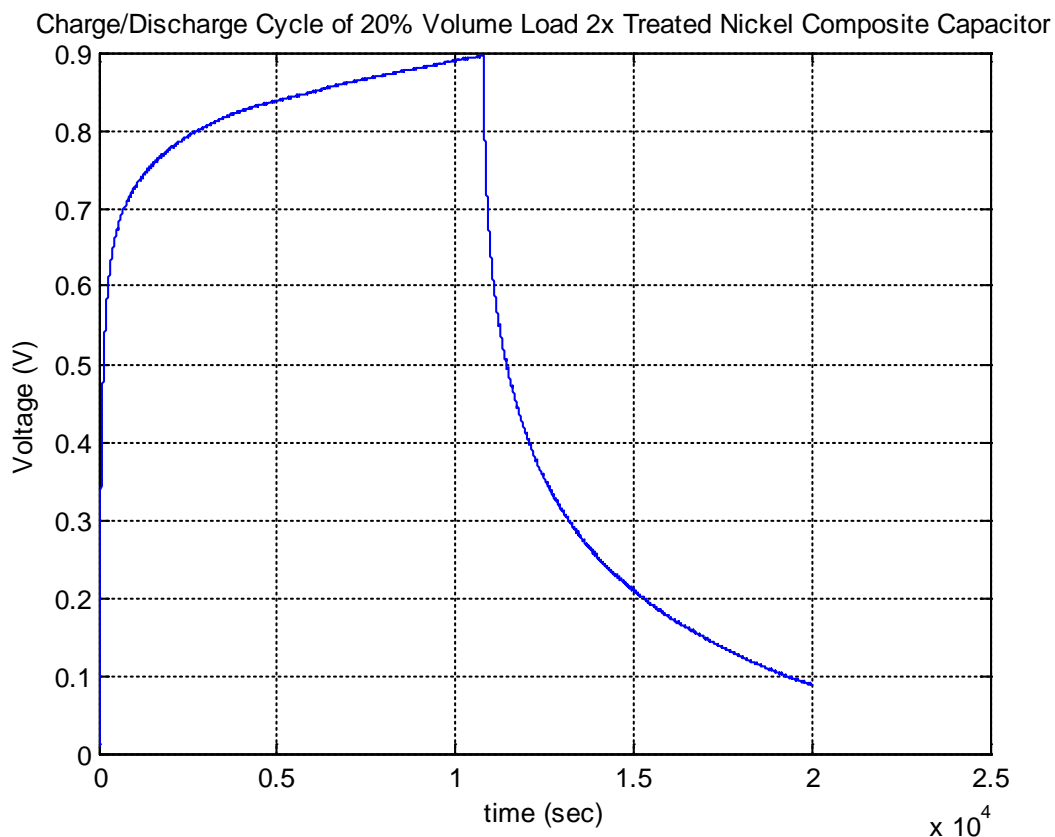
Figure 24. Charge/Discharge Cycle of 20% Volume Load 2x Treated Nickel CED
Capacitor

This result shows the general agreement between the shape of the voltage cycle curves of the commercial capacitor and the CED capacitor. Notable are the differences in voltage and time scales. Both capacitors failed to reach the full charging voltage, but the CED capacitor was far more limited and reaches less than 25% of the applied potential. However, noting the difference in time scales, the capacitance of the CED capacitor is vastly superior.

It is also notable that the methods employed to achieve high capacitance are very different. The commercial capacitor is designed on the basis of employing a low-permittivity dielectric material and capitalizing on high surface area and remarkably thin separation.   The CED is orders of magnitude thicker, but achieves remarkable capacitance based on the high dielectric constant of the MMD. This suggests that a CED fabricated to a very thin dimension could achieve even greater capacitance.

44

The charge and discharge portions are separated and analyzed to extract the capacitance and dielectric constant according to Equations 4 and 5. Plotting example charge and discharge characteristics from the commercial capacitor should ideally show two lines with equal slope. This would represent equal constant capacitance, since the series resistance is the same during charge and discharge. As shown in Figure 25, the discharge characteristic is more stable with nearly constant capacitance. The charge characteristic shows more variability at the beginning and end of the charge cycle. However, superimposing the two curves in Figure 26 demonstrates that the average capacitance is comparable over the majority of the cycle. The discharge is represented by the right axis and the charge by the left axis. The calculated capacitance of 138 μF shows reasonable agreement with the labeled rating and multimeter measurement. The result of this analysis generally suggests that it is preferable to measure capacitance during isolated discharge, but observing charge characteristics is also beneficial for consistency and verification.
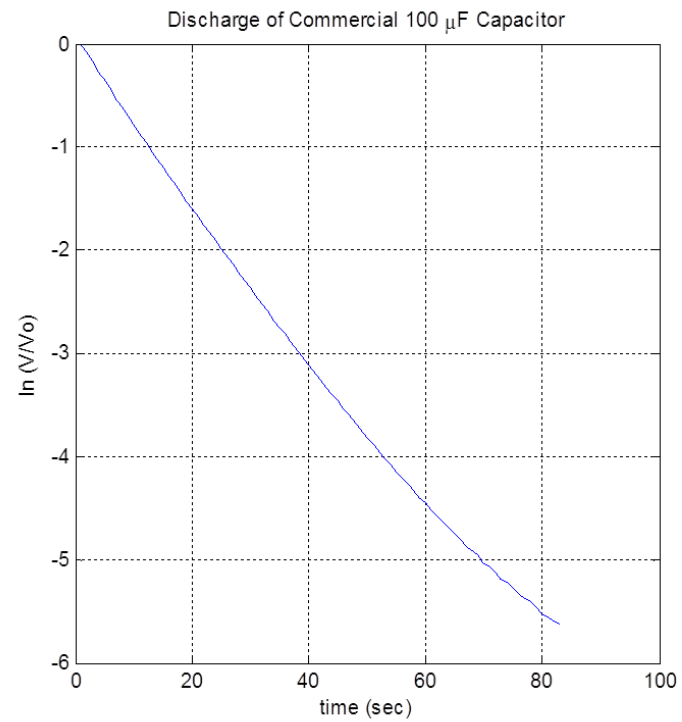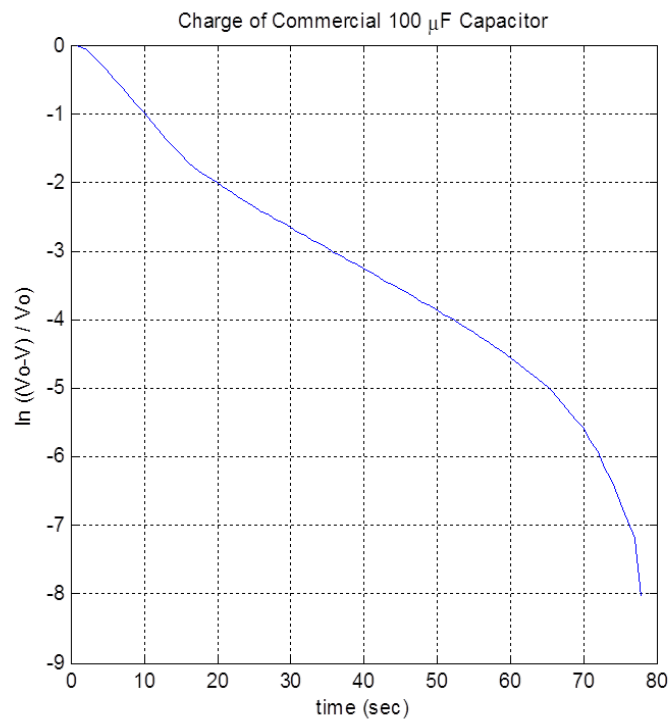
Figure 25.   Charge and Discharge Characteristics of 100 µF Commercial Capacitor

46
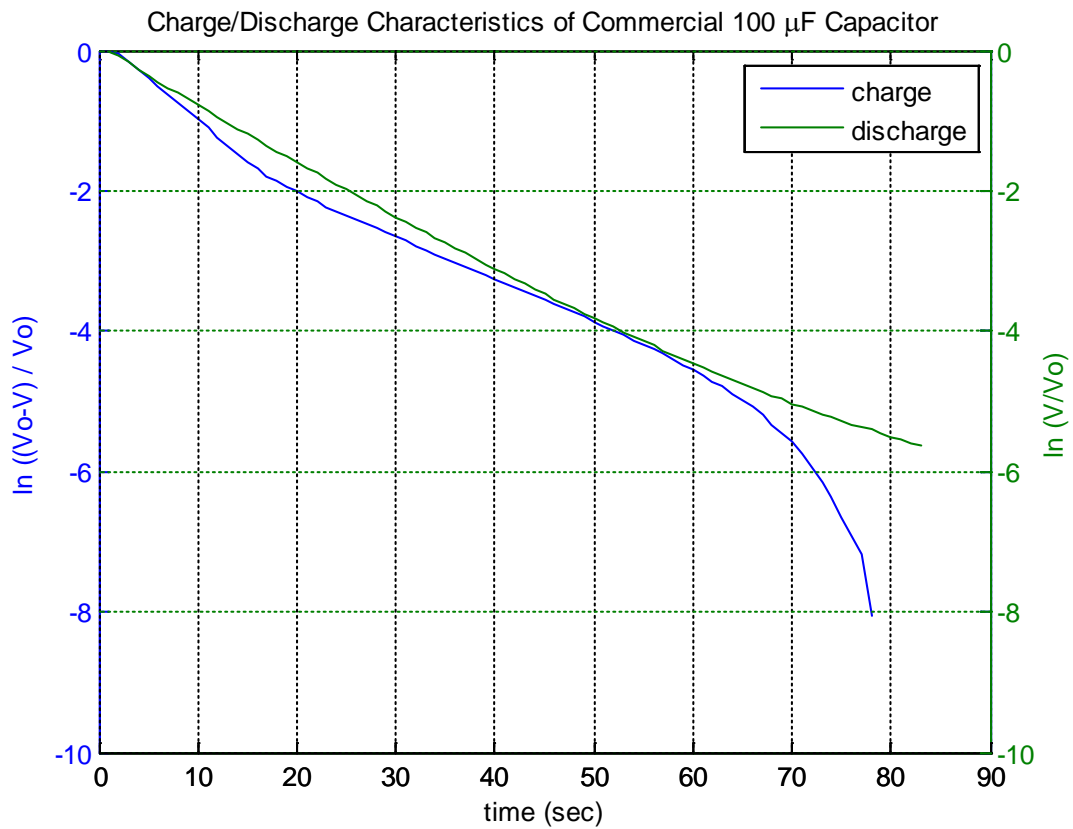
Figure 26.   Combined Charge/Discharge Characteristics of Commercial 100 µF Capacitor

The charge and discharge characteristic curves for the CED capacitor voltage cycle are similarly separated and analyzed.   The individual curves are shown in Figure 27.
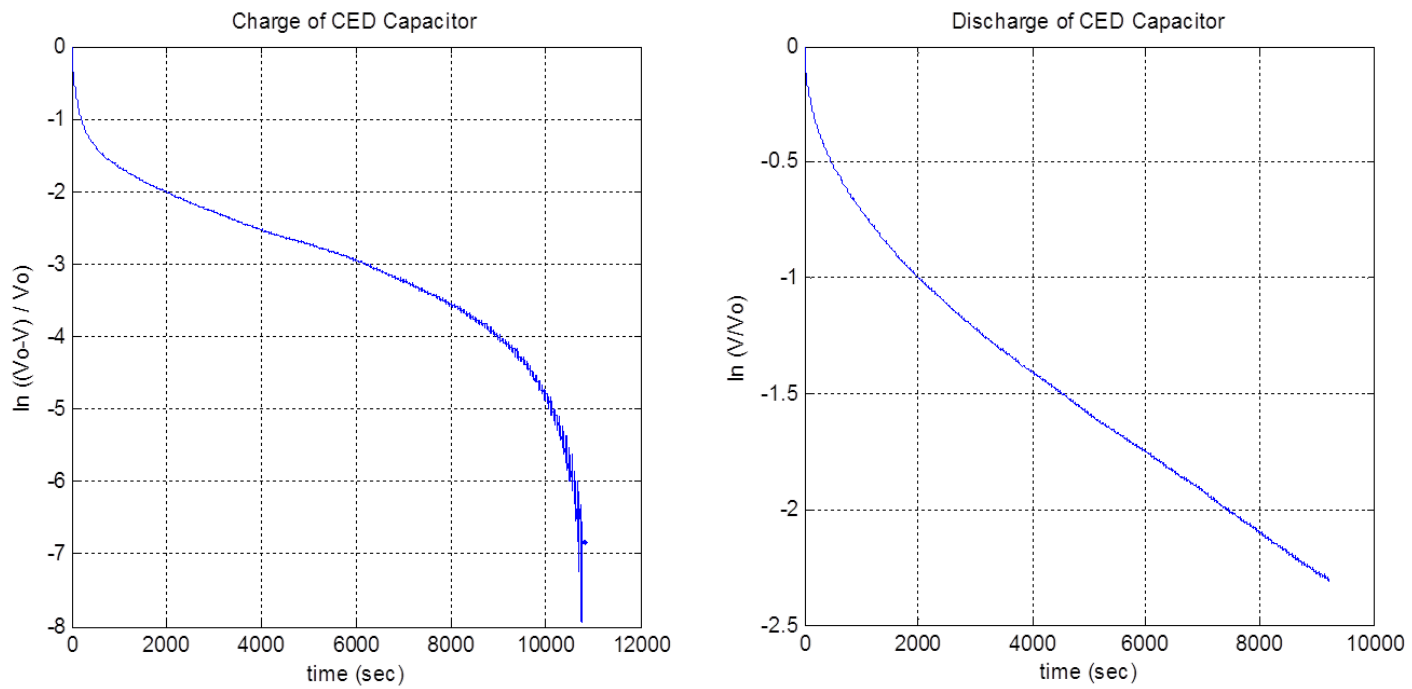
Figure 27.   Charge and Discharge Characteristics of 20% Volume Load with 2x Treated Nickel CED Capacitor

48

It is also important to note that the representation of voltage for each curve is inverted. Specifically, on the charge curve voltage goes up with time, and on the discharge curve voltage goes down with time. It was observed that during charging, both initially at low voltage and ultimately near the maximum voltage, the capacitance represented by the slope is highly variable. The highest and most constant capacitance occurred from approximately 1,000 to 8,000 seconds, representing voltage from 0.72 V to 0.88 V. This correlates to a dielectric constant of 3.7E9 over that range.

The discharge curve appears to demonstrate more stable capacitance, but the initial non-linear region encompasses most of the voltage range. At 2,000 seconds, the capacitor has discharged from the maximum 0.90 V down to 0.33 V. Constant capacitance is not demonstrated until relatively low voltage during cycling. Considering the discharge from initiation up to 8,000 seconds, the overall equivalent dielectric constant translates to 4.1E9. Considering only the linear region from 2,000 to 8,000 seconds, the dielectric constant is 5.6E9. These values differ by less than 50%, and are clearly consistent within an order of magnitude.

Superimposing the two curves in Figure 28 confirms that capacitance is comparable between charge and discharge, as the curves are relatively parallel in the linear regions. It is also notable that the charge characteristics become very noisy as the capacitor reaches ultimate voltage. The characteristic curve falls away toward vertical in the limit, as there is no subsequent voltage change once the capacitor is fully charged. This condition is consistent across all of the charge characteristics.
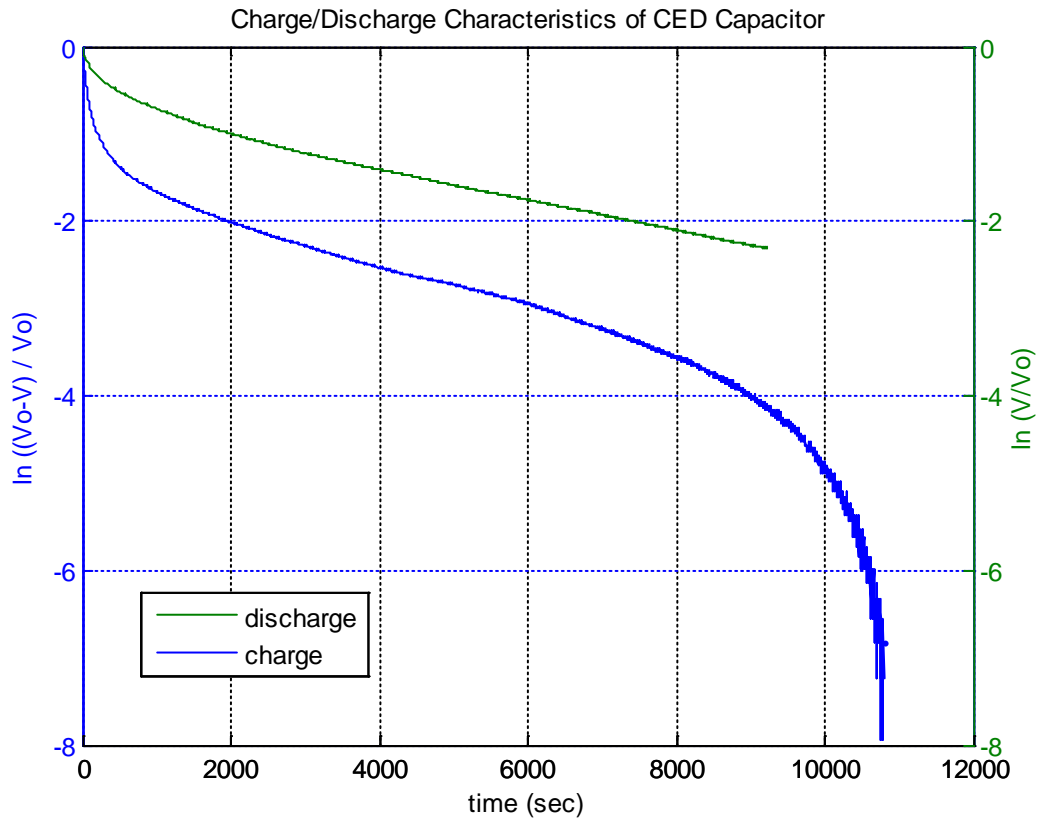
Figure 28. Combined Charge/Discharge Characteristics of 20% Volume Load with 2x Treated Nickel CED Capacitor

2. Current Delivery

Lower resistances were used to verify capacitor performance. To obtain higher currents, lower series resistance was employed during charge and discharge. The first resistor, measured as 2.67 kΩ by multimeter, was tested with the commercial 100 μF capacitor in the cycling circuit shown in Figure 8 with applied voltage of 10 V. Due to the low time constant, the voltage sampling rate was increased to 10 Hz for two charge/discharge cycles. The voltage response is shown in Figure 29.
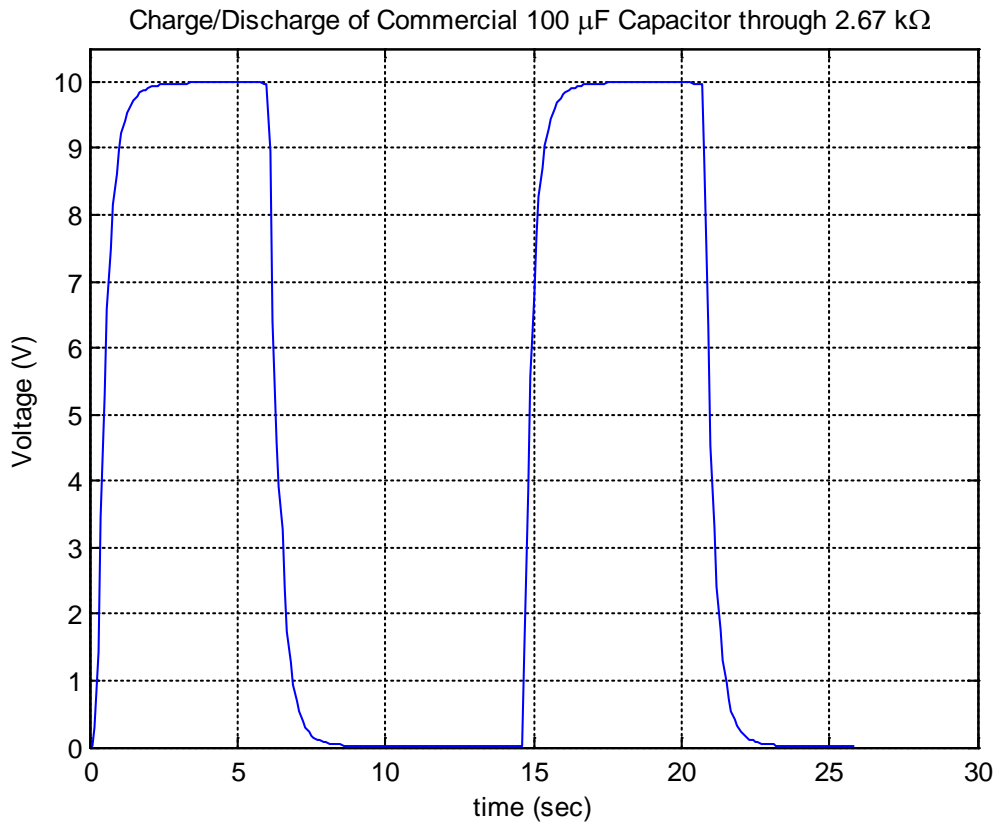
Figure 29. Charge/Discharge Cycles of Commercial 100 µF Capacitor through 2.67 kΩ

Unlike testing with the larger 99.2 kΩ resistor, the commercial capacitor was fully charged to equal the applied voltage. Capacitive behavior was also verified to be observable with the lower load resistance using a faster sampling rate. The charge and discharge characteristic curves are separated and analyzed for the first cycle and shown in Figure 30.
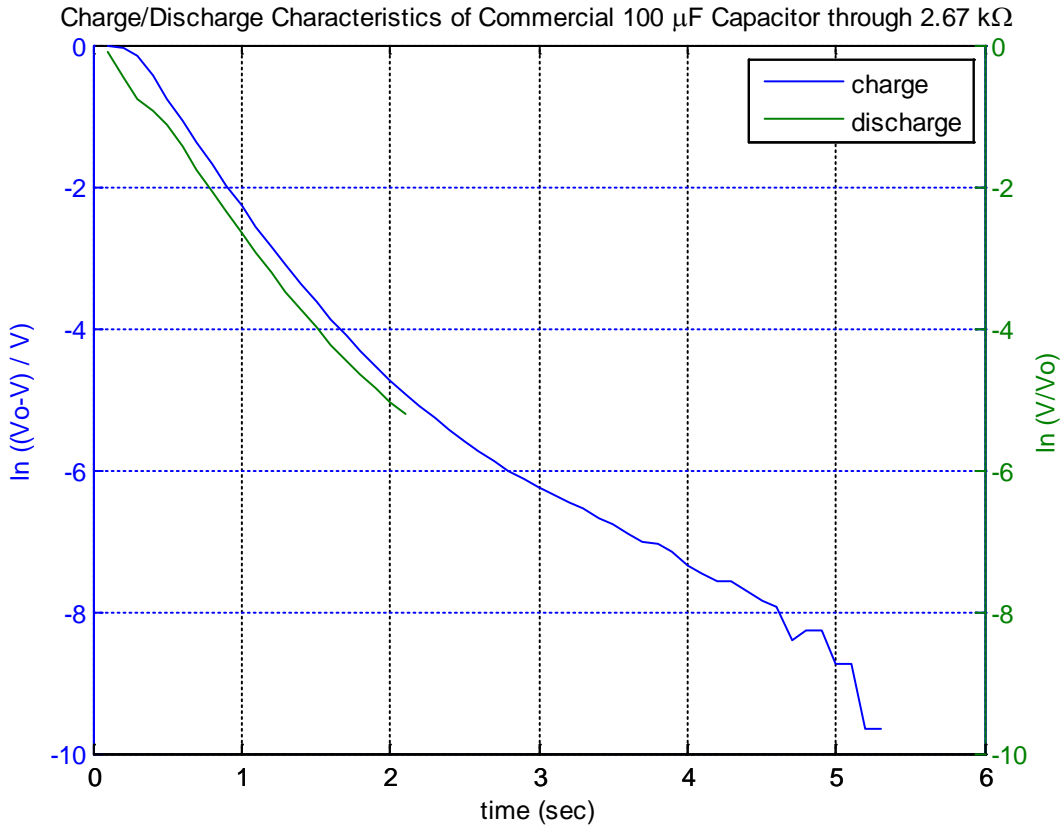
Figure 30.   Combined Charge/Discharge Characteristics of Commercial 100 µF Capacitor through 2.67 kΩ

The capacitance, as represented by the slope of the curves, was comparable during charge and discharge.   The capacitance was measured as 139 µF, demonstrating consistency in the measurement method with different load resistances.   The response is also relatively stable compared to the longer cycles with larger resistance.

Next, the results of testing a CED capacitor with 20% volume load of twice treated nickel powder using the 2.67 kΩ resistor are considered.   The CED capacitor was charged with 4 V and the dielectric thickness, d, was measured as 1.98 mm.   The voltage response is shown in Figure 31.

Figure 31. Charge/Discharge Cycle of 20% Volume Load with 2x Treated Nickel CED Capacitor through 2.67 kΩ

Interestingly, the capacitor quickly charged up to a higher voltage than observed using the larger 99.2 kΩ resistor. However, even with continued charging for an additional hour, the capacitor failed to reach half the charging voltage. Characteristic curves were derived for the discharge and the initial 250 seconds of the charge. The characteristic curves in Figure 32 show very inconsistent capacitance during both charge and discharge.
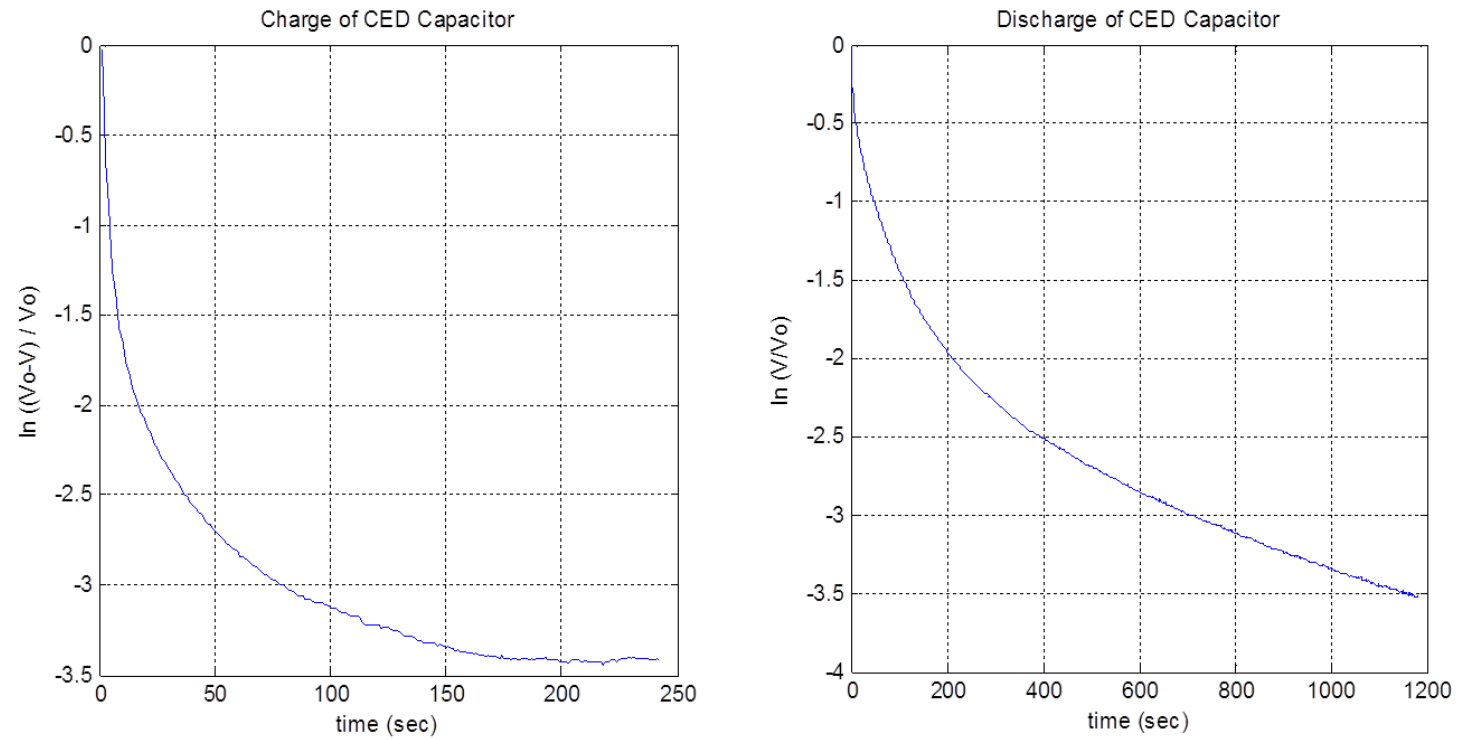
Figure 32. Charge and Discharge Characteristics of 20% Volume Load with 2x Treated Nickel CED Capacitor through 2.67 kΩ

No meaningful capacitance or dielectric constant can be extracted from this result. The charge characteristic is decidedly non-linear, and the discharge only achieves linear behavior at an insignificant voltage. Superimposing the charge and discharge curves in Figure 33 also shows the disparity in overall capacitance as indicated by the difference in time constant. The discharge lasted over five times as long as the charge.

Figure 33.   Combined Charge/Discharge Characteristics of 20% Volume Load with 2x Treated Nickel CED Capacitor through 2.67 kΩ

Considering these inconsistencies, the resistance of 2.67 kΩ was assessed to be too low for use in this experiment. Notably, the low resistance did result in higher voltage on charging. This was observed with the CED and commercial capacitors. However, the non-linear behavior on both charge and discharge and the disparity in time constant necessitate evaluation of another resistance.

A resistor measured as 20.2 kΩ by multimeter was employed to further evaluate the cycling behavior. The commercial capacitor was tested first, charged with 10 V, to observe the impact of the resistance on ultimate voltage. As seen in Figure 34, the capacitor charged up to a higher voltage than observed with the 99.2 kΩ resistor, but not to the full charging voltage as seen with the 2.67 kΩ resistor.
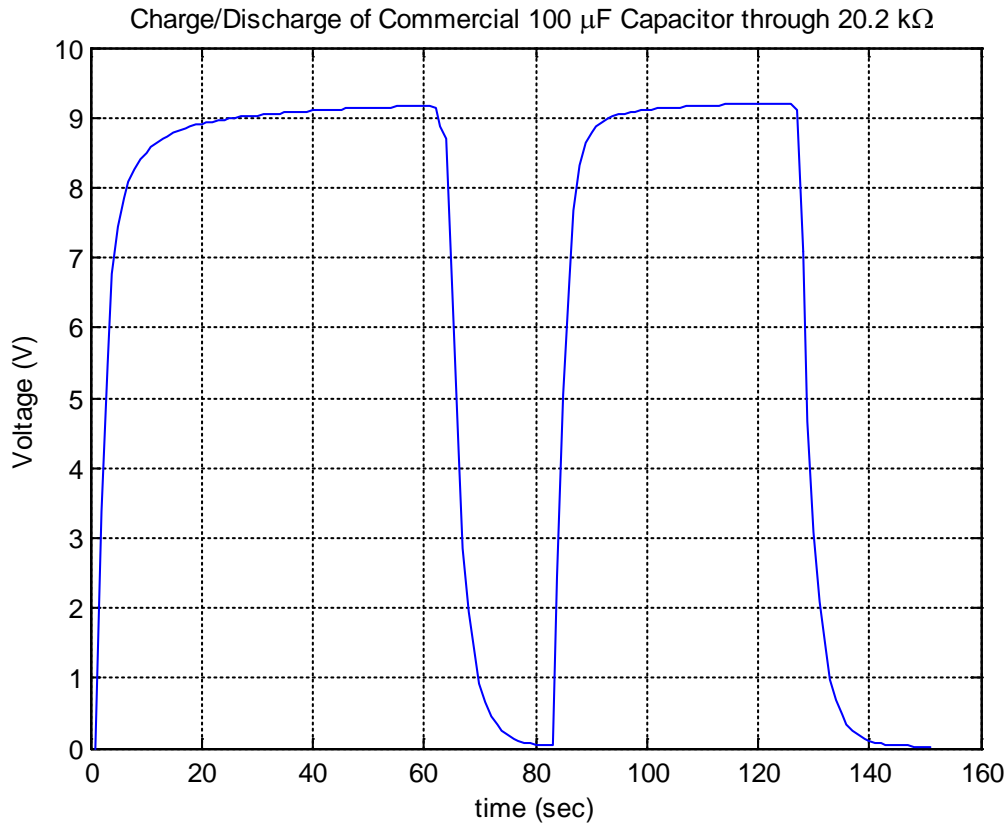
Figure 34.   Charge/Discharge Cycles of Commercial 100 µF Capacitor through 20.2 kΩ

This influence of charging current on the ultimate voltage is not understood. It is apparent that the capacitor charged up to near its ultimate voltage in less than approximately 15 seconds. At that time, the voltage was approximately 97% of its final value, and the subsequent minute of charging has little impact. This limited voltage behavior was also observed with the CED capacitor, so it is significant that the same phenomenon was witnessed with the commercial capacitor

The characteristic curves from the second charge/discharge cycle are shown in Figure 35. This shows a particularly variable capacitance, especially during charge. The capacitance was measured from the first 12 seconds of the discharge resulting in a value of 140 μF. This was again consistent with measurements from previous tests. The results of measuring capacitance from individual phases of the cycling experiments appear to be consistent, but the stability of the responses clearly suffers when compared to pure discharge tests. This is particularly true for lower resistances.
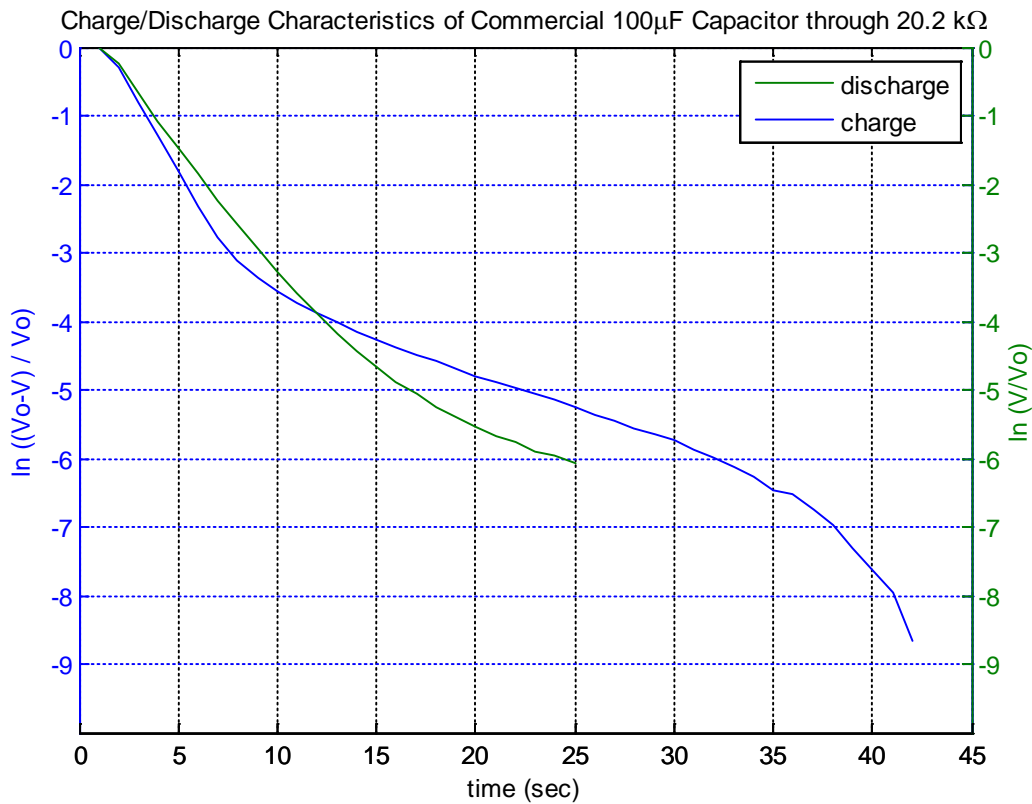
Figure 35. Combined Charge/Discharge Characteristics of Commercial 100 μF Capacitor through 20.2 kΩ

A CED capacitor was also analyzed by charge and discharge cycling with 20.2 kΩ resistance and applied voltage of 4 V. The capacitor is constructed with 20% volume load of twice treated nickel and the dielectric thickness, d, is 1.88 mm. The voltage response for three charge/discharge cycles is shown in Figure 36.
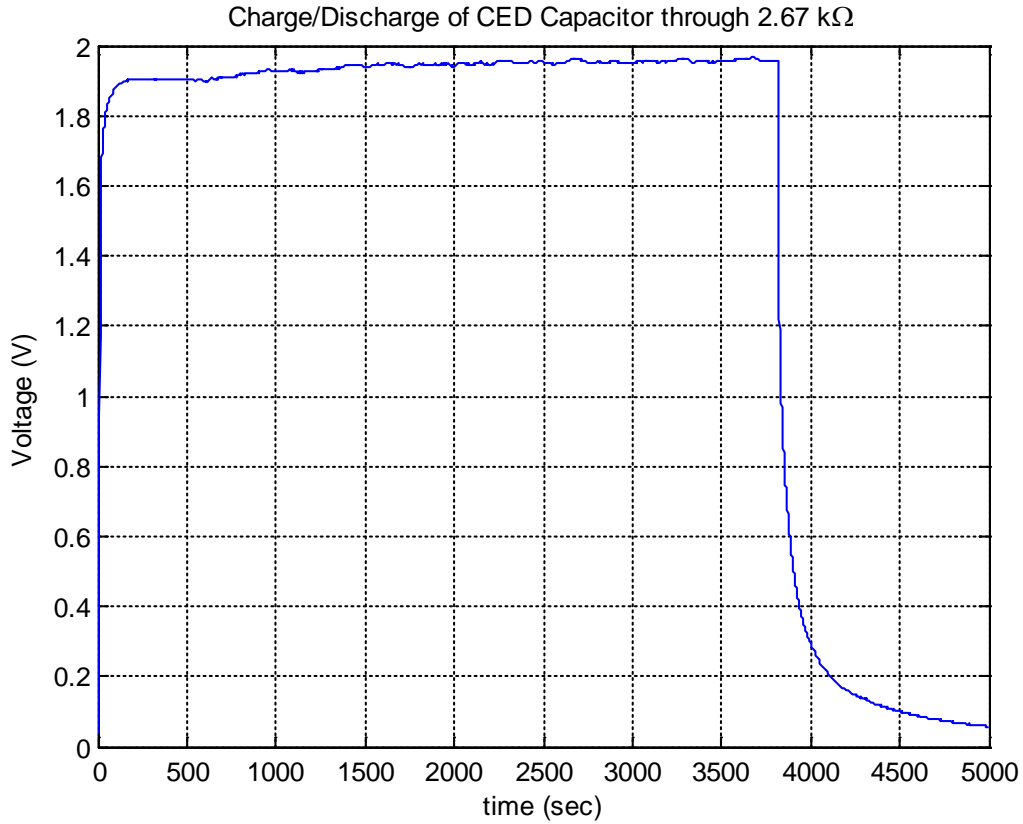
Figure 36.   Charge/Discharge Cycles of 20% Volume Load with 2x Treated Nickel CED Capacitor through 20.2 kΩ

The capacitor charged to a higher voltage than that tested with the 99.2 kΩ resistor, but lower than the 2.67 kΩ resistor.   This trend was also observed with the commercial capacitor.   The characteristic curves for the three charges and discharges are shown in Figure 37.
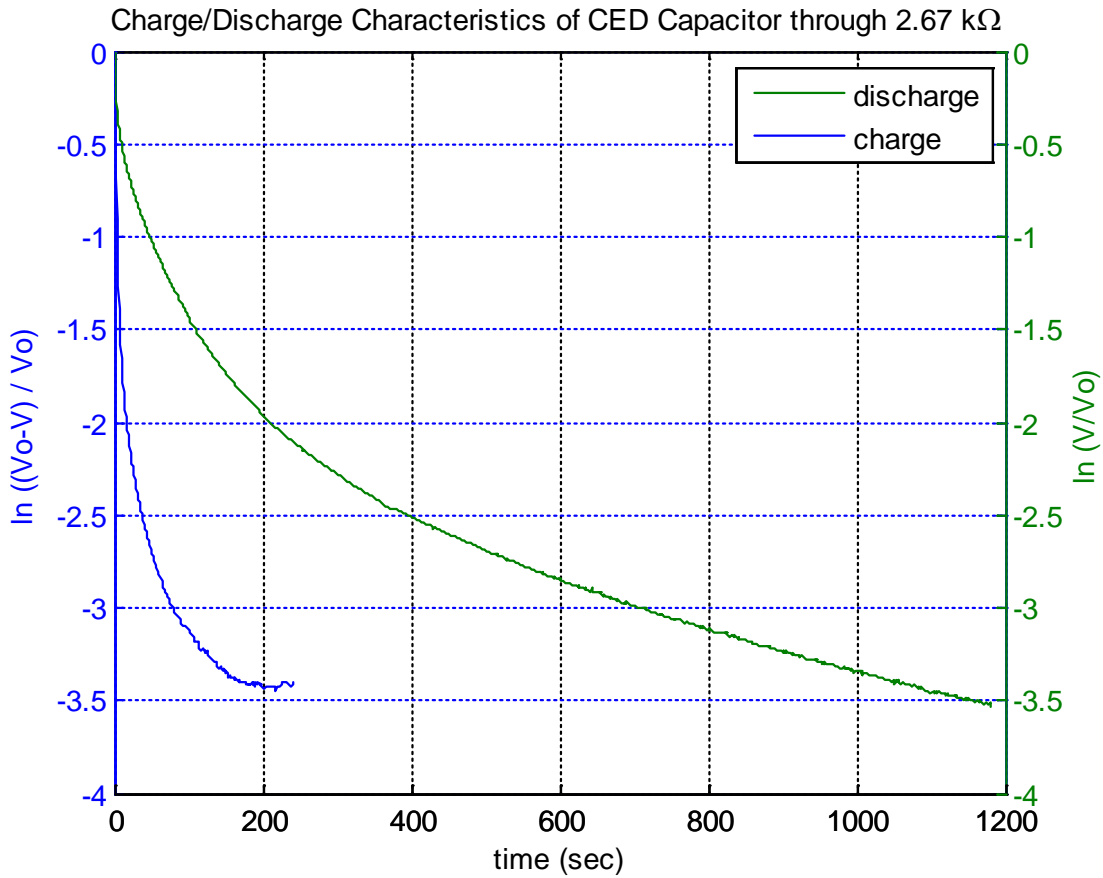
Figure 37.   Combined Charge/Discharge Characteristics of 20% Volume Load with 2x
Treated Nickel CED Capacitor through 20.2 kΩ

These characteristics are clearly more stable than those in Figure 33 resulting from the test with a 2.67 kΩ resistor. There is also strong consistency among the three cycles. The charge characteristics have long linear regions with good capacitance. The discharge characteristics present a gentle curvature, and only achieve reasonable linearity at relatively low voltages. While capacitance is not strictly constant throughout the cycle, meaningful parameters can be derived from the curves by considering best linear fits over relevant regions. Resulting dielectric constants with associated applicable voltage ranges were extracted from the curves and shown in Table 7.

	Operating Voltage Range	Dielectric Constant (ε_R) over Operating Voltage	Dielectric Constant (ε_R) over Entire Range
Charge 1	1.09 – 1.28 V	3.11E9	2.79E9
Charge 2	1.15 – 1.35 V	2.25E9	2.00E9
Charge 3	1.19 – 1.36 V	2.75E9	2.33E9
Discharge 1	0.44 – 0.16 V	3.87E9	4.88E9
Discharge 2	0.64 – 0.26 V	3.52E9	5.57E9
Discharge 3	0.69 – 0.26 V	4.23E9	5.70E9

Table 7.   Charge and Discharge Data for 20% Volume Load with 2x Treated Nickel CED Capacitor Cycled with 20.2 kΩ Resistor

The positive result from this test is considered a reasonable validation of capacitive behavior for the CED configuration. The capacitor demonstrated consistent, repeatable performance over multiple charge and discharge cycles with remarkable dielectric constant. This general behavior was observed to hold for multiple values of resistance, although consistency and stability suffered at low resistance.

3.   Other Factors Revisited

a.   *Thickness*

The dielectric thickness, *d*, was observed to have an impact on dielectric constant when tested with the HSA electrolyte matrix, and was therefore examined in the CED configuration. Section A.1 of this chapter demonstrates that the thinnest dielectrics exhibit the best performance with regard to dielectric constant and voltage. Additionally, thinner dielectrics are decidedly advantageous when specifically considering energy density. As shown previously in Equation 6, energy density has an inverse square dependence on dielectric thickness, *d*.

An especially thin CED capacitor was fabricated to revisit this factor in a charge/discharge cycling test. The composition was 20% volume load with twice treated

nickel and the dielectric thickness was 1.35 mm. The capacitor was charged with 4 V.

The voltage response is shown for two cycles in Figure 38.
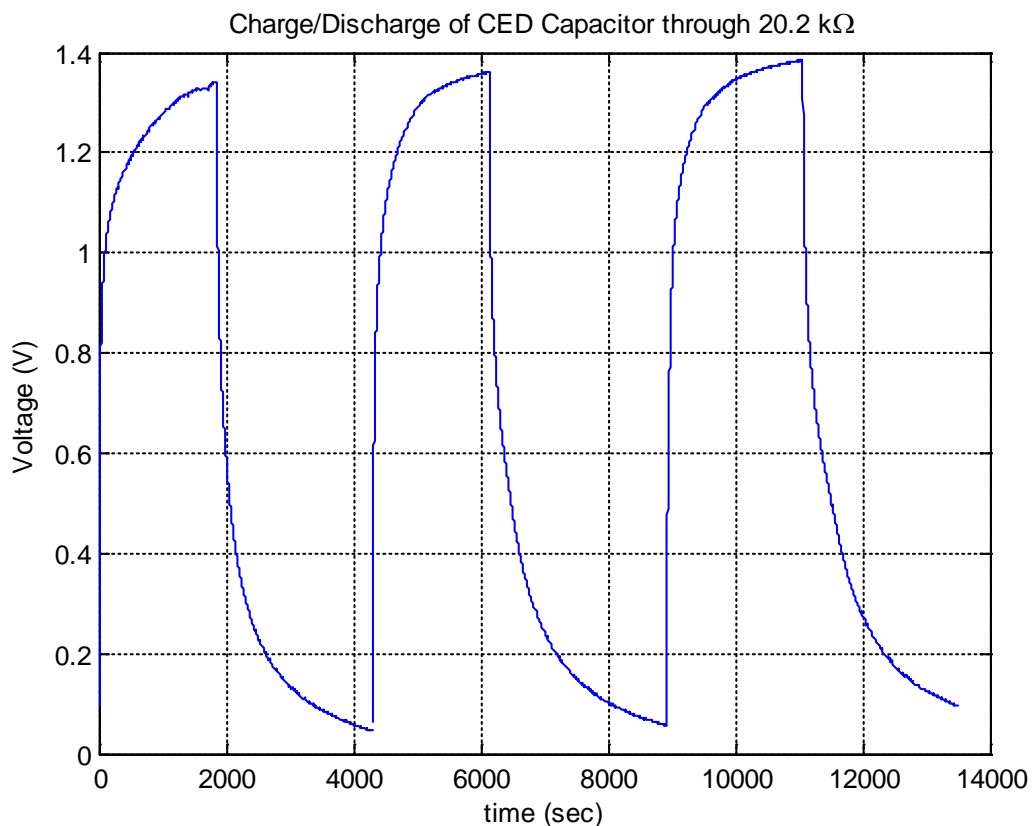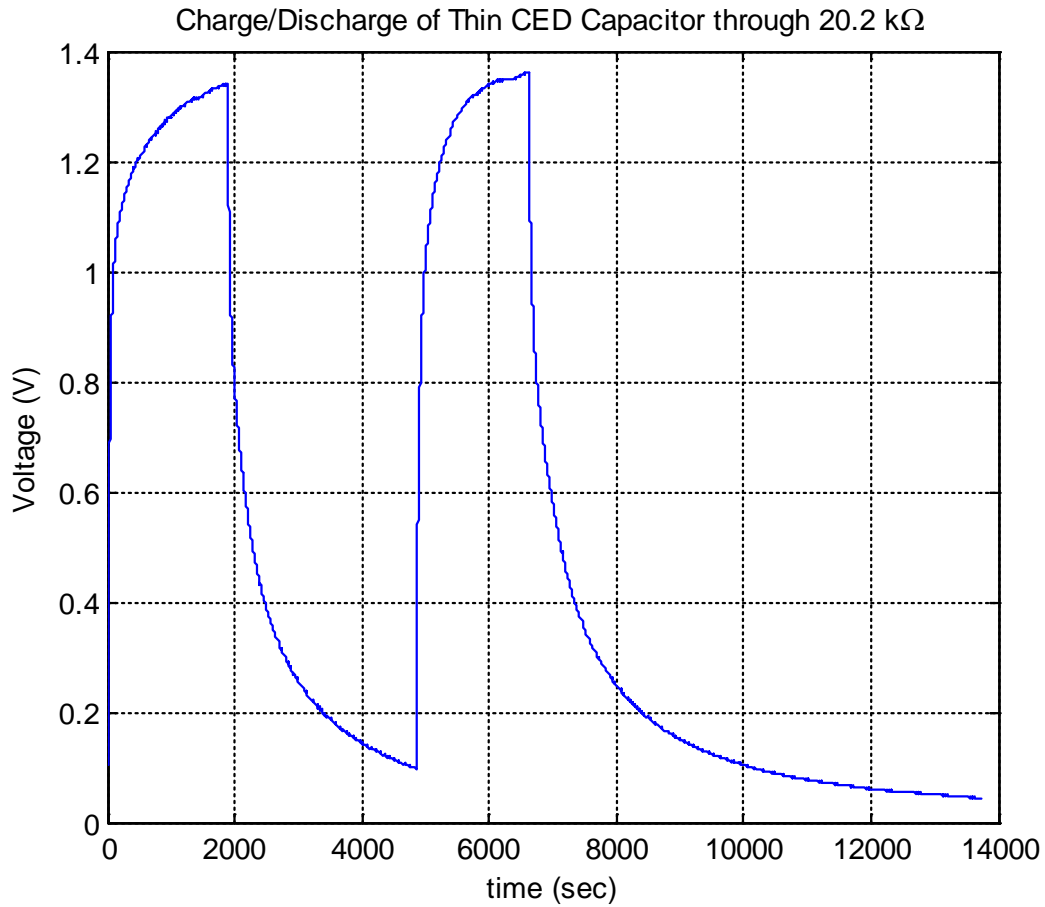

Figure 38.   Charge/Discharge Cycles of 20% Volume Load with 2x Treated Nickel Thin
CED Capacitor through 20.2 kΩ

The ultimate voltage is comparable to that observed with the standard
dielectric thickness using the same 20.2 kΩ resistor, and the overall curve appears
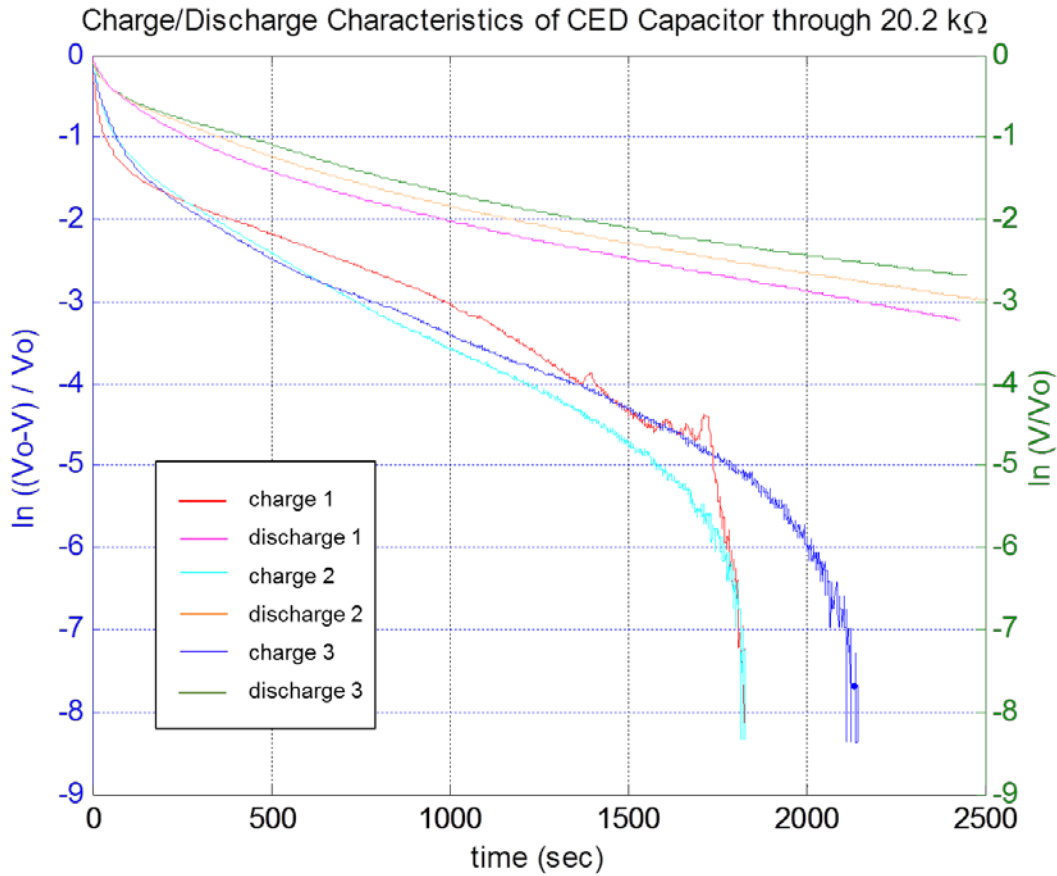similar. The characteristic curves for charges and discharges are shown in Figure 39.

Figure 39.   Combined Charge/Discharge Characteristics of 20% Volume Load with 2x
Treated Nickel Thin CED Capacitor through 20.2 kΩ

The results seem comparable to those from the standard CED capacitor. The specific parameters extracted from the characteristic curves are shown in Table 8.

	Operating Voltage Range	Dielectric Constant (ε_R) over Operating Voltage	Dielectric Constant (ε_R) over Entire Range
Charge 1	1.10 – 1.30 V	2.14E9	1.16E9
Charge 2	1.08 – 1.34 V	1.45E9	1.00E9
Discharge 1	0.66 – 0.32 V	3.21E9	3.51E9
Discharge 2	0.71 – 0.37 V	3.47E9	6.23E9

Table 8.   Charge and Discharge Data for 20% Volume Load with 2x Treated Nickel Thin CED Capacitor Cycled with 20.2 kΩ Resistor

This result shows that this decrease in thickness does not have an appreciable impact on the dielectric constant or operating voltage in the CED configuration subjected to charge/discharge cycling. Producing thinner dielectrics is also more practically challenging. Therefore, it was assessed that dielectrics of approximately 2 mm thickness are thin enough for this study.

Alternatively, a thicker dielectric layer was evaluated in the CED configuration. Constructed from the same relative composition, the dielectric was produced with 16 mL of HSA powder (3.5 g of alumina and 0.35 g of boric acid), 4 mL of twice treated nickel powder, and 5 mL of H_2O. The resulting dielectric thickness, d, was 2.90 mm. The capacitor was charged with 4 V, and cycled with the 20.2 kΩ resistor. The capacitor was subjected to two cycles similar to those for the standard and thin dielectrics, with a charge time of approximately 30 minutes. The capacitor was then allowed to fully discharge and submitted to a third cycle with a longer charge of approximately 45 minutes. The voltage response is shown in Figure 40.
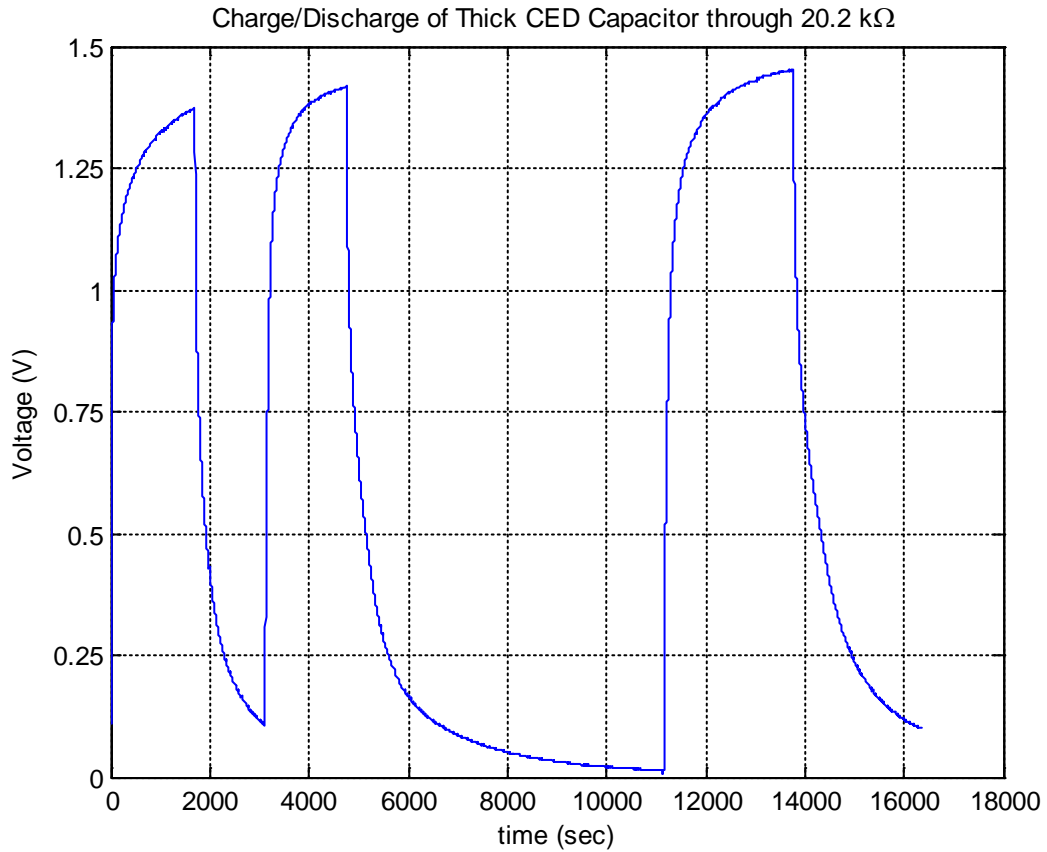
Figure 40. Charge/Discharge Cycles of 20% Volume Load with 2x Treated Nickel Thick CED Capacitor through 20.2 kΩ

The ultimate voltage and overall appearance of the curve is similar to other cycle tests conducted with the 20.2 kΩ resistance. The separated charge and discharge characteristics are shown in Figure 41.
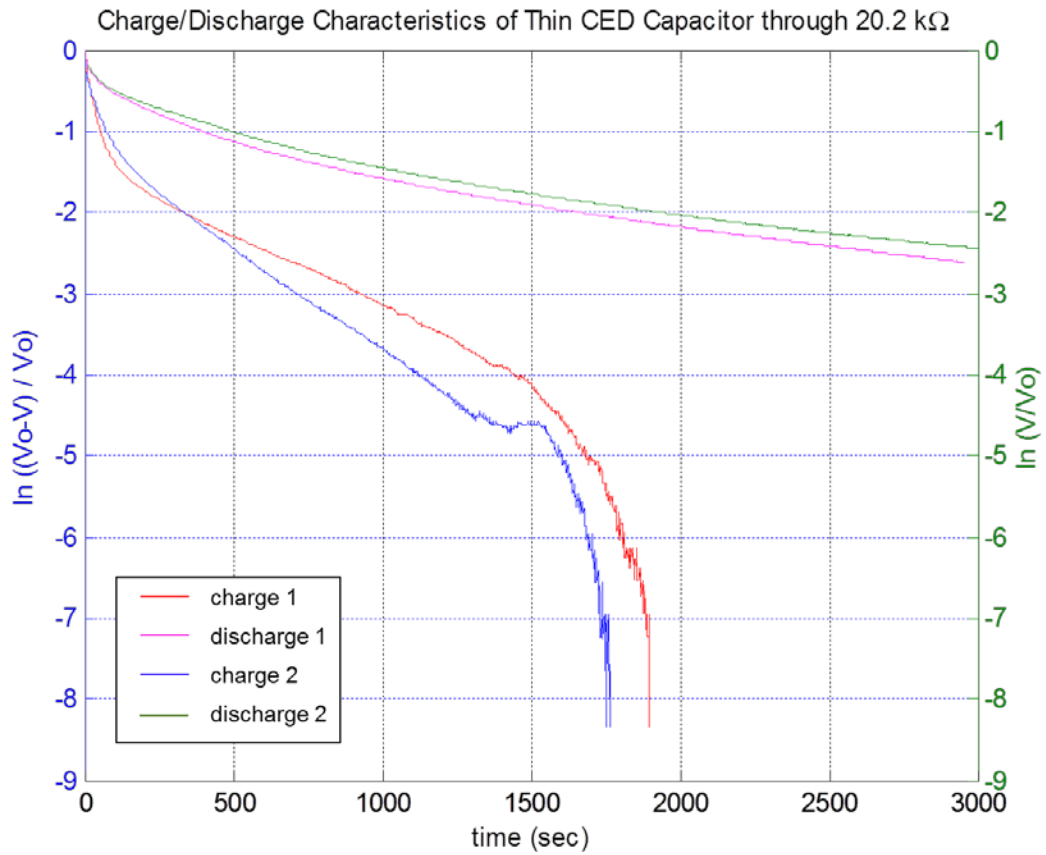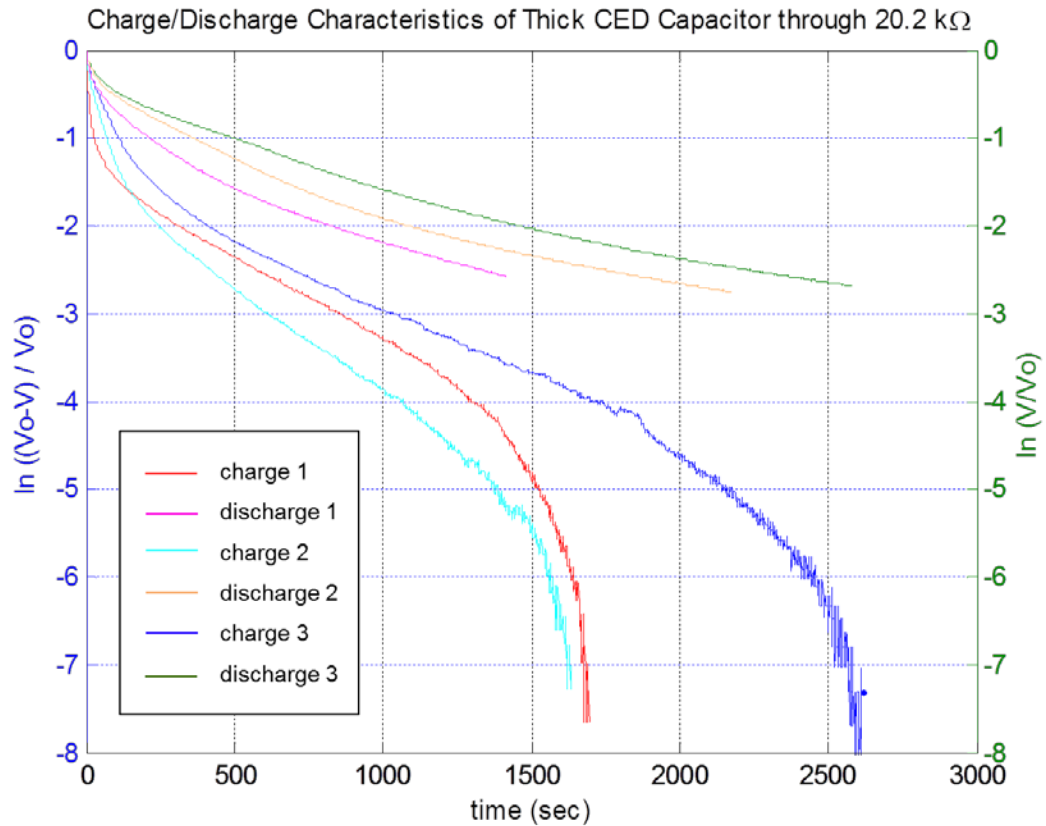
Figure 41.   Combined Charge/Discharge Characteristics of 20% Volume Load with 2x
Treated Nickel Thick CED Capacitor through 20.2 kΩ

The results once again seem comparable to those from the standard and thin CED capacitors. The specific parameters extracted from the characteristic curves are shown in Table 9.

	Operating Voltage Range	Dielectric Constant (ε_R) over Operating Voltage	Dielectric Constant (ε_R) over Entire Range
Charge 1	1.13 – 1.34 V	4.19E9	2.24E9
Charge 2	1.23 – 1.40 V	3.25E9	1.91E9
Charge 3	1.25 – 1.43 V	5.24E9	2.94E9
Discharge 1	0.70 – 0.25 V	3.95E9	3.69E9
Discharge 2	0.79 – 0.26 V	4.92E9	5.29E9
Discharge 3	0.83 – 0.29 V	6.78E9	6.59E9

Table 9.   Charge and Discharge Data for 20% Volume Load with 2x Treated Nickel Thick CED Capacitor Cycled with 20.2 kΩ Resistor

A modest but consistent improvement in dielectric constant and voltage is observed with increasing thickness. However, the increase in dielectric thickness reduces any net gain in energy density. The influence of dielectric constant on energy density is not as sensitive as thickness or voltage. Therefore, order of magnitude improvements in dielectric constant are generally required to achieve a conclusive result.

Recall that when considering only the HSA electrolyte as dielectric, the dielectric constant was inversely related to the dielectric thickness. In the CED configuration, the opposite trend is observed. The basis of this behavior is not understood. It is suspected that thicker composite dielectrics would mitigate the propensity for percolation if constituent nickel particles were not uniformly and completely insulated. However, this does not suggest lesser performance for thinner layers without excessive metal loading.

Although a trend is observed, the magnitude of the difference in dielectric constant is unremarkable. Hence the standard of approximately 2 mm is maintained as the objective dielectric thickness. It is also noteworthy that the dielectric thickness is subject to fairly wide variation. For all capacitors constructed to this standard objective

thickness using 15 mL of dry powder, the mean is 2.07 mm with a standard deviation of 0.23 mm, or approximately 11%. The practical difficulty associated with manually producing dielectric layers of strictly consistent and uniform thickness complicates precise control of this variable.

To summarize the impact of the various parameters on the capacitor energy density, Figure 42 shows the results for each cycle test using the 20% volume load twice treated nickel CED. The data is plotted with respect to thickness, with resistance indicated by color and charge or discharge indicated by symbol. Accounting for dielectric constant, maximum operating voltage, and dielectric thickness, the energy density is shown to be relatively consistent across the range of thicknesses. The thinnest dielectric appears to be consistently preferable, and measurements of charge cycles are typically superior to those of discharge cycles. The lowest resistance of 2.67 kΩ produced a dramatic negative effect, primarily due to the non-linearity of the response and inability to measure capacitance at relevant voltage. The other two resistance values of 20.2 kΩ and 99.2 kΩ demonstrated roughly consistent results for capacitor energy density.
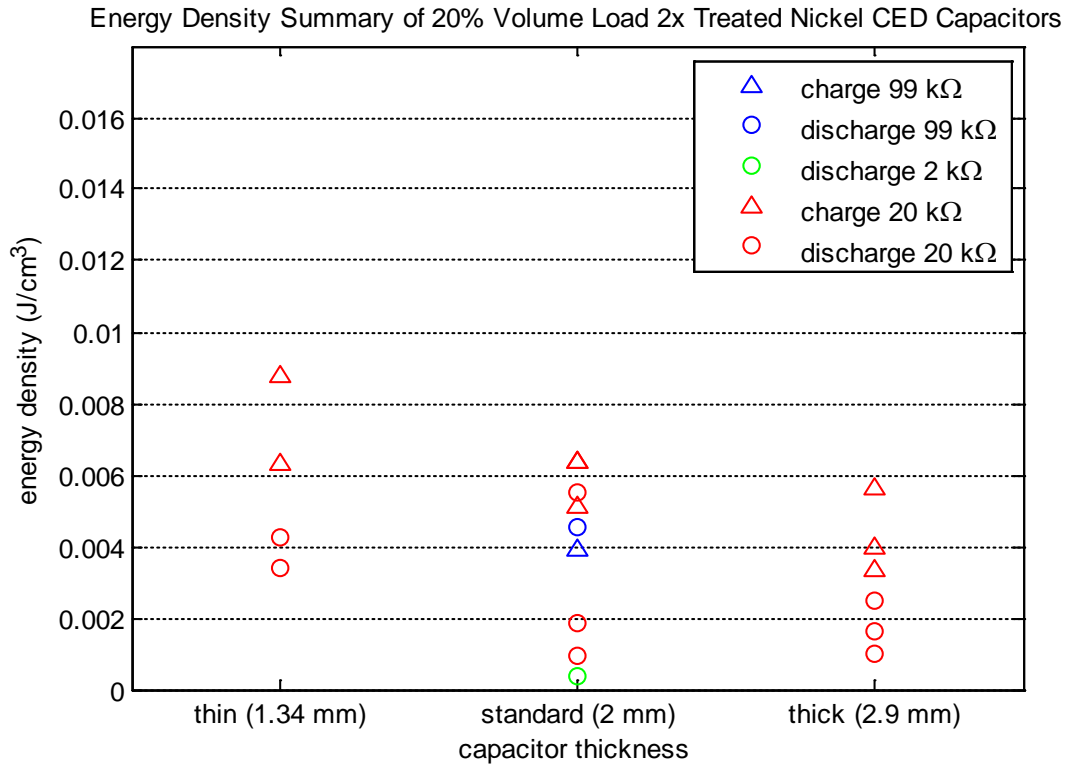
Figure 42.   Energy Density Summary of Cycle Tests for 20% Volume Load 2x Treated Nickel CED Capacitors

b.   *Voltage*

This study supposed charging voltage to be primarily inconsequential to capacitive performance in the described testing scenarios. Essentially, the only criteria is that the charging voltage be great enough to ensure that observed operating voltage is in fact the maximum achievable in that configuration. However, a precipitous initial voltage drop is observed across the range of all discharge tests and CED capacitors never fully reach the applied voltage in charging cycles. All composite capacitors were charged with 4 V, but observed maximum capacitor voltage never exceeded 2 V.

Based on this observation, a discharge test was conducted using lower charging voltage. The capacitor was charged with 1 V, which was typically observed to be within the operating voltage range. The dielectric thickness was 1.98 mm and was composed with 20% volume load of twice treated nickel. The test was conducted using the circuit shown in Figure 4 with a resistance of 20.2 kΩ. The objective of the test was

68

to observe whether the discharge continues to exhibit an abrupt initial drop in voltage. The resulting discharge characteristic is shown in Figure 43.
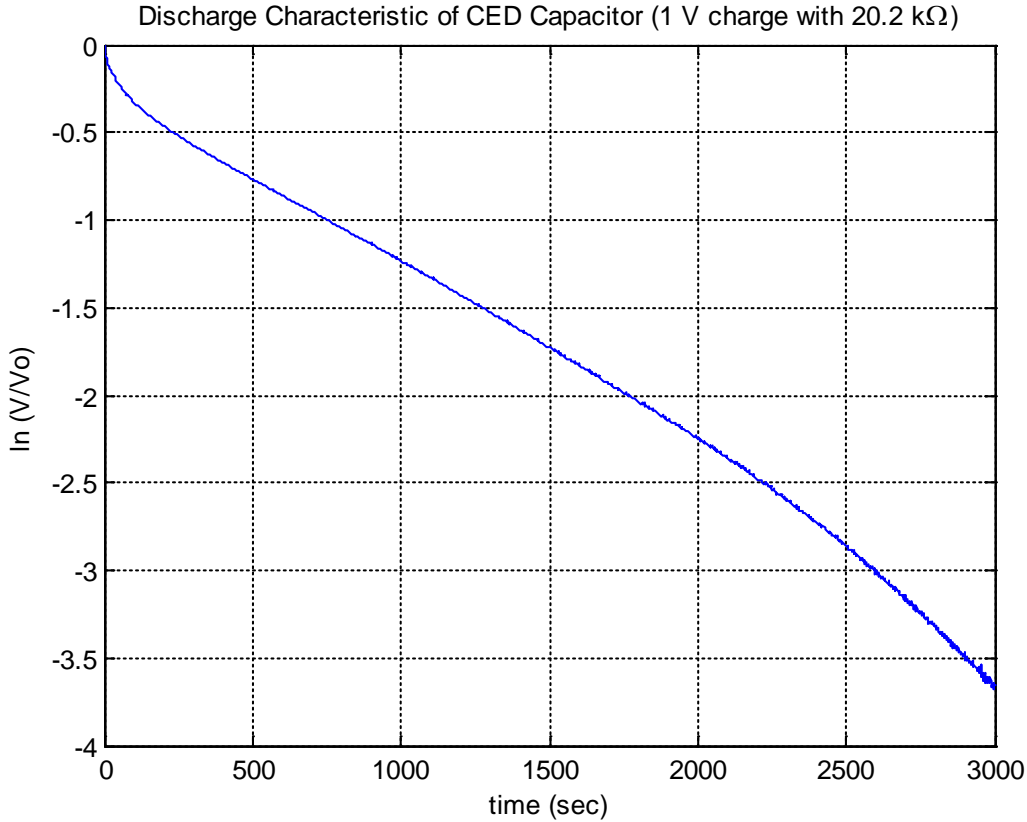
Figure 43.   Discharge Characteristic of 20% Volume Load with 2x Treated Nickel CED Capacitor (1V charging with 20.2 kΩ)

This result shows that the initial voltage drop before stable capacitance is relatively limited. The entirety of the discharge is considered linear, and the measured dielectric constant is 5.12E9 at the full charging voltage of 1 V. The limited voltage does noticeably affect the resultant energy density, which is calculated to be 5.78E-3 J/cm^3.

A charge/discharge cycle is also performed in the circuit shown in Figure 8 with applied potential of 1 V and a 20.2 kΩ resistor. The result is shown in Figure 44, and demonstrates significant inconsistency over two cycles. The first charge is very short, as is the second discharge. The ultimate voltage is significantly lower than the applied voltage.
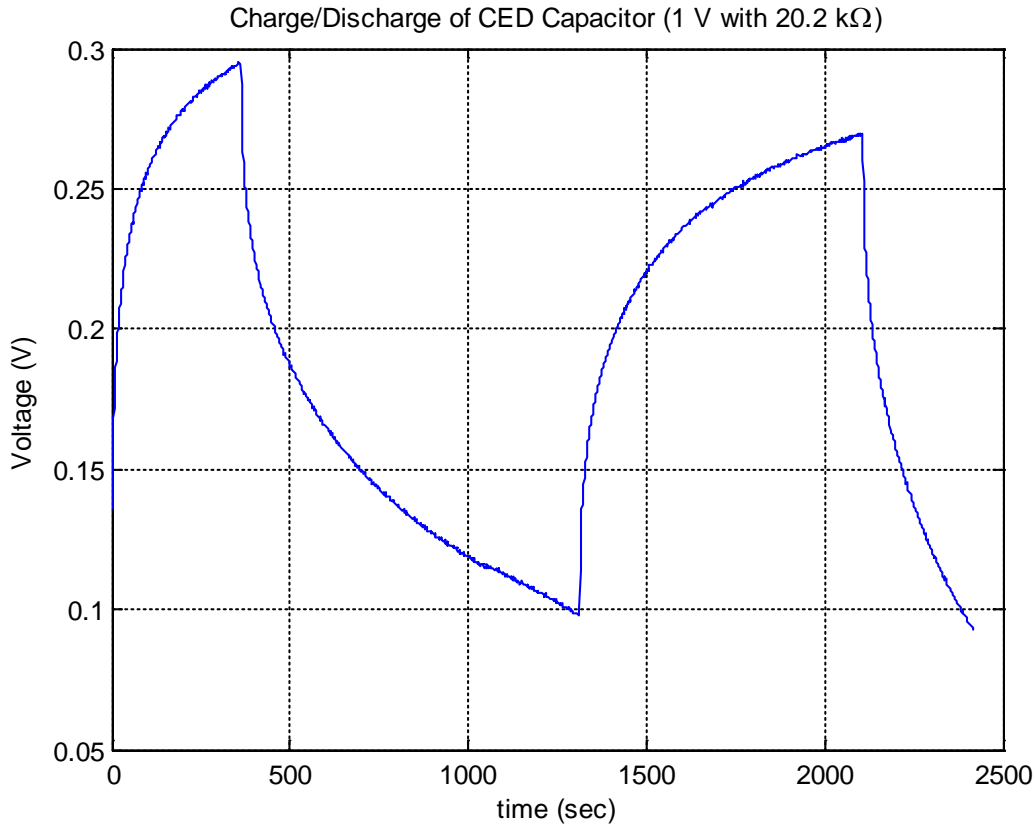
Figure 44. Charge/Discharge Cycles of 20% Volume Load with 2x Treated Nickel CED Capacitor (1 V charging through 20.2 kΩ)

The charge and discharge characteristics are shown in Figure 45. The plot confirms that the capacitance observed for each of the charge and discharge cycles is notably inconsistent. Additionally, even when charging voltage is less than the typical operating range, the capacitor still experiences an initial abrupt drop in voltage during discharges before achieving stable capacitance. Charges also do not reach stable capacitance until well into the cycle. This effect of initial instability is more pronounced than in the discharge-only test. The combined effect of the lower charging voltage and initial lagging response results in insignificant operating voltages in the constant capacitance regions.

Figure 45.   Combined Charge/Discharge Characteristics of 20% Volume Load with 2x Treated Nickel CED Capacitor (1 V charging through 20.2 kΩ)

The disparity in performance between discharge and cycling tests is not understood.   Comparing the results from all discharges, including those within cycle tests, the examples from discharge only tests have consistently higher operating voltages and generally more linear responses.   Cycling tests are informative for examination of capacitive behavior, but complicate the measurement of capacitance and dielectric constant.

4.   Alternate Composition

This test examined the influence of electrolyte composition on the performance of the CED capacitor.   An electrolyte of aqueous 1 M KOH is used instead of boric acid powder and water.   The dielectric thickness, d, is 1.65 mm and the composition consists of:

- 12 mL alumina (2.5 g)
- 3 mL 2x treated nickel powder
- 3.5 mL 1 M KOH.

The 20% volume load with twice treated nickel CED capacitor is subjected to a standard discharge test using a load resistor of 20.2 kΩ. The capacitor is charged with 4 V for 16 minutes. The resulting discharge characteristic is shown in Figure 46.

Discharge of CED Capacitor with KOH electrolyte
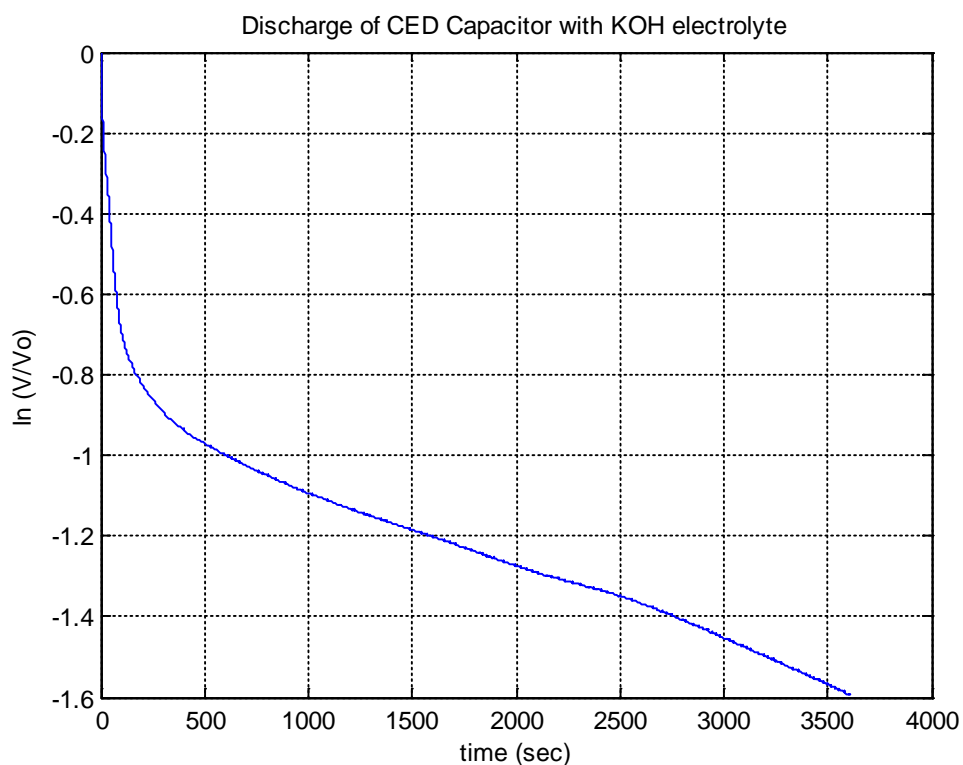
Figure 46. Discharge of 20% Volume Load with 2x Treated Nickel CED Capacitor with KOH Electrolyte

It can be seen that the initial discharge is significant before the achievement of stable capacitance. The discharge characteristic is stable at low voltage, with a reasonably constant slope. The parameters of the discharge are shown in Table 10.

Composition	Dielectric Thickness (d)	Initial Discharge Voltage (V_0)	Dielectric Constant (ε_R)	Operating Voltage
12 mL alumina (2.5 g) 3 mL treated nickel 3.5 mL KOH	1.65 mm	1.81 V	2.10E10	0.74 V

Table 10.   CED Capacitor with 20% Volume Load Twice Treated Nickel and KOH Electrolyte Discharge Test Data

It can be seen that while the initial voltage was reasonably high compared with other compositions, the operating voltage was very low. The dielectric constant was the highest observed, but the low operating voltage makes the result less significant. The resulting energy density is 0.019 J/cm^3.

Next, the same capacitor was examined by charge and discharge cycling. Using 4 V charging voltage and a 20.2 kΩ resistor, the capacitor was subjected to two cycles. The voltage response is shown in Figure 47.
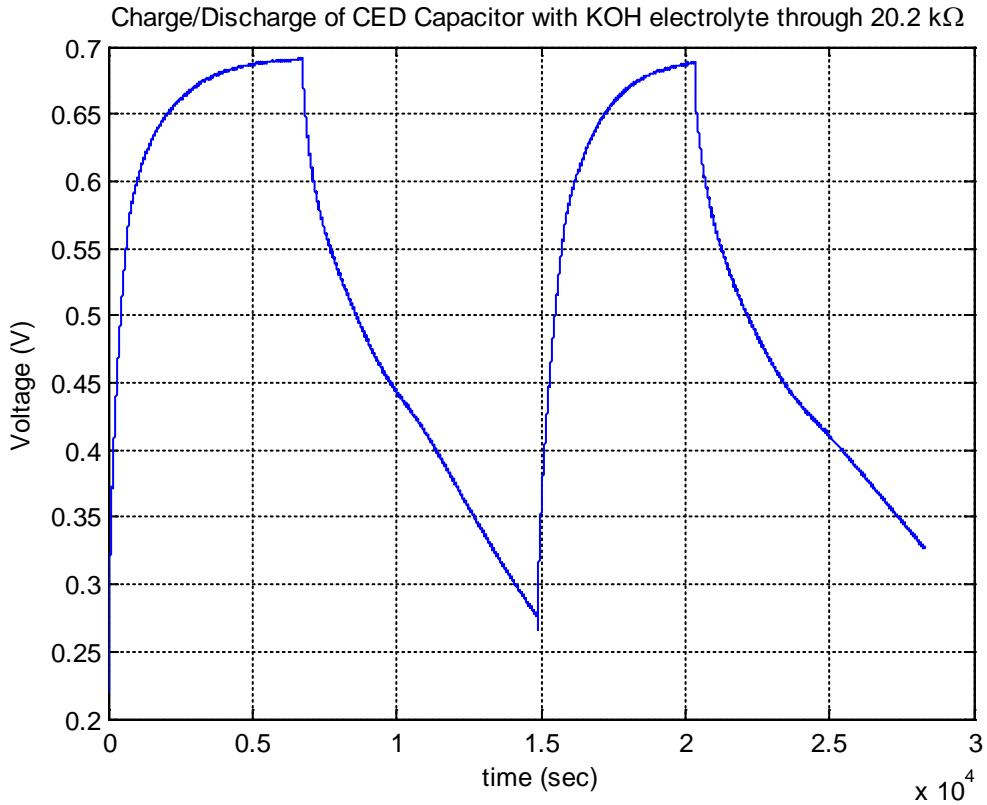
Figure 47.   Charge/Discharge Cycles of 20% Volume Load with 2x Treated Nickel KOH
Electrolyte CED Capacitor through 20.2 kΩ

It can be seen that the ultimate voltage of the capacitor is very limited. The CED capacitors using boric acid electrolyte generally failed to reach 25% of the charging voltage, but this iteration is even more restricted. The capacitor never reaches a voltage of 0.7 V when charged through the resistor. The separated charge and discharge characteristics are shown in Figure 48 and the parameters measured from the cycles are shown in Table 11.
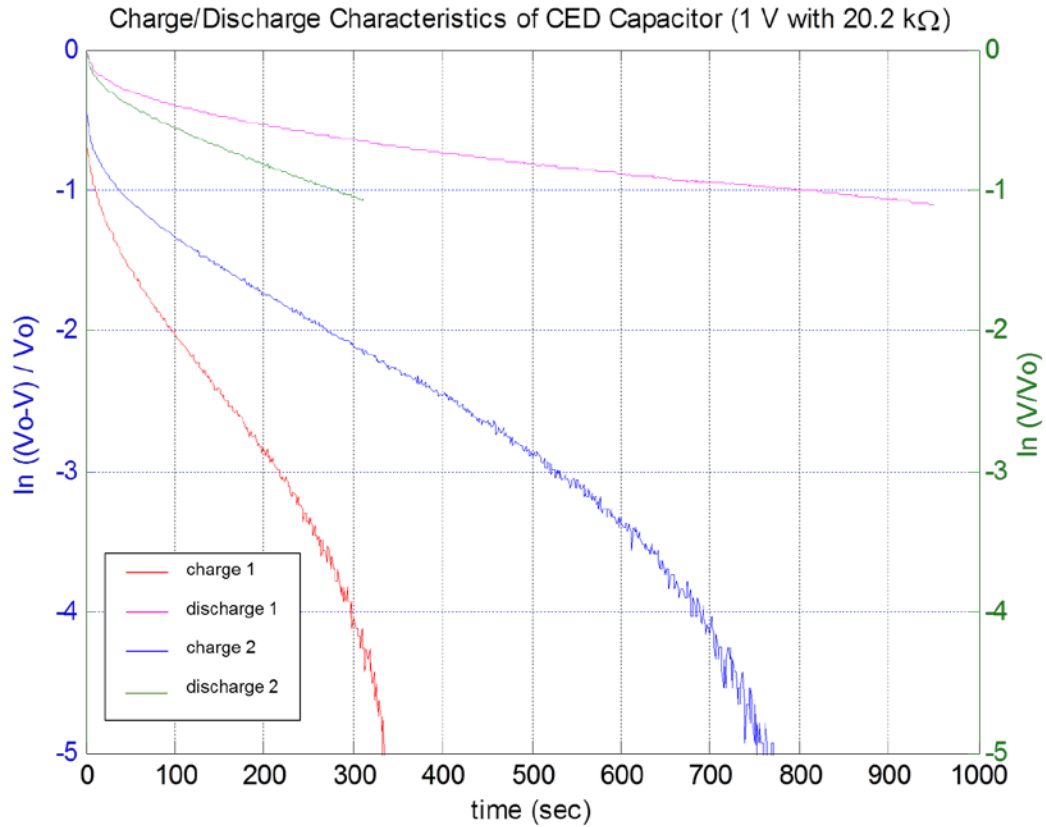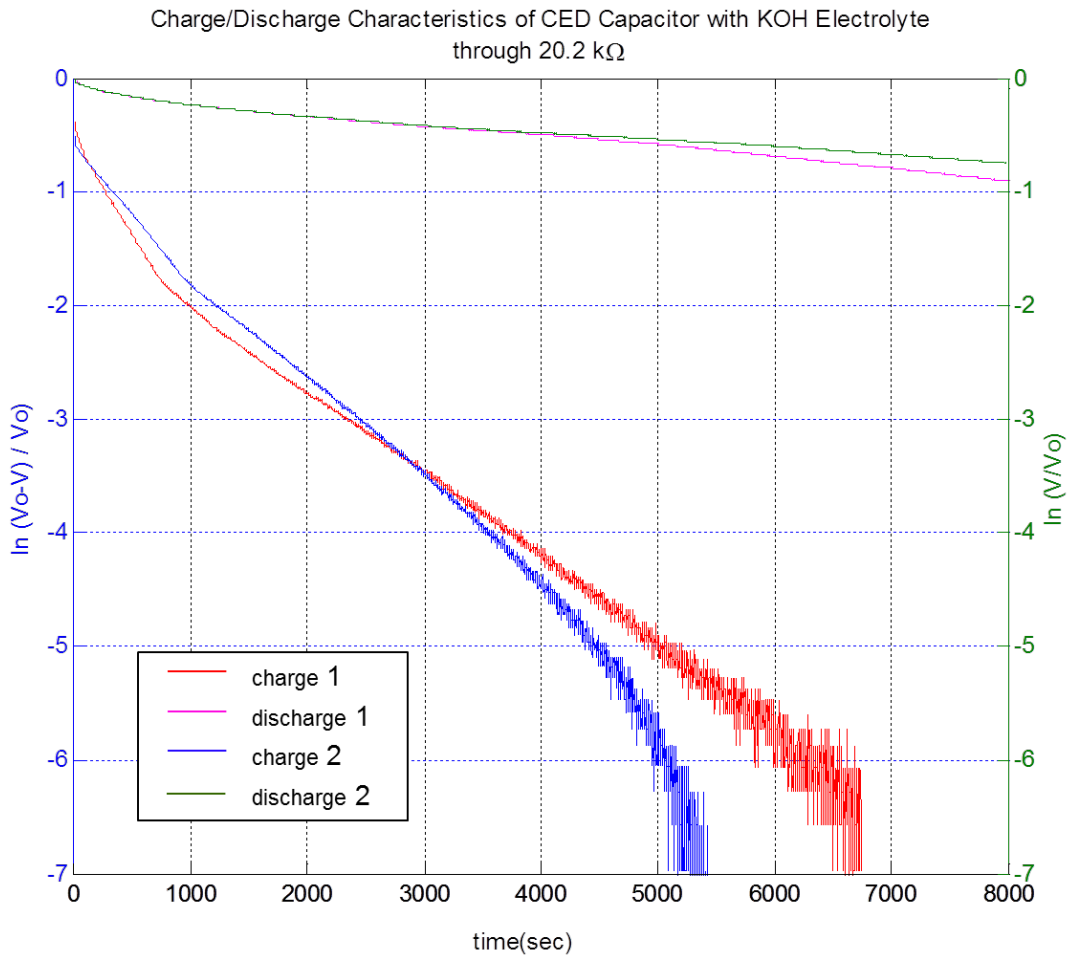
Figure 48.   Combined Charge/Discharge Characteristics of 20% Volume Load with 2x
Treated Nickel KOH Electrolyte CED Capacitor through 20.2 kΩ

The charge and discharge characteristic curves are stable, with relatively little initial lag in reaching a constant capacitance. Also of note, both charge curves exhibit a distinctive corner in the characteristic coinciding with a voltage of approximately 0.57 V. The cause of this abrupt shift in capacitance is not understood, but was consistent over both charges at the same voltage.

75

	Operating Voltage Range	Dielectric Constant (ε_R) over Operating Voltage	Dielectric Constant (ε_R) over Entire Range
Charge 1	0.60 – 0.68 V	6.42E9	4.91E9
Charge 2	0.58 – 0.67 V	5.50E9	4.42E9
Discharge 1	0.56 – 0.31 V	4.89E10	3.91E10
Discharge 2	0.54 – 0.38 V	6.19E10	4.40E10

Table 11.   Charge and Discharge Data for 20% Volume Load with 2x Treated Nickel KOH Electrolyte CED Capacitor Cycled with 20.2 kΩ Resistor

The data show that the dielectric constants for dielectrics using KOH electrolyte are consistently higher than those dielectrics with boric acid. However, the voltage is also notably lower.

IV.   CHARACTERIZATION

A.   X-RAY DIFFRACTION (XRD)

1.   Method Description

X-Ray diffraction (XRD) is used to determine the crystal structure of a specimen. This can be used to determine composition of a material by comparing the measured parameters of the specimen crystal structure with a database of known materials. The process of XRD analysis consists of passing current through an X-ray tube to a metal source. As inner valence electrons of the metal source are knocked out, outer valence electrons drop to a lower energy level and X-ray radiation is emitted. X-rays are directed to irradiate the sample specimen, and are diffracted according to the arrangement of crystallographic planes in the sample. The number of diffracted X-rays is counted across a range of diffraction angles, or 2-θ angles. The resulting spectrum indicates the crystallographic orientation and structure spacing and can be correlated with known compositions.

A Philips 1830 Analytical X-ray Diffractometer is used for this study. The X-ray tube uses a copper source with primary K_α wavelength of 1.54 Å. The range of 2-θ angle studied is from 25 to 90 degrees. The step size increment is 0.02 degrees, and the time at each step is one second. The nickel powder samples are placed on a low-background silicon plate to prevent interference in the range of analysis. The current is set to 30 mA and the voltage is set to 35 kV.

2.   Analysis

The nickel powder surface treatment with H_2O_2 is intended to create an insulating oxide layer. In order to characterize the resulting treated nickel particles and ascertain the existence of the insulating surface layer, XRD analysis was used to examine nickel powder before and after varying levels of H_2O_2 surface treatment. The spectrum result from the untreated nickel powder is shown in Figure 49. Using X'Pert HighScore analysis software, the spectrum is determined to match conclusively with nickel, with no significant impurities.
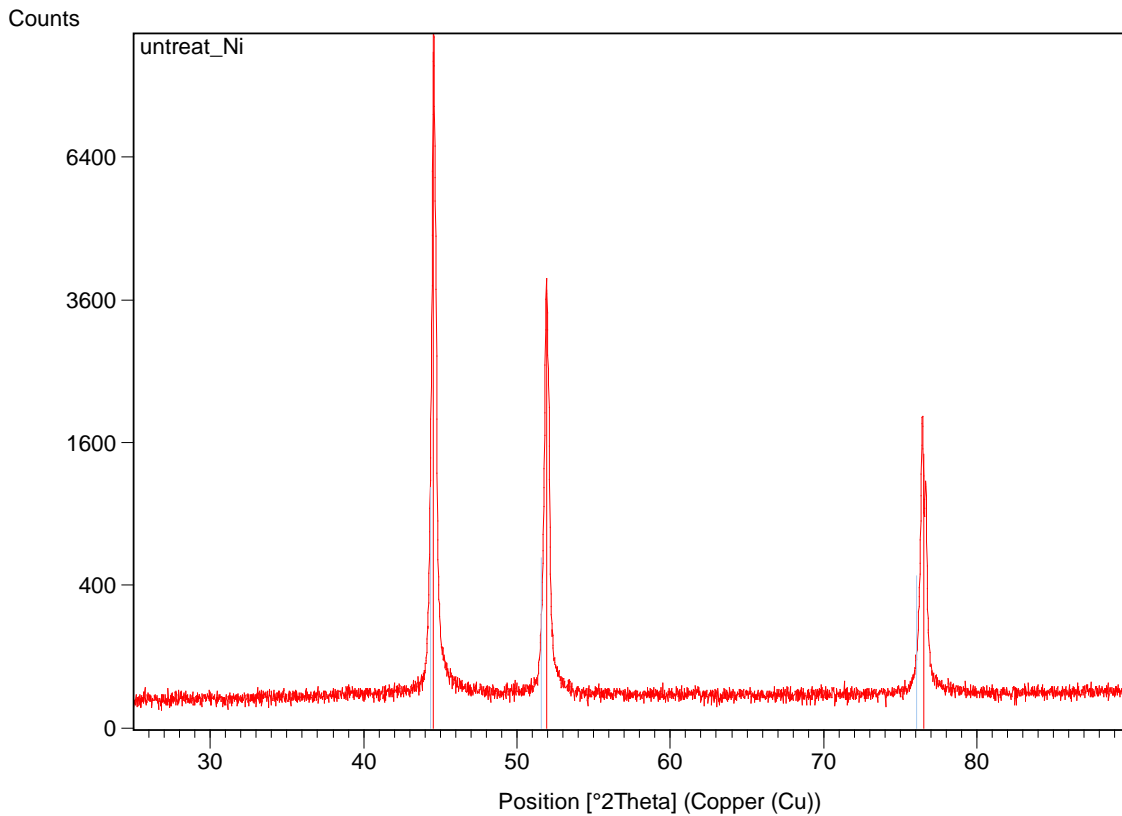
Figure 49. XRD Spectrum for Untreated Nickel Powder

Figure 50 shows the resulting spectra from one, two, and four times treated nickel superimposed with the untreated nickel. It is clear that there is no detectable difference in the crystal structure or composition of the different powders.
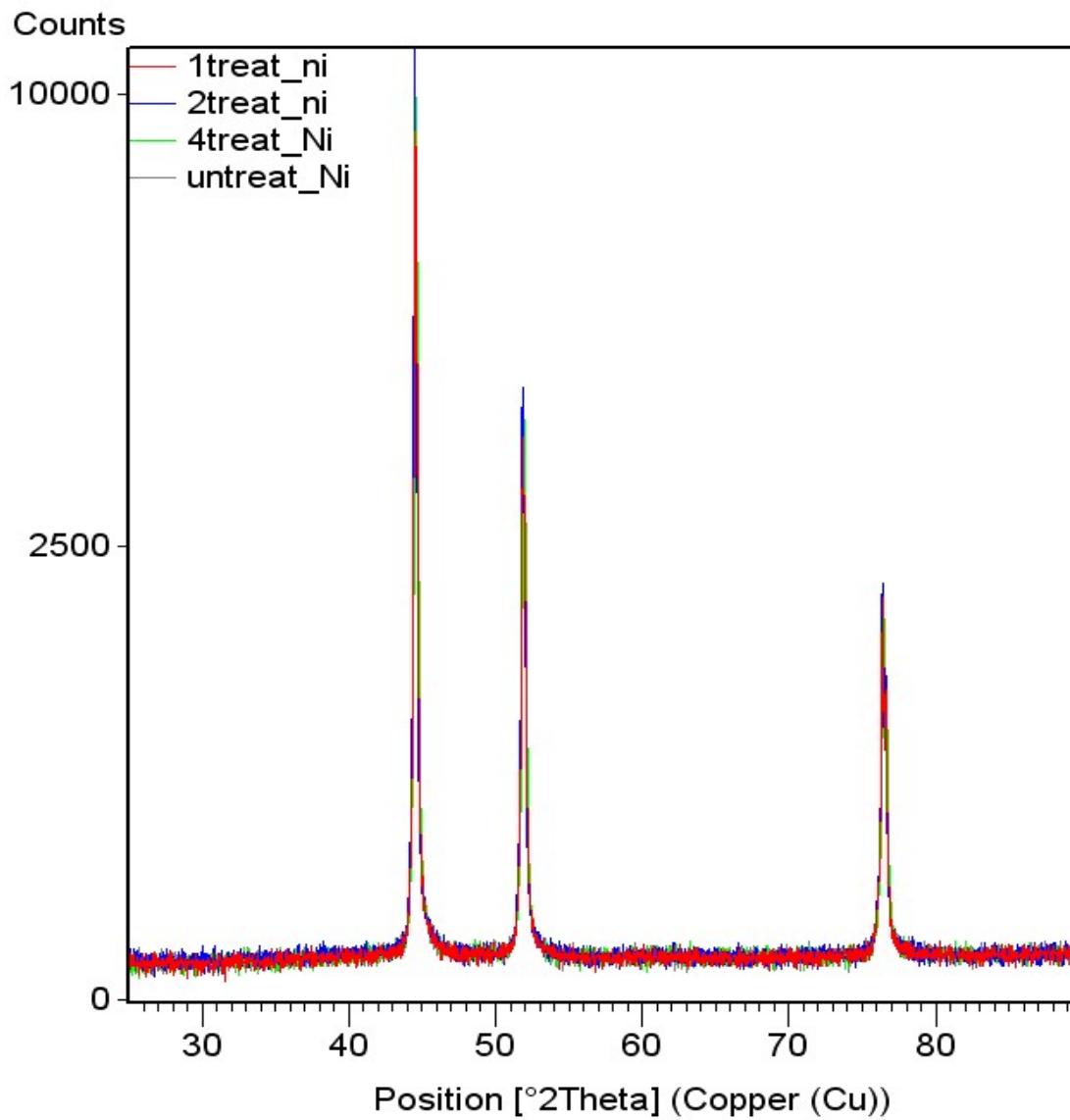
Figure 50. Superimposed XRD Spectra for Untreated, 1x, 2x, and 4x Treated Nickel Powder

Additionally, Figure 51 shows the spectrum for the twice treated nickel powder along with blue lines indicating the expected peaks associated with nickel oxide. This result demonstrates that the H_2O_2 surface treatment process does not generate an oxide phase in sufficient quantity to be detectable by XRD.
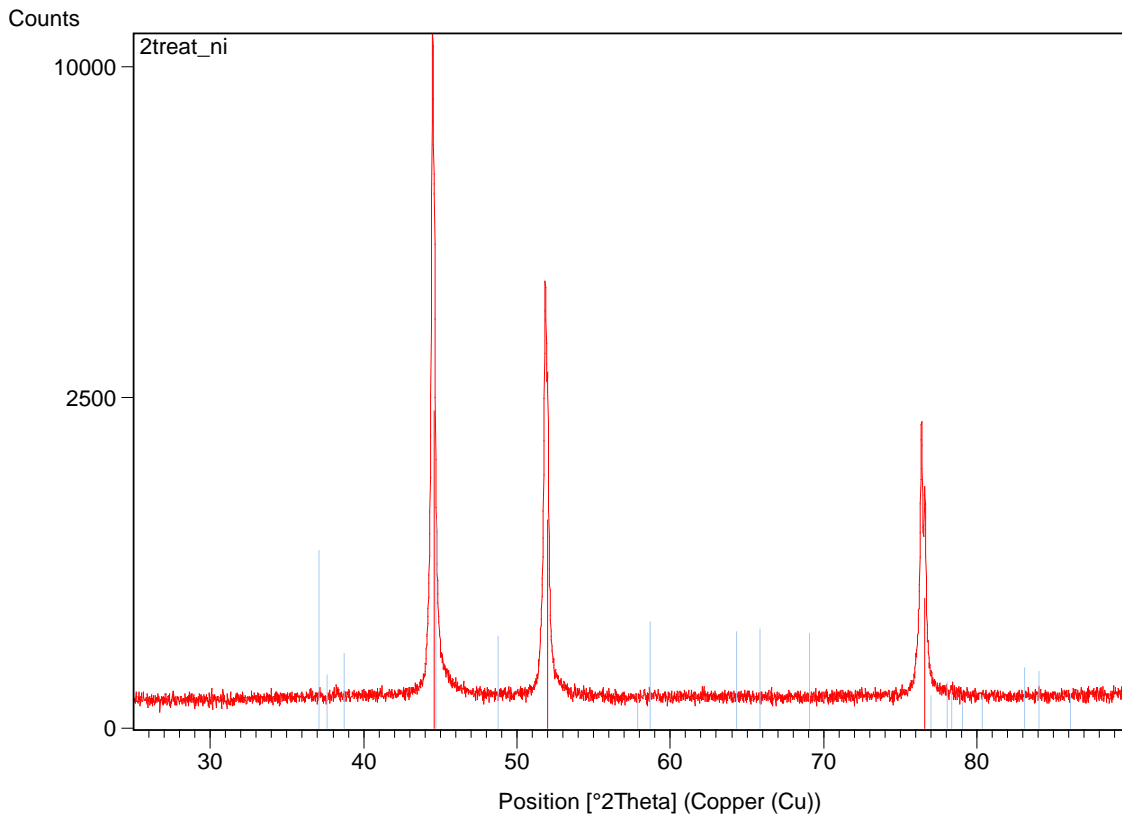
Figure 51.   XRD Spectrum for 2x Treated Nickel with Indication of Expected Nickel
Oxide Peaks

B.   SCANNING ELECTRON MICRSOCOPY (SEM)

1.   Method Description

Scanning Electron Microscopy (SEM) is used to image and examine a sample at high magnification.   A field emission gun is mounted in a column above the sample chamber and generates an electron beam, which is incident on the specimen.   The beam is generated at a specified energy level determined by an applied voltage potential, primarily 20 kV for this study.   The beam is controlled and directed by a series of lenses and electromagnetic coils and is focused on the sample.   Incident electrons are scattered, diffracted, or transmitted upon reaching the sample. Scattered electrons are collected and used to generate images of the sample surface.

Secondary electrons are also ejected from sample atoms upon incidence of the generated beam, which results in the generation of X-ray radiation as higher-energy electrons assume lower-energy states. The energy of these generated X-rays is specific to the source element from which they originated. The resulting spectrum of X-ray counts and their energies can therefore be used to determine the material composition of the sample. This process is referred to as energy dispersive X-ray spectroscopy (EDS).

In addition to using an electron beam for imaging and analysis, a focused ion beam (FIB) can also be used. Gallium ions are produced by using a tungsten filament to ionize a pool of liquid gallium. The ions produce a beam with application of a voltage potential and are focused with the same lenses and coils used for the electron beam. The gallium ions impact the surface of the sample and can mill away material with nano-scale control. This allows single particles to be cross-sectioned for analysis of surface layers and internal compositions. Varying applied voltage and current controls the energy and number of ions produced in the process, and therefore permits precision milling of the sample.

2.   Analysis

a.   Imaging

The first step in the SEM analysis comprised obtaining images of the untreated nickel powder to gain an appreciation for particle characteristics and size. Figure 50 shows a representative image of the untreated nickel powder at 500x magnification. It can be seen that the particle size is inconsistent. Smaller individual particles have diameters on the order of 10 µm, while there are many larger apparent conglomerate structures with diameters on the order of 150 µm.
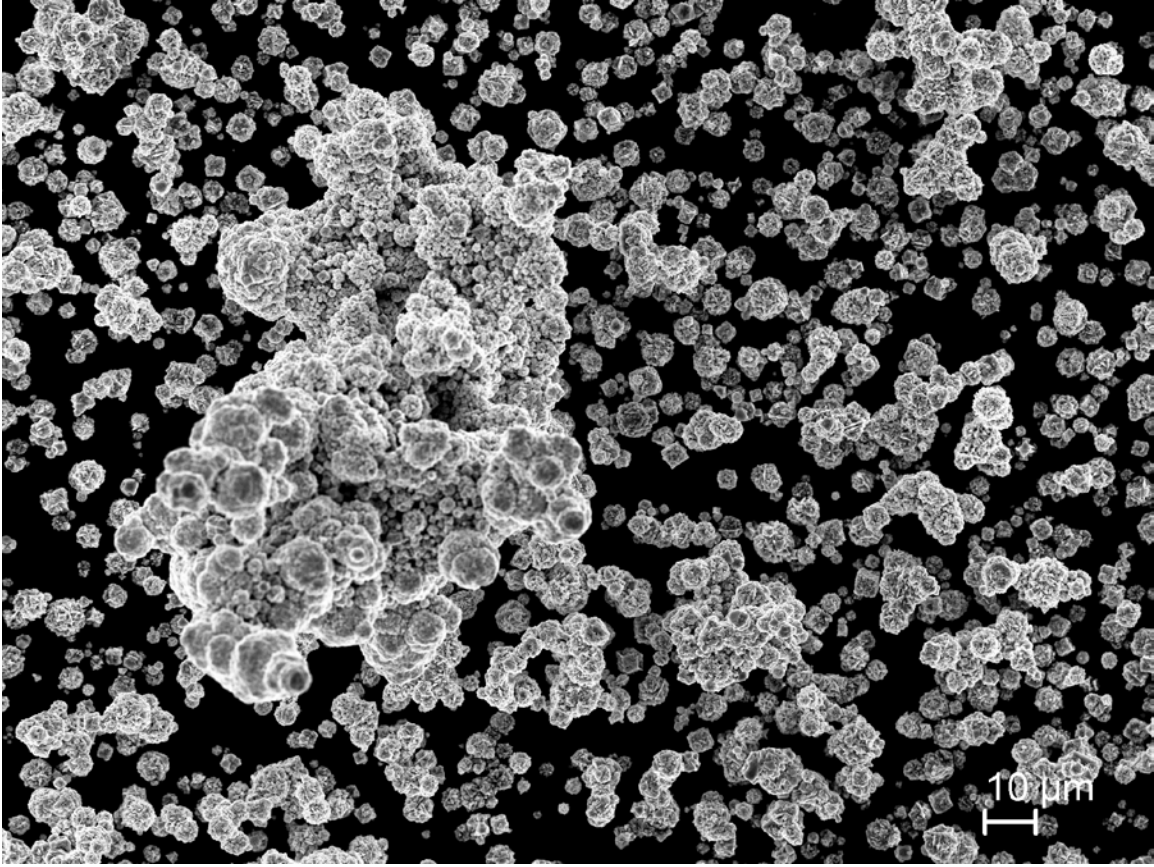
Figure 52.   SEM Image of Untreated Nickel Powder (500x)

Higher magnification images are collected to examine the nature of the particle structure and surface. Figure 53 shows a representative image of the untreated nickel powder at 5kx magnification. It shows the general shape of the conglomerate particle structures that are seemingly composed of assemblies of the smaller individual spherical particles with sharp protruding ridges.
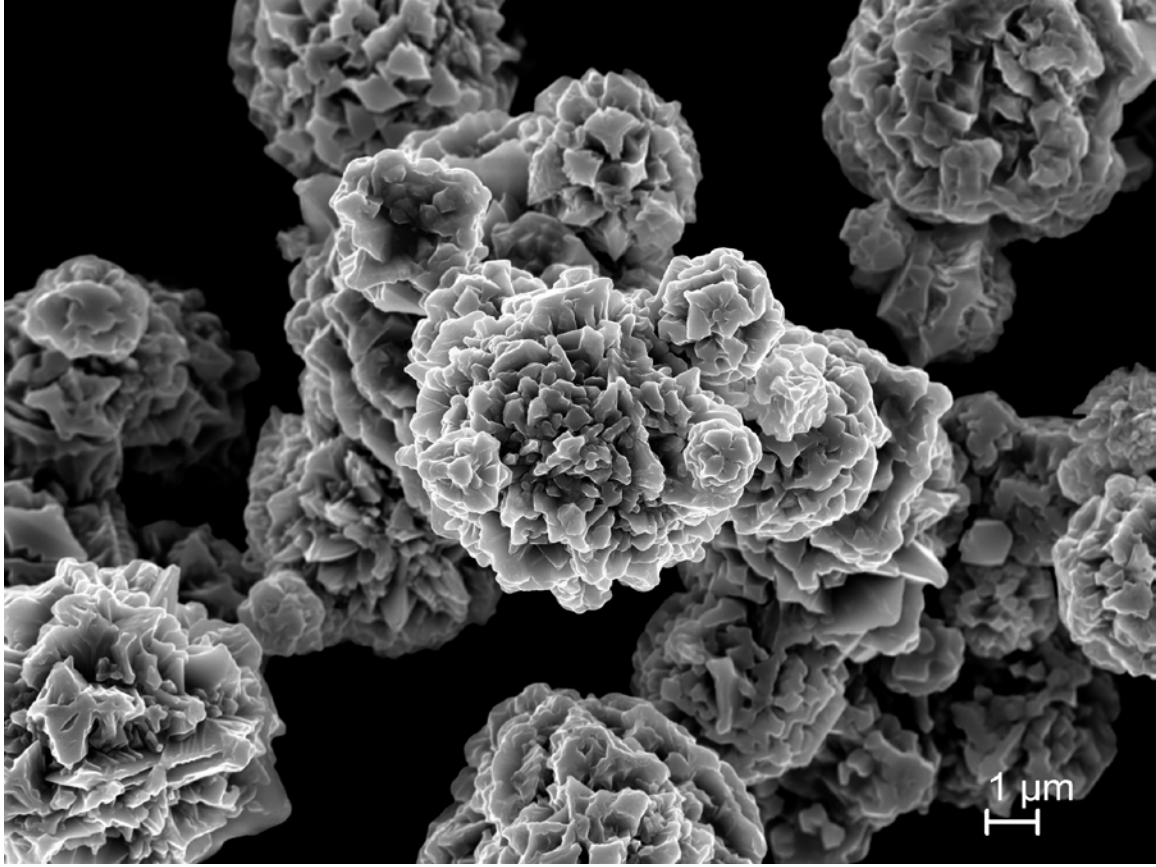
Figure 53.   SEM Image of Untreated Nickel Powder (5kx)

Comparable images are collected for particles with varying levels of surface treatment. Figures 54 and 55 are examples of the once treated nickel powder at 500x and 5kx magnifications.   It can be seen in the wide-angle image that overall appearance of the powder has not significantly changed. Large conglomerations are still present, although the largest of these appear smaller than the largest conglomerations in the untreated powder. The largest assemblies observed have diameters on the order of 100 µm.
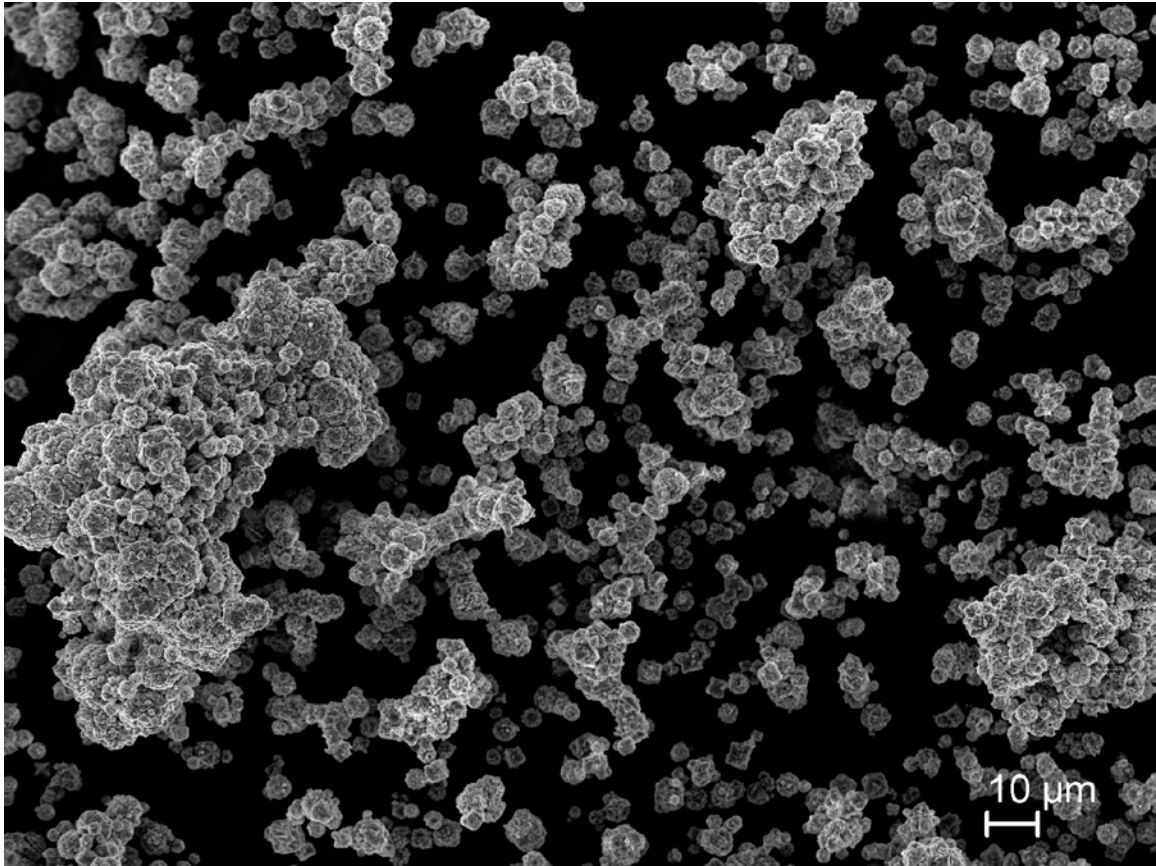
Figure 54.   SEM Image of 1x Treated Nickel Powder (500x)

The closer view in Figure 55 seems to indicate an interesting effect of the H_2O_2 surface treatment. Namely, the particle ridge protrusions appear somewhat rounded or softened compared to those seen in the untreated powder.
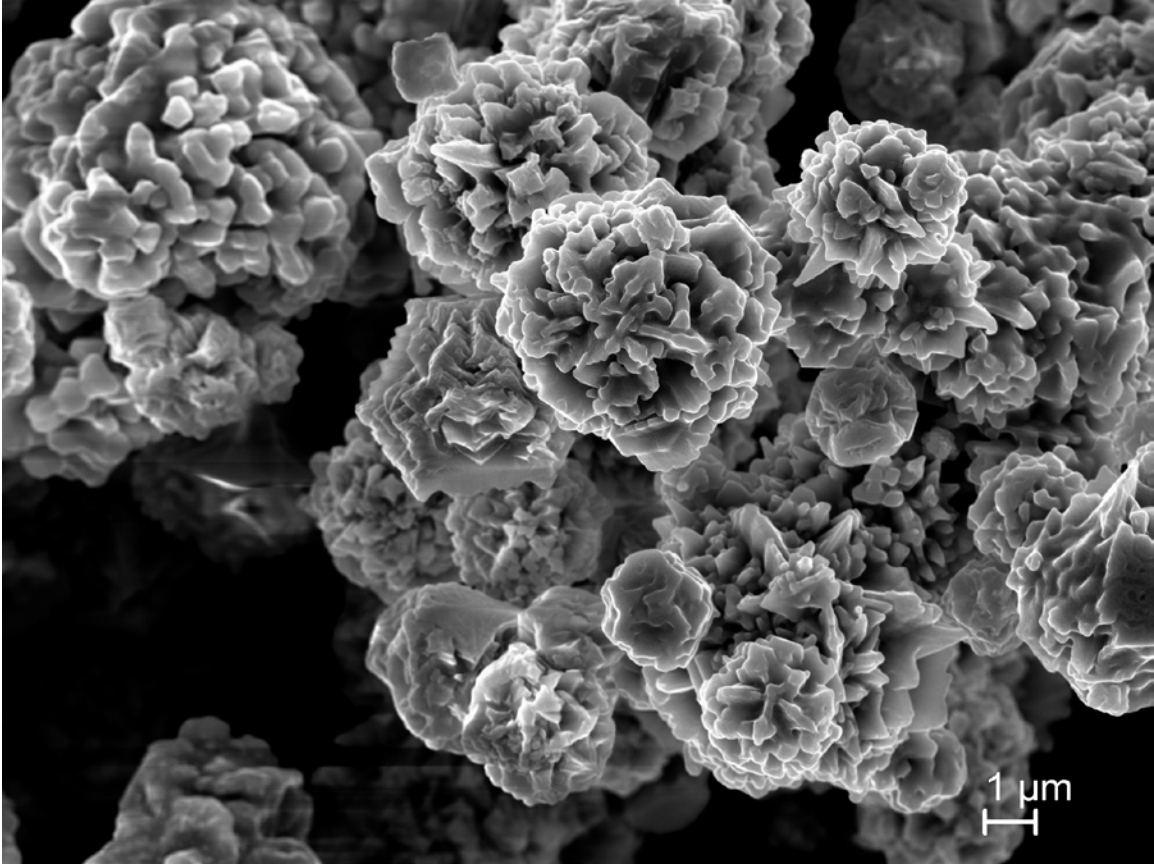
Figure 55.   SEM Image of 1x Treated Nickel Powder (5kx)

The most noticeable difference between the untreated and treated particles is only evident at higher magnifications. Carefully examining the texture of the particle surfaces shows that the roughness of the particle surface is influenced by the H_2O_2 treatment. Figure 56 shows images of untreated and once treated particles at 80kx magnification.
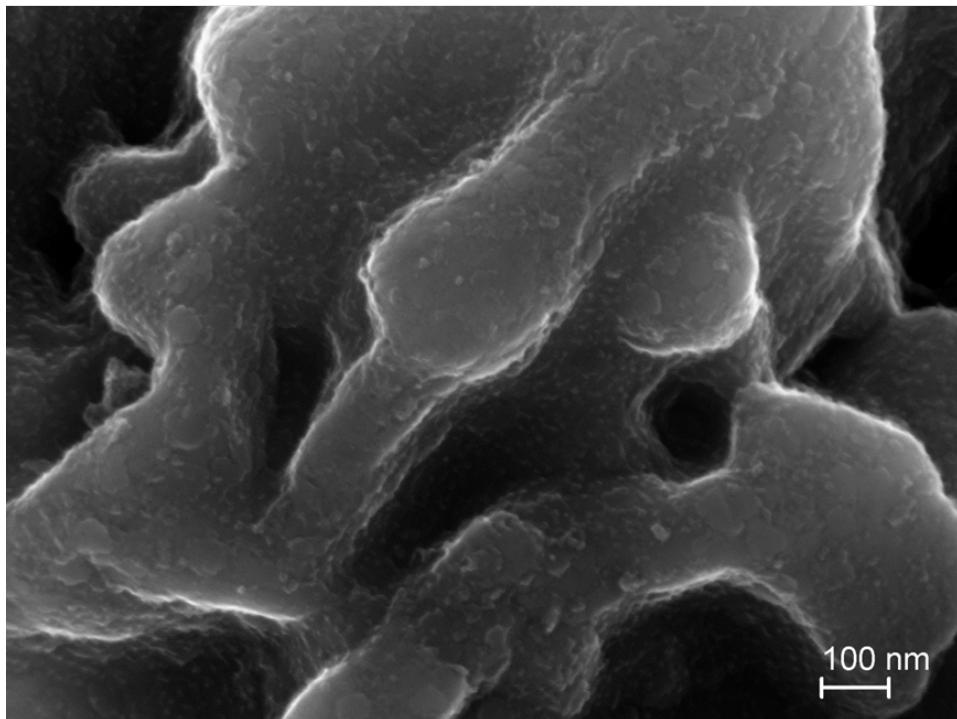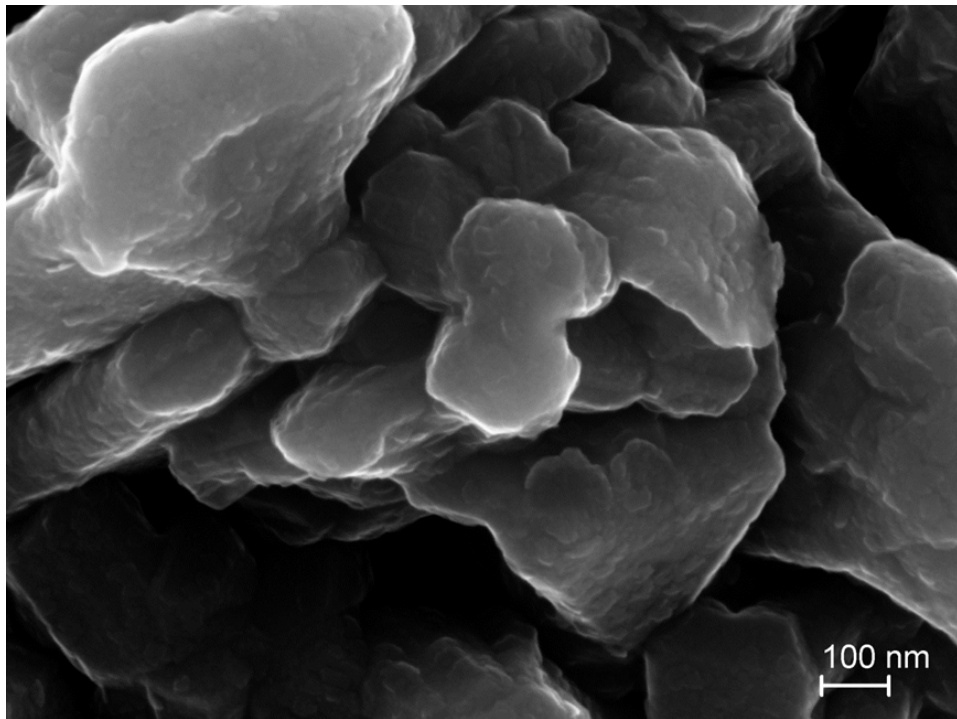
Figure 56.   SEM Images of (top) Untreated and (bottom) 1x Treated Nickel Powder (80kx)

This trend is further examined with increasing levels of H_2O_2 treatment. There is some indication of increased surface roughness with increasing treatment, but not as significant or consistent as the impact of the first treatment. Figure 57 shows images of particles after two through five treatments at 80kx magnification.
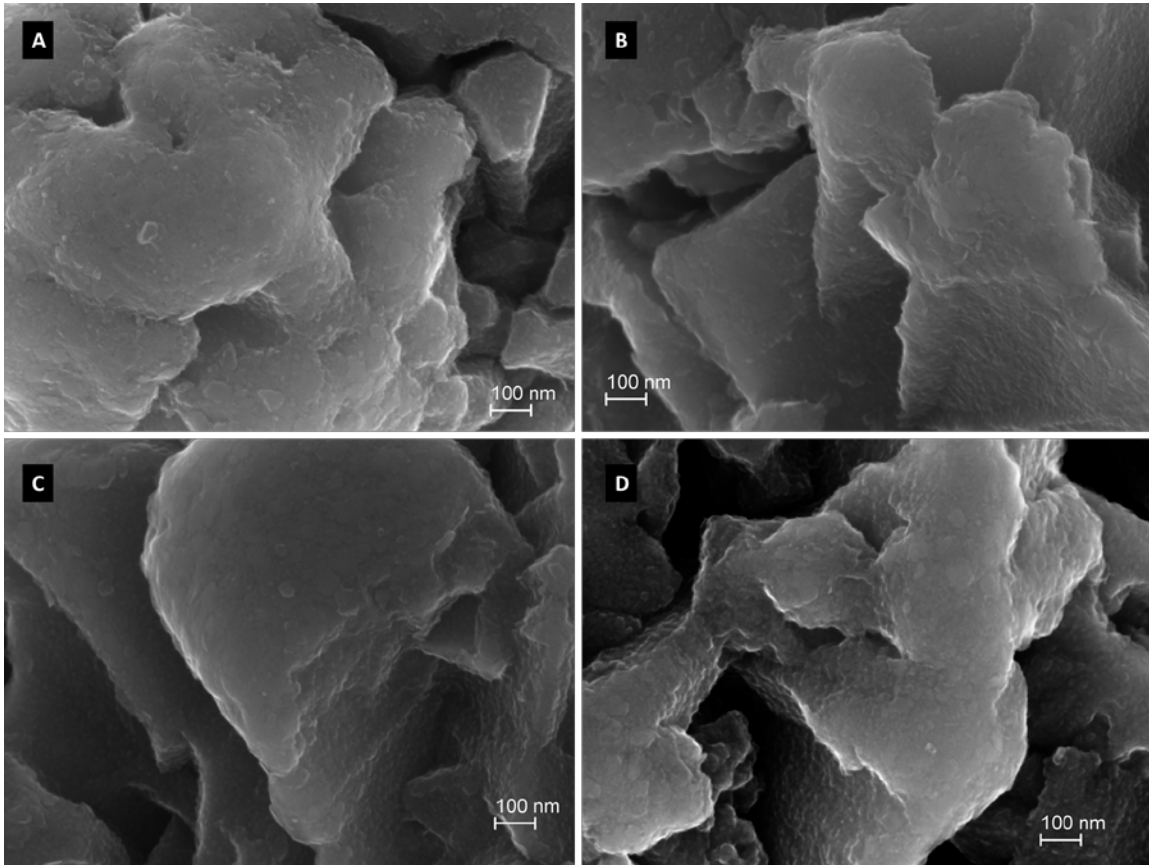
Figure 57. SEM Images of Nickel Powders (A) 2x Treated, (B) 3x Treated, (C) 4x Treated, (D) 5x Treated. (80kx)

b. *Energy Dispersive X-ray Spectroscopy (EDS)*

In addition to imaging, EDS is performed on the particles of varying treatment. Spectrums are collected over a 100 second period from an image at 30kx magnification. The resulting spectrum for the untreated nickel powder is shown in Figure 58. Using EDAX Genesis software with Peak Identification, the constituent elements are determined and labeled. It can be seen that nickel is the dominant constituent, with carbon and oxygen peaks practically absent. The source images are displayed in the inset.
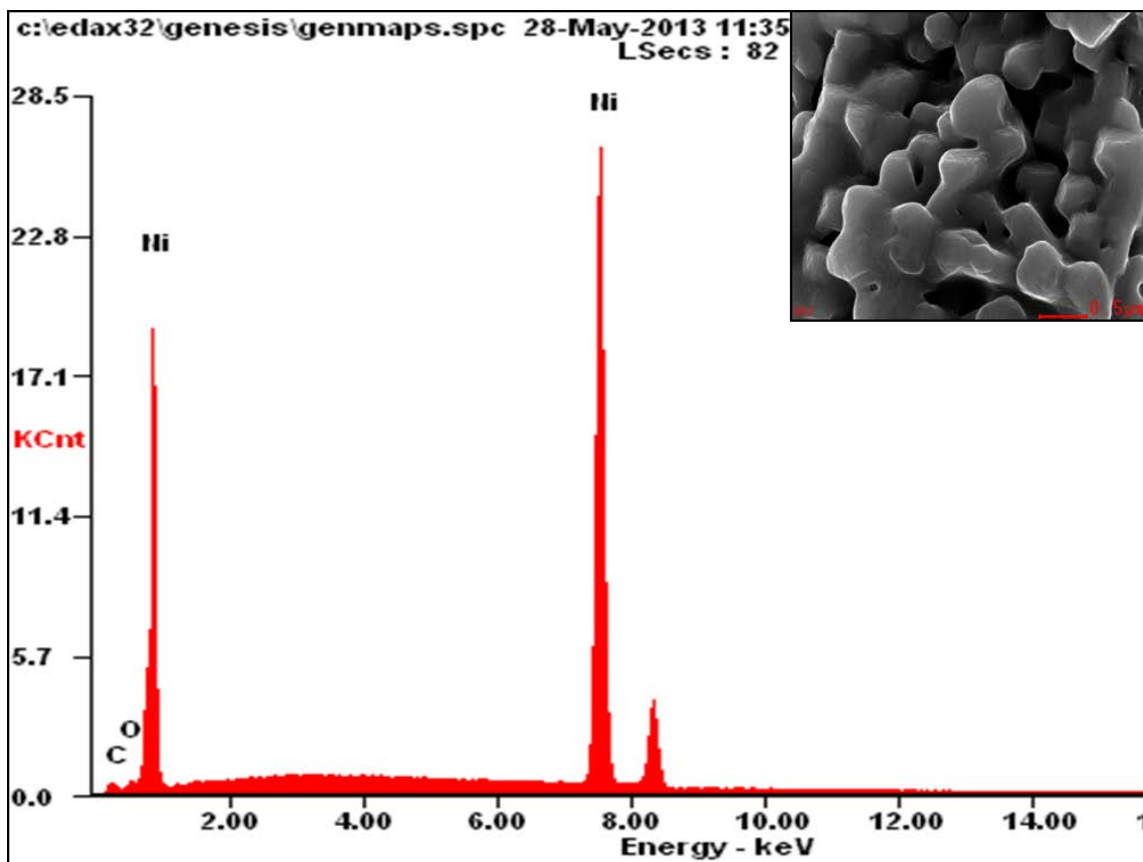
Figure 58.   EDS Spectrum of Untreated Nickel Particle (30kx)

For comparison, a spectrum is also collected from untreated powder at 1kx magnification.   Shown in Figure 59, this spectrum shows more noticeable carbon and oxygen peaks collected from the wider background, specifically the carbon tape that is used to mount the powder sample.
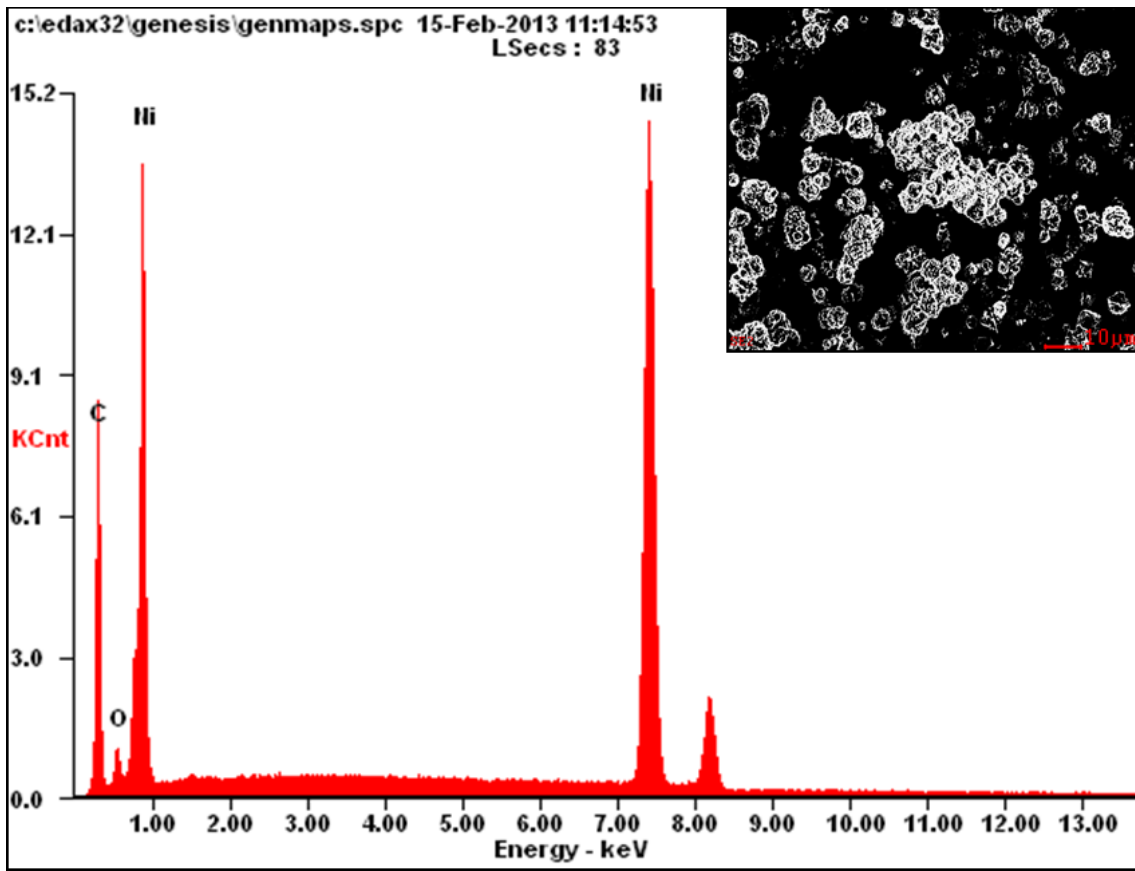
Figure 59.   EDS Spectrum of Untreated Nickel Powder (1kx)

To assess whether an insulating oxide layer is formed on the metal particles, EDS spectra are collected from treated particles. Figure 60 shows the spectrum collected from once treated nickel powder. It can be seen there is no discernible difference from the spectrum shown in Figure 58 from the untreated powder, with no appreciable oxygen peak.
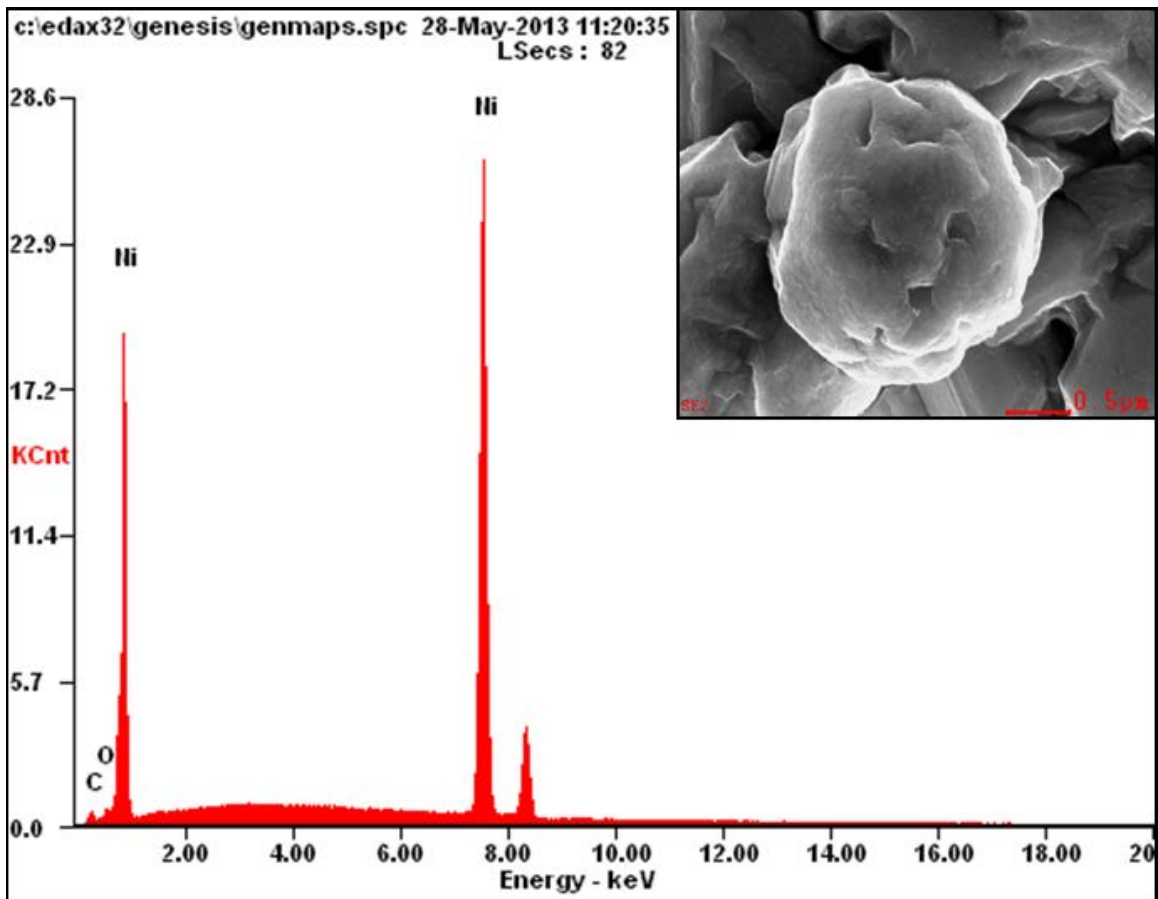
Figure 60.   EDS Spectrum of 1x Treated Nickel Particle (30kx)

Increasing levels of surface treatment additionally have no impact on the EDS analysis result. Figure 61 shows the spectra collected from twice treated and four-times treated particles. Similarly, there is no detectable oxygen peak and the spectra are practically identical to the untreated powder. As with XRD, EDS is unable to definitively detect the presence of an insulating oxide layer on the nickel particles.
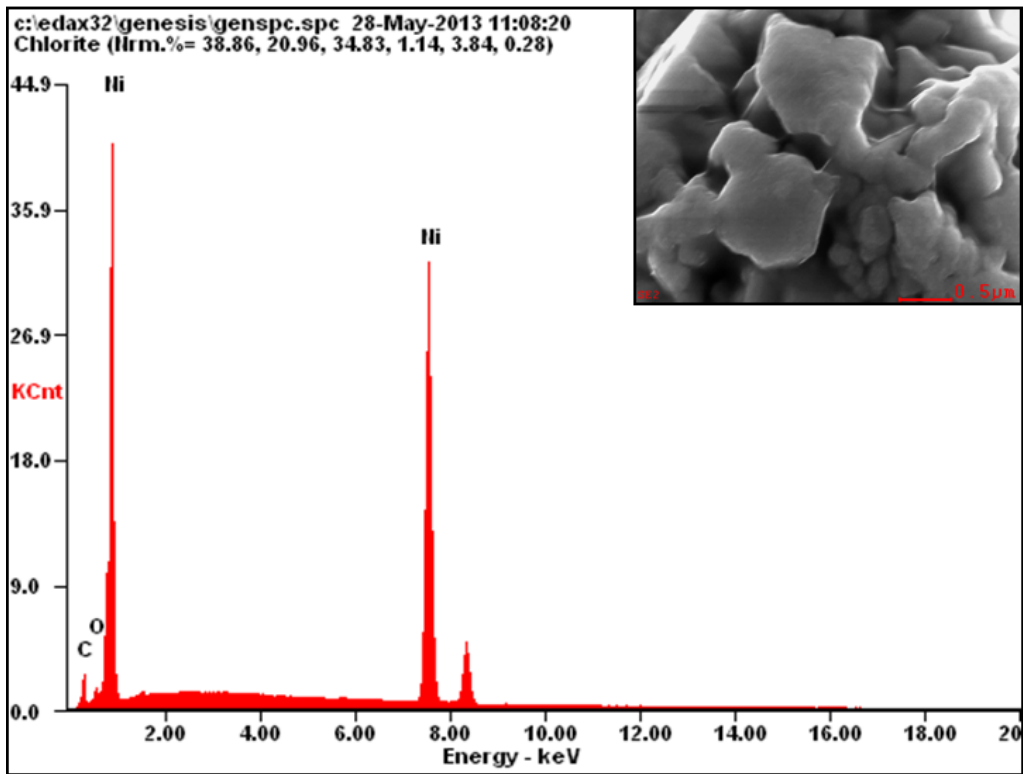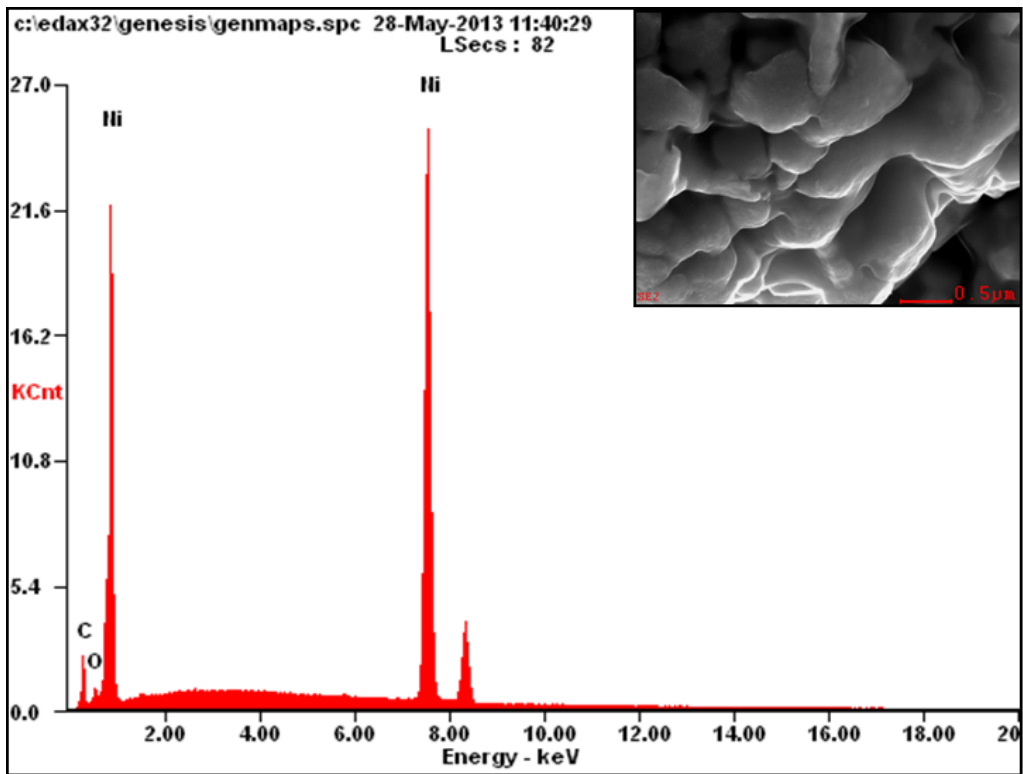
Figure 61.   EDS Spectra of (top) 2x Treated and (bottom) 4x Treated Nickel Particles (30kx)

91

c.   ***Focused Ion Beam (FIB)***

In order to more directly examine the impact of surface treatment, FIB milling was used to cross-section individual powder particles. Twice treated nickel powder produces the best results in composite dielectrics and shows evidence of substantial surface roughening by SEM imaging. Thus, the twice treated powder was selected for analysis by FIB sectioning and comparison to untreated powder.

The FIB milling is accomplished by sectioning individual representative particles from the untreated and twice treated powder SEM samples. The first pass was performed with application of 30 kV and 2 nA to mill for a depth of 4 µm. A second polishing pass was performed with application of 30 kV and 200 pA to mill an additional 1 µm for a net depth of 5 µm.

The resulting sectioned particle of untreated powder is shown in Figure 62 at a magnification of 5kx. Some internal grain structure is visible on the polished surface. The protruding ridges seem to be extensions of individual grains in a particularly uniaxial direction, which is notably off angle from the vertical cutting direction.
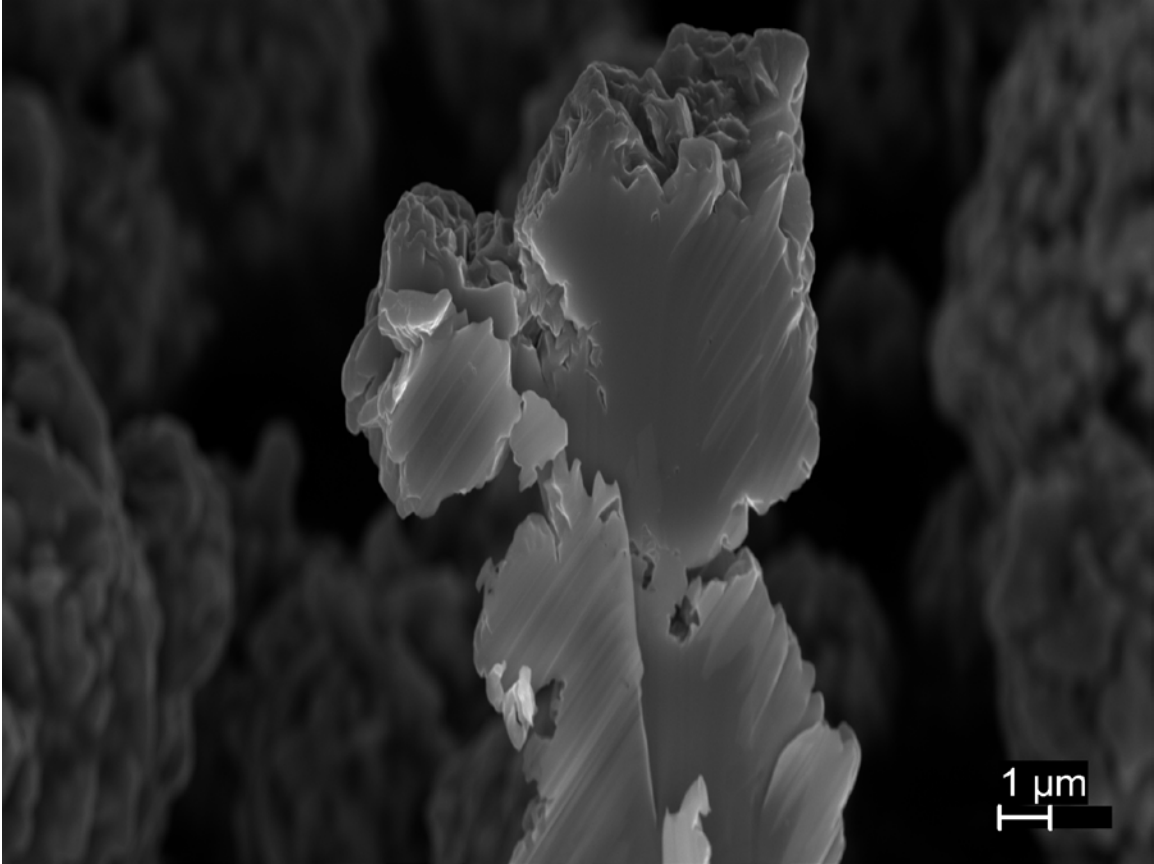
Figure 62.   SEM Image of Untreated Nickel Powder after FIB Sectioning (5kx)

A closer look shows the seamless transition between the polished cut surface and the textured outer particle surface. Figure 63 shows the edge of the sectioned particle at 30kx magnification.
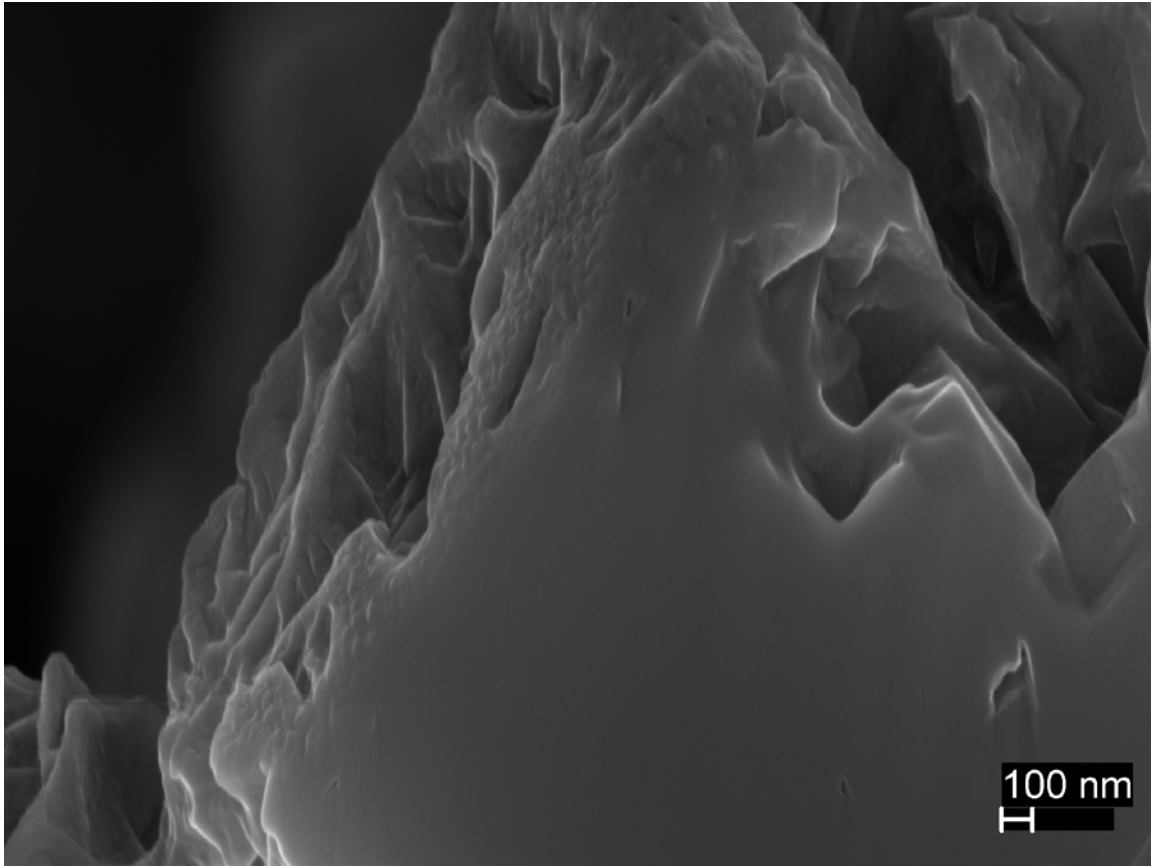
Figure 63.   SEM Image of Untreated Nickel Powder after FIB Sectioning (30kx)

The sectioned particle of twice treated nickel powder is shown in Figure 64. The same long uniaxial grain alignment is observed leading to protruding surface ridges.   There is no obvious indication of a unique surface layer encapsulating the particle.
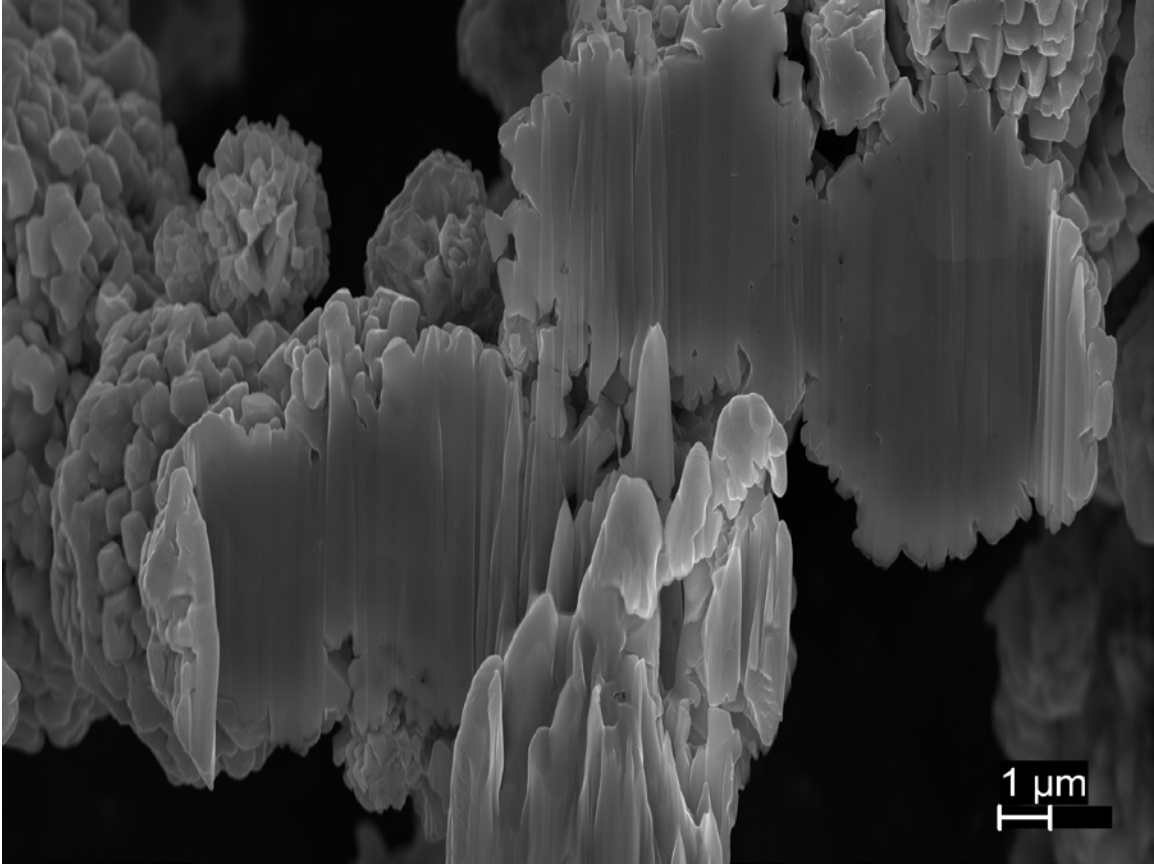
Figure 64.   SEM Image of 2x Treated Nickel Powder after FIB Sectioning (5kx)

Figure 65 further examines the edge of the particle surface and polished cut face.   At 30kx and 80kx magnification, there is also no indication of a uniquely structured surface layer.
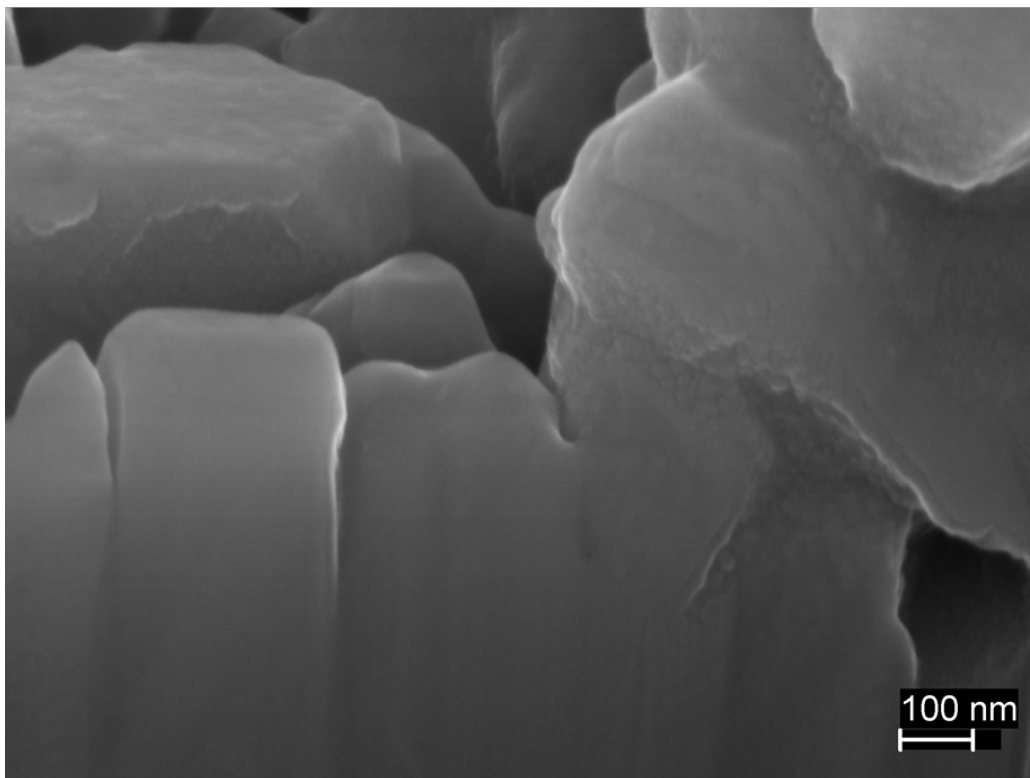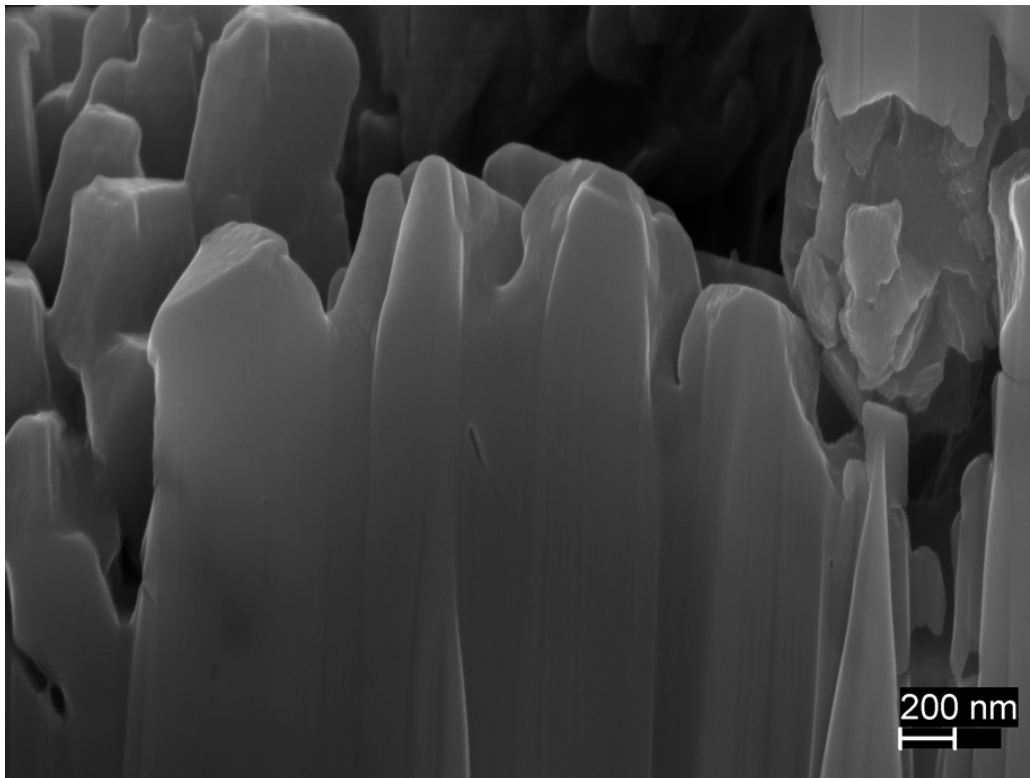
Figure 65.   SEM Images of 2x Treated Nickel Powder after FIB Sectioning (30kx top, 80kx bottom)

After sectioning of the treated particle, EDS spot analysis is conducted to compare the spectra collected from the core and the surface of the particle. This process provides another observation of the absence of any compositionally unique surface layer. The resulting spectra are shown in Figure 66.
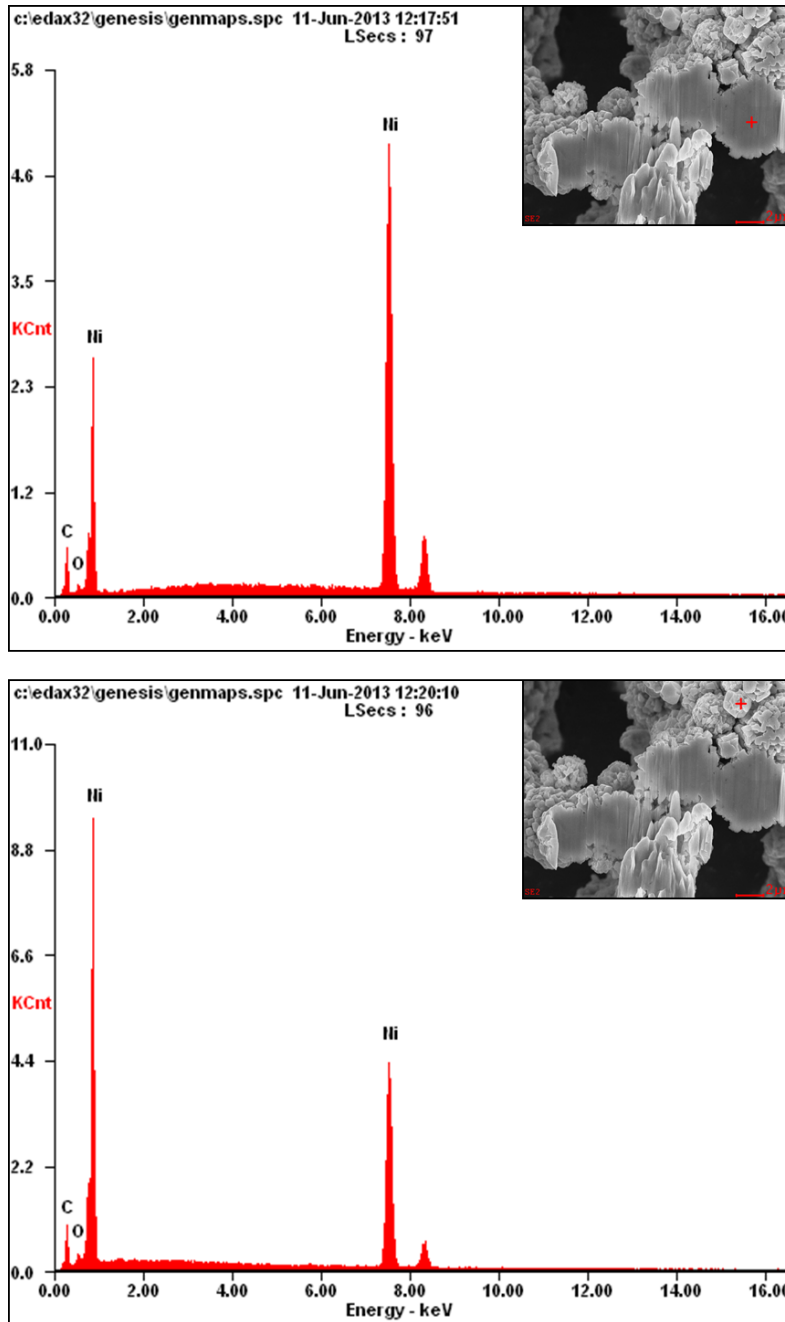
Figure 66.   EDS Spectra from FIB Sectioned 2x Treated Particle (top) Core and (bottom) Surface (5kx)

In summary, efforts by XRD, SEM imaging, EDS, and FIB sectioning were unable to identify the existence of an insulating oxide layer on the nickel particles. Despite this negative result from characterization techniques, there is a measurable difference in treated and untreated powders both in terms of resistance and dielectric performance.

C.   RESISTANCE

As described is Chapter II, Section B.3.b with the voltage divider circuit shown in Figure 15, resistance checks are performed on untreated and treated nickel powders. The measured resistance and applied voltage results for powders of varying treatment are shown in Figure 67 on a log plot. Each powder is measured at least three times in the voltage divider circuit and the values are averaged for each applied voltage. The complete results are included in the Appendix.
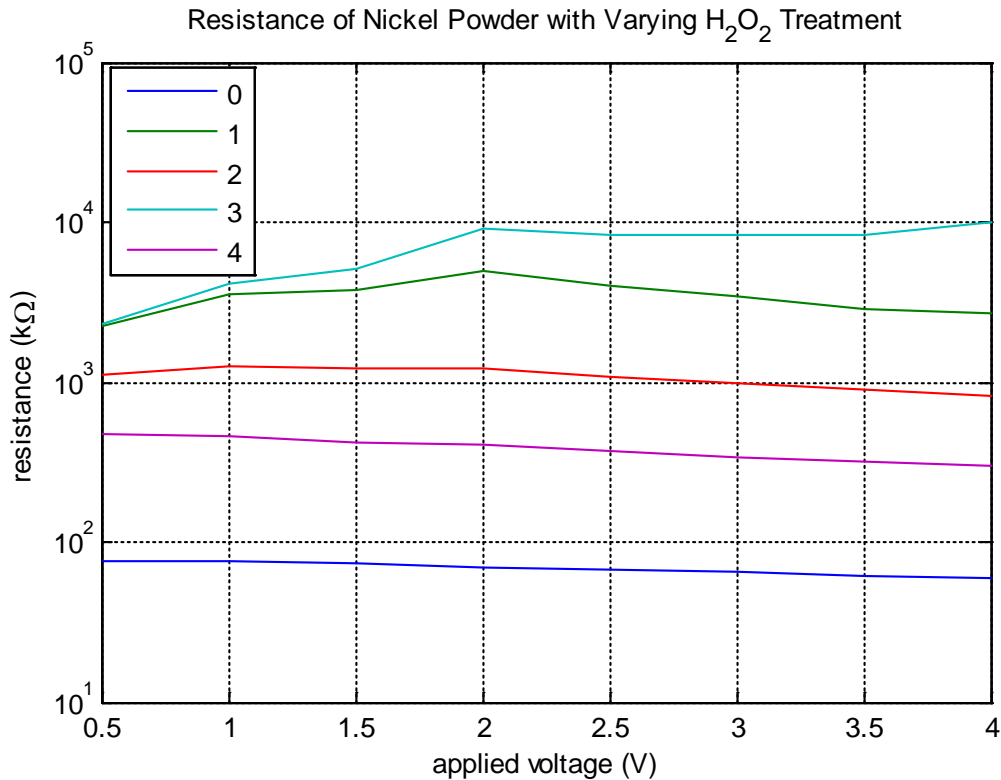
Figure 67.   Resistance of Nickel Powder with Varying Levels of H_2O_2 Surface Treatment

It can be seen that the untreated powder exhibits low resistance, less than 100 kΩ on average across the range of applied voltage. After one, two, and three treatments, the powder consistently exhibits resistance of at least 1 MΩ. Notably after a fourth treatment, the resistance drops off to approximately 400 kΩ. This effect suggests that excess treatments may lead to breakdown or spalling of any supposed insulating layer.

D. SUMMARY

A range of characterization efforts were not able to definitively establish the existence of an insulating oxide layer. The specific impact of the H_2O_2 surface treatment process is not well-known. SEM imaging revealed indications of particle surface roughening. Tellingly, resistance measurements demonstrated the remarkable insulating capacity of nickel powder after just one H_2O_2 surface treatment. The impact of surface treatment is also demonstrated in the ability to load treated nickel particles in higher volume fractions in composite capacitor dielectrics.

THIS PAGE INTENTIONALLY LEFT BLANK

V. DISCUSSION

A. OBSERVATIONS AND APPLICATION

There are a number of notable findings in this study. First, it was shown that dielectric constants achievable by using the MMD method can be orders of magnitude greater than those of single material dielectrics. Second, a new CED configuration of the MMD concept was developed. Third, this class of composite dielectric was shown to have exceptional dielectric constant, but suffered from limited maximum voltage. Fourth, it was shown that obstacles associated with loading percolation-limited conductive particles in high volume fractions can be overcome. Furthermore, it is suggested that although the concept of loading conducting, high-permittivity particles into dielectrics is established, the physics associated with composite dielectric behavior near the percolation threshold is not well understood.

The application of the treated metal particle MMD concept is observed in the measured dielectric constant. A CED composed of a wetted mixture of alumina, boric acid, and treated nickel powders demonstrated a dielectric constant on the order of 10^{10}. The capacitor is verified to function consistently over multiple cycles at voltages around 1 V.

B. UNPRECEDENTED DIELECTRIC CONSTANTS

The single material with the highest observed dielectric constant is $BaTiO_3$, with reported values of order 10^4 depending on purity and grain size [24]–[26]. In contrast, dielectric constants of 10^{10} are demonstrated by MMD materials in the CED configuration examined in this study. The performance was verified by repeated voltage cycling of capacitors. This finding is consistent with the hypothesis that surface-insulated conductive materials should be superior capacitor dielectrics.

It is further emphasized that the devices produced herein are not supercapacitors, but standard electrostatic capacitors. Supercapacitors leverage extreme electrode surface areas to produce exceptional capacitance. Therefore, they can exhibit increasing capacitance with greater volume and thickness. This is not true with electrostatic capacitors that behave according to Equation 2. Specifically, capacitance is inversely

related to dielectric thickness. This behavior is consistent with the CED capacitors produced in this study.

These observations support the validity of the dramatic primary finding of this study: Multi-material dielectrics in the CED configuration have dielectric constants orders of magnitude greater than any observed in single materials.

C.   OPERATING VOLTAGE LIMITATIONS

Operating voltages of the MMD-CED dielectrics are a significant limitation to the net energy density and practicality of these devices. Particularly during charge and discharge cycling, capacitors demonstrated a restrictive limitation in ultimate voltage. In isolated discharge tests, the operating voltage was limited to approximately 1.3 V. During charge and discharge cycling, discharge operating voltages were limited to approximately 0.8 V. In all cases in this study, the ultimate voltage on CED capacitors was less than 2 V. The limitation in operating voltage is similar to that observed in supercapacitors associated with the breakdown of electrolyte.

1.   Voltage Limits in MMD

It should be considered if the root cause of the observed voltage limitation is inherent to MMD materials. Specifically, is the exceptional relative permittivity of the dielectric material inherently limited to operation below some voltage threshold? It is hypothesized here that the voltage limitation is the result of other constituent elements of the composite. In particular, it is argued that in the CED configuration, the discharge occurs through the liquid electrolyte phase rather than the MMD component. Thus, the voltage limit should be a function of electrolyte chemistry and capacitor thickness, implying higher voltages and energy densities are achievable.

A series of observations support the concept of discharge occurring through the liquid electrolyte phase. First, the voltage limit was impacted by the use of an alternate electrolyte. Employing KOH as the aqueous electrolyte limited the maximum operating voltage to approximately 0.7 V, while capacitors with boric acid electrolyte operated with high permittivity up to approximately 1.3 V. This is evidenced in Tables 5, 10, and 11.

The impact of electrolyte chemistry on operating voltage is well documented in supercapacitors, and remains a research focus area [4], [18], [21]. Second, the voltage limit appears to be related to the dielectric layer thickness. Although not specifically evaluated in this study, the general trend is noticeable in the data from Tables 7, 8, and 9 that the operating voltage tends to increase with increasing dielectric thickness. This suggests the discharge limit is a function of the voltage gradient, which is supported by the dependence of breakdown voltage on the electrolyte resistivity [51].

It is important to point out that while it is suggested that increasing dielectric thickness could lead to increased operating voltage, this does not directly result in increased energy density. This concept was previously discussed in Chapter III, Section B.3.a and illustrated in Equation 6. Specifically, energy density is proportional to the voltage squared, and inversely proportional to thickness squared. Therefore, any gain in voltage must outpace increases in thickness.

2.   Dielectric Loss and Relaxation

The initial drop in voltage on discharge for all capacitors tested could be related to the concepts of dielectric loss or dielectric relaxation. In an ideal capacitor, all of the energy added and stored in the electric field can be recovered. In reality, all of this energy is not fully recoverable. These factors are well documented in AC capacitor applications.

Dielectric loss is related to the energy that is lost to dielectric heating during switching of applied electric field polarity as charges must overcome opposition in their displacement through the dielectric. This factor is related to the equivalent series resistance (ESR) of a capacitive element and is a function of the complex nature of permittivity [52]–[53].

Similarly, dielectric relaxation refers to the delay observed before a constant dielectric constant is reached upon switching the polarity of an applied electric field. This factor is also related to the complex definition of permittivity [52]–[53].

This study considered only performance in DC circuits. It is suspected that upon initial switching in charging and discharging, the influence of dielectric loss or relaxation is particularly pronounced with the CED capacitor. A full frequency analysis is required to characterize the ESR of a CED capacitor and determine the influence of complex loss or relaxation on the observed dielectric constant.

It is also interesting to note that the commercial capacitor demonstrated non-ideal performance aspects. Specifically, during charging cycles the capacitor did not fully reach the applied charging voltage as shown in Figures 23 and 34. Additionally, the charge and discharge characteristics shown in Figure 35 demonstrate significant non-linearity. These points reinforce that even standard commercial capacitors regularly exhibit non-ideal behavior.

D.   IMPLICATIONS FOR A THEORETICAL MODEL

A model of the MMD-CED configuration must be consistent with a number of observations from experimental results, including:

- unprecedented dielectric constants of the electrolyte capacitors without nickel loading,

- orders of magnitude increase in dielectric constant observed with the addition of metal particles, both treated and untreated,

- limited maximum voltage,

- the impact of electrolyte on the observed maximum voltage,

- the relation between dielectric thickness and observed maximum voltage, and

- the finding that metal particle addition increases the observed operating voltage.

A qualitative appreciation for these observations is presented in the following model. Further work will be required to develop a fuller, more rigorous construct.

It is theorized that various mechanisms of capacitance are active in the CED. One of these mechanisms is the previously described high polarizability of conductive material that permits a thorough redistribution of charge within individual metal particles. This supports the definitive increase in dielectric constant observed with the addition of nickel powder to the CED. A second mechanism which may be active is a kind of

double-layer capacitance similar to that observed in electrochemical systems. Specifically, high surface area alumina powder used as the base dielectric ceramic matrix provides a large available surface area for engagement of charged particles in the electrolyte material. Hydroxyl charge groups present on the surface of the alumina particles are available to hydrogen ions in the acid electrolyte. This arrangement permits formation of dipoles at the surface of the alumina particles, and may account for the remarkable capacitance observed in the pure electrolyte dielectrics noted in Table 3. The geometry is illustrated in Figure 68.
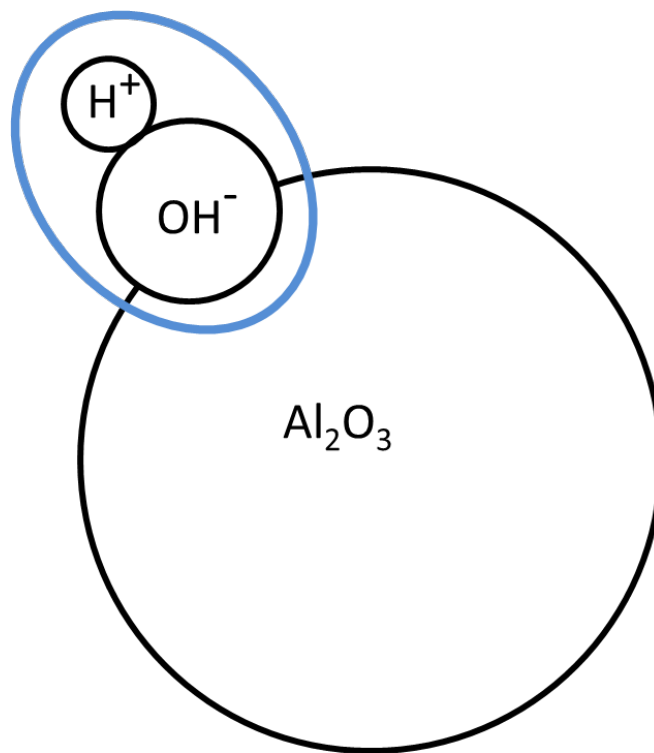
Figure 68.   Model of Alumina Particle with Dipole Pair

However, these hydrogen ions in the electrolyte composite also present a potential path for charge break down with sufficient applied potential. Alumina and metal particles do not completely occupy the volume of the dielectric. Space between these particles can be filled with aqueous electrolyte, permitting the flow of charged ions through the acid between electrodes. This concept is depicted in Figure 69, with metal particles omitted for clarity.
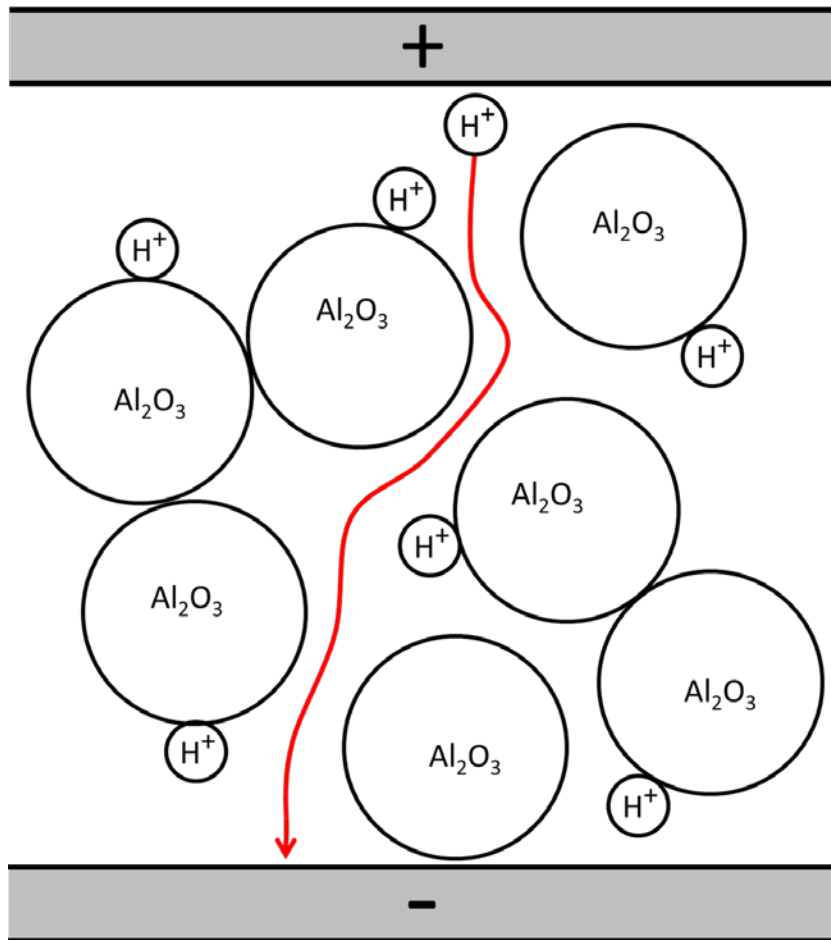
Figure 69.   Model of Charge Flow Through Dielectric Electrolyte

This postulated model of charge storage indicates that limited operating voltage may be inherent to the use of aqueous electrolyte in the dielectric matrix. Specifically, the propensity of charges to flow through the aqueous phase of the dielectric medium is a function of the strength of the electric field, and hence the applied voltage and thickness of the layer. Increasing the thickness of the layer with constant applied voltage would decrease the strength of field, and consequently the migration of charged ions. It follows that an increased operating voltage would be permitted before breakdown.

Limited operating voltage is a challenge also faced by supercapacitors, as discussed in Chapter I, Section C.2. The implementation of more stable electrolytes operating in excess of 3 V has been a significant avenue for performance improvement in

106

that technology [21], [54]. Alternate electrolyte chemistry or a different configuration of composite dielectric that does not include aqueous electrolyte may similarly improve voltage and energy density in MMD designs.

E.   METAL PARTICLE INSULATING SURFACE LAYER

The increased volume loading of insulated particles in the CED was a significant finding. It is shown that by a simple surface treatment process, the resistance of metal powders can be increased by at least an order of magnitude. Essentially, a bed of conductive nickel powder can be made into an insulating material by a simple soak in H_2O_2. The existence of any insulating surface oxide layer could not be verified by various characterization efforts and there is no observable change in mass or density of the metal powder. Only through direct resistance measurement is the existence of the insulating layer confirmed. This observation suggests that the insulating layer must be very thin, possibly less than 100 atomic layers. There is indication that the surface treatment has an impact on the surface texture of the metal particles.

The difference in performance between CED capacitors constructed with insulated and conductive particles validates the significance of this finding. Capacitors produced with dielectrics containing untreated, conductive nickel particles were not functional at volume fractions above 25%. Constructing capacitors with treated powders permits metal particle volume loading of at least 40%. This effect is not fully explored in this study. The original objective of maximizing dielectric constant and energy density led to the observation of functional capacitor dielectrics with high metal volume fractions. However, the upper bound of this observation is not captured in this study. High volume fractions are not tested over a range of surface treatments.

F.   SUMMARY

In summary, this study accomplishes validation of the CED concept and examines specific factors influencing capacitor performance. Previously unreported dielectric constants are observed and conductive particles are loaded in high volume fractions in a composite dielectric. However, the capacitors suffer from limited operating voltages and

appear particularly susceptible to complex loss behavior. A concept model is postulated for the mechanisms of charge storage and voltage limitations.

VI. RECOMMENDED FUTURE WORK

Continuation of this research could take several directions. One aspect suggesting further consideration is the examination of alterative variants of insulated conducting particles. Particularly of interest based on parallel investigations is the suitability of carbon particles coated in tetraethyl orthosilicate (TEOS) to create an insulating silica layer [55].

Another aspect for study is to focus on improving the voltage limitation by adjusting the composition of the matrix phase. The relative composition and selected constituent chemicals were held mostly constant for this study. Alternate investigations of the acid or base solution used in the electrolyte, and its relative amount with respect to the base ceramic powder, should be continued. Organic electrolytes with established higher breakdown voltages should lead to increases in operating voltage and energy density. Alternate ceramics could also be considered to capitalize on higher relative permittivity in the dielectric matrix phase. Loading insulated conductive particles into $BaTiO_3$ powder is an interesting prospective concept.

The relationship between the dielectric thickness and breakdown voltage should also be refined. Certainly a thinner dielectric is preferable for energy density and capacitance, but not if the voltage limit is strictly tied to the dielectric thickness.

More intentional consideration of high volume loading also justifies further study. This study demonstrated that insulated metal particles can be loaded into the electrolyte matrix in volume fractions up to 40%. Determining the upper bound of this effective volume loading and the factors which influence that limit would comprise a significant result.

A dedicated study of oxidizing surface treatments could also support this concept. This study demonstrated that the described H_2O_2 surface treatment succeeded in insulating the nickel powder, but the specific mechanism is not understood. Varying the parameters of the surface treatment process and application of additional characterization methods could inform a more optimal particle treatment regimen.

THIS PAGE INTENTIONALLY LEFT BLANK

APPENDIX

A.   DUPLICATE CAPACITOR TESTING

The results shown in Table 10 are duplicate tests not previously described in this study. The corresponding energy densities are represented on Figure 22.

Nickel Volume Loading (Treatment)	Composition	Dielectric Thickness (d)	Initial Discharge Voltage (V_0)	Dielectric Constant (ε_R)	Operating Voltage
20% (untreated)	12 mL alumina (2.4 g) 0.24 g boric acid 3 mL treated nickel 3.5 mL H_2O	1.73 mm	1.69 V	3.56E9	1.10 V
20% (3x treated)	12 mL alumina (2.5 g) 0.25 g boric acid 3 mL treated nickel 3.5 mL H_2O	2.39 mm	1.76 V	4.23E9	1.19 V
20% (2x treated)	12 mL alumina (2.5 g) 0.25 g boric acid 3 mL treated nickel 3.5 mL H_2O	2.18 mm	1.85 V	5.34E9	1.25 V
20% (2x treated)	12 mL alumina (2.5 g) 0.25 g boric acid 3 mL treated nickel 3.5 mL H_2O	1.98 mm	1.50 V	2.84E9	1.08 V
20% (1x treated)	12 mL alumina (2.5 g) 0.25 g boric acid 3 mL treated nickel 3.5 mL H_2O	2.11 mm	1.62 V	3.38E9	1.20 V
30% (2x treated)	10.5 mL alumina (2.2 g) 0.22 g boric acid 4.5 mL treated nickel 3.5 mL H_2O	1.98 mm	1.77 V	5.07E9	1.24 V
40% (2x treated)	9 mL alumina (1.8 g) 0.18 g boric acid 6 mL treated nickel 3.9 mL H_2O	1.85 mm	0.82 V	(No measurable result)	
40% (3x treated)	9 mL alumina (1.8 g) 0.18 g boric acid 6 mL treated nickel 3.9 mL H_2O	2.03 mm	1.69 V	5.63E9	1.26 V

Table 12.   Duplicate CED Capacitor Discharge Test Results

B.   RESISTANCE TESTING

The values shown in Tables 13 through 17 are voltages recorded by conducting resistance checks using the voltage divider circuit shown in Figure 15. All values are recorded in volts.   Each table contains results from a specific level of surface treatment. Each series of voltage measurement is repeated several times and recorded in respective columns.   Particularly, in Table 13, eight iterations are conducted due to higher variability in the result.

$V_{applied}$	V_{powder}							
0	0.026	0.024	0.234	0.210	0.002	0.318	0.293	0.158
0.5	0.035	0.033	0.317	0.288	0.003	0.442	0.406	0.221
1	0.072	0.068	0.618	0.565	0.006	0.884	0.814	0.440
1.5	0.106	0.101	0.890	0.826	0.009	1.305	1.200	0.648
2	0.141	0.134	1.145	1.074	0.012	1.721	1.564	0.850
2.5	0.173	0.166	1.367	1.290	0.015	2.118	1.919	1.040
3	0.204	0.199	1.592	1.500	0.018	2.498	2.263	1.220
3.5	0.236	0.233	1.720	1.683	0.020	2.855	2.575	1.398
4	0.267	0.264	1.900	1.857	0.023	3.206	2.886	1.527

Table 13.   Resistance Check Voltage Measurements for Untreated Nickel Powder

$V_{applied}$	V_{powder}		
0	0.345	0.342	0.344
0.5	0.482	0.475	0.479
1	0.980	0.964	0.974
1.5	1.475	1.444	1.466
2	1.984	1.928	1.970
2.5	2.477	2.386	2.458
3	2.973	2.826	2.947
3.5	3.469	3.246	3.436
4	3.974	3.667	3.930

Table 14.   Resistance Check Voltage Measurements for 1x Treated Nickel Powder

$V_{applied}$	V_{powder}		
0	0.330	0.329	0.328
0.5	0.460	0.459	0.458
1	0.929	0.927	0.926
1.5	1.390	1.385	1.383
2	1.854	1.847	1.844
2.5	2.297	2.289	2.283
3	2.732	2.722	2.716
3.5	3.151	3.151	3.143
4	3.577	3.575	3.567

Table 15.   Resistance Check Voltage Measurements for 2x Treated Nickel Powder

$V_{applied}$	V_{powder}		
0	0.342	0.344	0.343
0.5	0.479	0.479	0.480
1	0.976	0.976	0.978
1.5	1.470	1.470	1.474
2	1.976	1.976	1.983
2.5	2.468	2.468	2.477
3	2.961	2.960	2.973
3.5	3.454	3.454	3.469
4	3.955	3.954	3.974

Table 16.   Resistance Check Voltage Measurements for 3x Treated Nickel Powder

$V_{applied}$	V_{powder}		
0	0.340	0.245	0.342
0.5	0.427	0.337	0.476
1	0.850	0.656	0.966
1.5	1.254	0.945	1.449
2	1.655	1.223	1.942
2.5	2.022	1.468	2.417
3	2.379	1.695	2.890
3.5	2.720	1.915	3.359
4	3.056	2.120	3.828

Table 17.   Resistance Check Voltage Measurements for 4x Treated Nickel Powder

THIS PAGE INTENTIONALLY LEFT BLANK

LIST OF REFERENCES

[1]   A. Nishino, "Capacitors: operating principles, current market and technical trends," *Journal of Power Sources*, vol. 60, pp. 137–147, June 1996.

[2]   Z. Yang, J. Zhang, M.C.W. Kintner-Meyer, X. Lu, D. Choi, J.P. Lemmon, and J. Liu, "Electrochemical energy storage for green grid," *Chemical Reviews*, vol. 111, no. 5, pp. 3577–3613, March 2011.

[3]   V. Presser, C.R. Dennison, J. Campos, K.W. Knehr, E.C. Kumbur, and Y. Gogotsi, "The electrochemical flow capacitor: A new concept for rapid energy storage and recovery," *Advanced Energy Materials*, vol. 2, no. 7, pp. 895–902, May 2012.

[4]   O. Haas and E.J. Cairns, "Electrochemical energy storage," *Annual Reports on the Progress of Chemistry. Section C,* vol. 95, pp. 163–198, 1999.

[5]   J.C. Anderson, "Dielectric Breakdown," in *Dielectrics*, New York: Reinhold Publishing, 1964, ch. 8, pp. 98–120.

[6]   D.R. Lohrmann, D. Ma, and D. Wu, "On energy density in dielectrics," Naval Research Laboratory, Washington, D.C., Rep No. NRL/MR/5747--98--8197, 1998.

[7]   A.E. Curtright and J. Apt, "The character of power output from utility-scale photovoltaic systems," *Progress in Photovoltaics: Research and Applications*, vol. 16, pp. 241–247, September 2007.

[8]   J. Apt, "The spectrum of power from wind turbines," *Journal of Power Sources*, vol. 169, pp. 369–374, June 2007.

[9]   J. Cho, P.G. Bruce, N.-S. Choi, Z. Chen, S.A. Freunberger, X. Ji, Y.-K. Sun, K. Amine, G. Yushin, and L.F. Nazar, "Challenges facing lithium batteries and electrical double-layer capacitors," *Angewandte Chemie International Edition*, vol. 51, no. 40, pp. 9994–10024, October 2012.

[10]   J. Schindall, "The charge of the ultra-capacitors," *IEEE Spectrum*, vol. 44, pp. 42–46, November 2007.

[11]   M. Jayalakshmi and K. Balasubramanian, "Review: Simple capacitors to supercapacitors," *International Journal of Electrochemical Science,* vol. 3, pp. 1196–1217, January 2008.

[12]   L. Wei and G. Yushin, "Capacitive Electric Storage," in.*The World Scientific Handbook of Energy,* G.M Crawley, Ed. Singapore: World Scientific Publishing, 2012, pp. 373–404.

[13]   A. Dehbi, W. Wondrak, Y. Ousten, and Y. Danto, "High temperature reliability testing of aluminum and tantalum electrolytic capacitors," *Microelectronics Reliability*, vol. 42, pp. 835–840, June 2002.

[14]   S. Niwa and Y. Taketani, "Development of new series of aluminium solid capacitors with organic semiconductive electrolyte (OS-CON)," *Journal of Power Sources*, vol. 60, pp. 165–171, June 1996.

[15]   H. Yamamoto, M. Oshima, M. Fukuda, I. Isa, and K. Yoshino, "Characteristics of aluminum solid electrolytic capacitors using a conducting polymer," *Journal of Power Sources*, vol. 60, pp. 173–177, June 1996.

[16]   A.K. Shukla, S. Sampath, and K. Vijayamohanan, "Electrochemical supercapacitors: Energy storage beyond batteries," *Current Science,* vol. 79, no. 12, pp. 1656–1661, December 2000.

[17]   V. Khomenko, E. Raymundo-Piñero, E. Frackowiak, and F. Béguin, "High-voltage asymmetric supercapacitors operating in aqueous electrolyte," *Applied Physics A: Materials Science & Processing,* vol. 82, no. 4, pp. 567–573, March 2006.

[18]   C. Liu, Z. Yu, D. Neff, A. Zhamu, and B.Z. Jang, "Graphene-based supercapacitor with an ultrahigh energy density," *Nano Letters,* vol. 10, no. 12, pp. 4863–4868, December 2010.

[19]   S. Boukhalfa, K. Evanoff, and G. Yushin, "Atomic layer deposition of vanadium oxide on carbon nanotubes for high-power supercapacitor electrodes," *Energy & Environmental Science*, vol. 5, pp. 6872–6879, May 2012.

[20]   T. Liu, H. Zhang, F. Wang, J. Shi, P. Ci, L. Wang, S. Ge, Q. Wang, and P.K. Chu, "Three-dimensional supercapacitors composed of $Ba_{0.65}Sr_{0.35}TiO_3$ (BST)/NiSi$_2$/silicon microchannel plates," *Materials Science and Engineering B*, vol. 176, no. 5, pp. 387–392, March 2011.

[21]   B.E. Conway and W.G. Pell, "Double-layer and pseudocapacitance types of electrochemical capacitors and their applications to the development of hybrid devices," *Journal of Solid State Electrochemistry,* vol. 7, no. 9, pp. 637–644, September 2003.

[22]   M. Mastragostino, C. Arbizzani,, and F. Soavi, "Polymer-based supercapacitors," *Journal of Power Sources*, vol. 97-98, pp. 812–815, July 2001.

[23]   C. Arbizzani, M. Mastragostino, and F. Soavi, "New trends in electrochemical supercapacitors," *Journal of Power Sources*, vol. 100, pp. 164–170, November 2001.

[24] K. Kinoshita and A. Yamaji, "Grain-size effects on dielectric properties in barium titanate ceramics," *Journal of Applied Physics,* vol. 47, no.1, pp. 371–373, January 1976.

[25] G. Arlt, D. Hennings, and G. de With, "Dielectric properties of fine-grained barium titanate ceramics," *Journal of Applied Physics,* vol. 58, pp. 1619–1625, August 1985.

[26] J.C. Burfoot and G.W. Taylor, "Non-switching applications," in *Polar Dielectrics and Their Applications*, Berkeley and Los Angeles: University of California Press, 1979, ch. 17, pp. 359–402.

[27] F. El Kamel and P. Gonon, "Enhancement of the double-layer capacitance in $BaTiO_3$:H-based solid electrolyte," *Journal of the Electrochemical Society*, vol. 157, no. 3, pp. G91–94, January 2010.

[28] M. Maglione, C. Elissalde, and U-C. Chung, "Interface control in $BaTiO_3$ based supercapacitors," *Proceedings of SPIE*, vol. 7603, pp. 76030U–176030U-5, February 2010.

[29] J.C. Anderson, "Dielectric Devices," in *Dielectrics*, New York: Reinhold Publishing, 1964, ch. 10, pp. 143–163.

[30] B. Skinner, T. Chen, M.S. Loth, and B.I. Shklovskii, "Theory of volumetric capacitance of an electric double-layer supercapacitor," *Physical Review E*, vol. 83, no. 5, pp. 056102-1–056102-10, May 2011.

[31] H. Kishi, Y. Mizuno, and H. Chazono, "Base-metal electrode-multilayer ceramic capacitors: Past, present and future perspectives," *Japanese Journal of Applied Physics*, vol. 42, pp. 1–15, January 2003.

[32] R.D. Weir and C.W. Nelson, "Electrical-energy-storage unit (EESU) utilizing ceramic and integrated-circuit technologies for replacement of electrochemical batteries," U.S. Patent 7 033 406, April 25, 2006.

[33] R.D. Weir and C.W. Nelson, "Utilization of poly(ethylene terephthalate) plastic and composition-modified barium titanate powders in a matrix that allows polarization and the use of integrated-circuit technologies for the production of lightweight ultrahigh electrical energy storage units (EESU)," U.S. Patent 7 466 536, December 16, 2008.

[34] F. Zhang , T. Zhang , X. Yang , L. Zhang , K. Leng , Y. Huang, and Y. Chen, "A high-performance supercapacitor-battery hybrid energy storage device based on graphene-enhanced electrode materials with ultrahigh energy density," *Energy & Environmental Science*, vol. 6, pp. 1623–1632, March 2013.

[35]   R.A. Dougal, S. Liu, and R.E. White, "Power and life extension of battery-ultracapacitor hybrids," *IEEE Transactions on Components and Packaging Technologies*, vol. 25, no. 1, pp. 120–131, March 2002.

[36]   C. Pecharromán, F. Esteban-Betegón, J. F. Bartolomé, S. López-Esteban, and J. S. Moya, "New percolative BaTiO3 - Ni composites with high and frequency independent dielectric constant," *Advanced Materials,* vol. 13, no. 20, pp. 1541–1544, October 2001.

[37]   Y.J. Wu, S.H. Su, J.P. Cheng, and X.M. Chen, "Spark plasma sintering of Barium Zirconate Titanate/Carbon nanotube composites with colossal dielectric constant," *Journal of the American Ceramic Society,* vol.94, no. 3, pp. 663–665, March 2011.

[38]   Z. Ghallabi, M. Arous, A. Kallel, I. Royaud, G. Boiteux, and G. Seytre, "Giant permittivity in three-phase PVDF composites," in *2010 10th IEEE International Conference on Solid Dielectrics*,IEEE. doi: 10.1109/ICSD.2010.5568044.

[39]   D. Gerenrot, L. Berlynad, and J. Phillips, "Random network model for heat transfer in high contrast composite materials," *IEEE Transactions on Advanced Packaging,* vol. 26, no. 4, pp. 410–416, November 2003.

[40]   J.P. Calame, "Evolution of Davidson-Cole relaxation behavior in random conductor-insulator composites," *Journal of Applied Physics,* vol. 94, no. 9, pp. 5945–5957, November 2003.

[41]   D. Wilkinson, J.S. Langer, and P.N. Sen, "Enhancement of the dielectric constant near a percolation threshold," *Physical Review B,* vol. 28, no.2, pp. 1081–1087, July 1983.

[42]   R.C. McPhedran and D.R. McKenzie, "Exact solutions for transport properties of arrays of spheres," *Proceedings of the First Conference on the Electrical Transport and Optical Properties of Inhomogeneous Media*, Columbus, OH, 1977, pp. 294–299.

[43]   D.J. Bergman and Yoseph Imry, "Critical behavior of the complex dielectric constant near the percolation threshold of a heterogeneous material," *Physical Review Letters,* vol. 39, no. 19, pp. 1222–1225, November 1977.

[44]   A.K. Sarychev and V.M. Shalaev, "Percolation Threshold: Singularities in Metal-dielectric Composites," in *Electrodynamics of Metamaterials,* Singapore: World Scientific Publishing, 2007, ch. 1, sec. 2, pp. 11–18.

[45]   C. Pecharromán and J.E. Iglesias, "Effective dielectric properties of packed mixtures of insulator particles," *Physical Review B*, vol. 49, no. 11, pp. 7137–7147, March 1994.

[46]   R. Ulrich, L. Schaper, D. Nelms, and M. Leftwich, "Comparison of paraelectric and ferroelectric materials for applications as dielectrics in thin film integrated capacitors," *The International Journal of Microcircuits and Electronic Packaging*, vol. 23, no. 2, pp. 172–180, 2000.

[47]   J.C. Anderson, "General Properties," in *Dielectrics*, New York: Reinhold Publishing, 1964, ch. 1, pp. 1–20.

[48]   J. Phillips and B. Scanlan, "Multi-material dielectrics: Novel class of super high dielectric constant materials incorporated into energy storage devices," unpublished.

[49]   L.Z. Liu, X.H. Gao, L. Weng, H. Shi, and C. Wang, "Preparation of high-dielectric-constant Ag@Al2O3/Polyimide composite films for embedded capacitor applications," in *2012 IEEE 10th International Conference on the Properties and Applications of Dielectric Materials*, IEEE. doi: 10.1109/ICPADM.2012.6318901.

[50]   J.C. Anderson, "Measurement of Permittivity," in *Dielectrics*, New York: Reinhold Publishing, 1964, ch. 2, pp. 21–38.

[51]   F.J. Burger and J. Wu, "Dielectric Breakdown in Electrolytic Capacitors," *Journal of the Electrochemical Society*, vol. 118, no. 12, pp. 2039–2042, December 1971.

[52]   A. von Hippel, "Theory," in *Dielectric Materials and Applications*, New York: The Technology Press of M.I.T. and John Wiley & Sons, 1954, ch. 1, pp. 3–46.

[53]   H. Fröhlich, "Macroscopic Theory," in *Theory of Dielectrics*, London: Oxford University Press, 1958, ch. 1, pp. 1–14.

[54]   X. Andrieu, L. Josset, and B. Pichon, "A High Energy Density Supercapacitor," *Proceedings of the Symposium on Electrochemical Capacitors II*, vol. 96, no. 25, pp. 202–207, 1997.

[55]   D. Lenard, "High dielectric constant multi-material dielectric capacitors," M.S. thesis, Dept. Mech. Eng., Naval Postgraduate School, Monterey, CA, 2013.

THIS PAGE INTENTIONALLY LEFT BLANK

INITIAL DISTRIBUTION LIST

1.   Defense Technical Information Center
        Ft. Belvoir, Virginia

2.   Dudley Knox Library
        Naval Postgraduate School
        Monterey, California